# THERMOGRAPHY AND COMPUTATIONAL ANALYSIS OF WATER INGRESS IN HONEYCOMB COMPOSITE PANELS

**by**

**CLETUS MATTHEW MAGODA**

**Student No. 203131851**

**Thesis submitted in fulfilment of the requirements for the degree**

**Doctor of Engineering in Mechanical Engineering**

**in the**

**Faculty of Engineering and the Built Environment**

**at the**

**Cape Peninsula University of Technology**

**Supervisor:** Prof Tiyamike Ngonda

**Co-supervisor:** Prof Vladamir Vavilov

**Bellville Campus**

**November 2024**

## CPUT copyright information

## DECLARATION

I, **Cletus Matthew Magoda**, declare that I am the sole author of this thesis and that no part of this thesis has been published or submitted for publication. The contents of this thesis represent my own unaided work, and this is a true copy of my thesis, including any final revisions, as approved by my institution's research committee. Lastly, it represents my own opinions and not necessarily those of the Cape Peninsula University of Technology.

Signed  Date **18/11/2024**

## ABSTRACT

This research presents the results of experimental and numerical investigations on water ingress trapped in honeycomb panels. Ingress of atmospheric water in aircraft honeycombs may cause damage to aircraft. The percentage of water/ice filling honeycomb cells is an important factor in possible cell wall damage. This study is focused on the analysis of the following inspection parameters: 1) influence of panel orientation (horizontal, vertical and Inclined at 30° and 60°) on the efficiency of water detection, 2) efficiency and optimisation of a heating technique in evaluating water ingress, 3) influence of water/ice phase transformation on the detectability of water ingress, 4) quantifying of the water ingress.

The numerical analysis was conducted by using the finite difference algorithms (ThermoCalc-3D), image processing algorithms (ThermoFit Pro), finite difference algorithms with only radiation heat transfer boundary condition ( ThermoCalc-3D-radiation), and Normalization image processing algorithm (ThermoDouble software), and the experiments were conducted by using active and passive infrared thermography to evaluate the detectability of water ingress and image processing in the cases where a test panel is placed in different spatial orientations. The samples with water and ice were tested and analysed using several data processing algorithms in the ThermoFit software to enhance water detection performance. The Maximum surface differential temperature signals ($\Delta T$), running contrast ($C_m$) and their observation times ($t_{\Delta T}$ and $t_{Cm}$) were recorded and analysed for both samples with water and ice in the honeycomb cells. The signal-to-noise ratio (SNR) concept was used to compare the efficiency of image processing algorithms in inspecting water ingress in honeycomb panels with varying water content, spatial orientation and water/ice phase transformation.

The computational results indicate that cells filled with water (100%) in a horizontal panel (180°) exhibit the highest differential temperature signal ($\Delta Tm$) of 30.1°C and a running contrast ($C_m$) of 0.88. In contrast, cells filled with 50% water in the same orientation show a $\Delta T_m$ of 27°C and a $C_m$ of 0.14. For the panel in a vertical position, the recorded $\Delta T_m$ and $C_m$ values are 30.0°C and 0.82, respectively. The inclined panel (60°) with 50% water-filled cells shows the optimal $\Delta T_m$ and $C_m$ values of 30.1°C and 0.83.

These computational trends are supported by the experimental data, which demonstrate that the horizontal panel (180°) filled with 100% water yields the highest $\Delta T_m$ of 6.5°C and $C_m$ of 0.7. The same panel orientation with 50% water-filled cells results in a $\Delta Tm$ of 3.96°C and $C_m$ of 0.59. The vertical panel shows a $\Delta T_m$ of 4.8°C and $C_m$ of 0.55. The inclined panel (60°) with 50% water-filled cells yields optimal values of 3.71°C for $\Delta T_m$ and 0.58 for $C_m$.

To assess the efficiency of data processing and improve water ingress detection (visibility), computing the Signal-to-Noise Ratio (SNR) during image processing is essential. Using a

single image processing algorithm (Fourier phase 3rd harmonic) across all scenarios, the horizontal panel with 100% water-filled cells recorded an SNR of 88.1, while the vertical and inclined (60°) panels recorded SNRs of 21.9 and 20.2, respectively.

The qualitative data indicate that the variation in $\Delta T_m$ and $C_m$ across panel orientations is minimal, suggesting that panel orientation has little impact on the detection of water ingress. This implies that water visibility is primarily dependent on water content rather than the panel's orientation.

Quantifying the amount of water trapped in honeycomb cells is crucial. From the calibration curve, it was observed that passive heating results in a maximum $\Delta T_m$ of 11°C, which remains constant as water content increases, due to the rapid thermal equilibrium between the panel and the environment. Active heating, on the other hand, generates a $\Delta T_m$ of 27°C, with a positive correlation to increasing water content.

These findings suggest that active heating provides a more reliable calibration curve, while passive heating is better suited for detecting the presence of water ingress.

The overall findings from this study make a valuable contribution to aircraft fuselage maintenance and provide useful data for aviation engineers to quantify water content in the cells of honeycomb panels.

## PUBLICATIONS ARISING FROM THE STUDY

| Chapter | Journal article | Status |
|---|---|---|
| 3 & 4 | Magoda, C.M., Ngonda, T.N., Vavilov, V.P. and D. Yu. Kladov (2024). Evaluating Water Ingress in Glass Fiber Plastic/Nomex Honeycomb Panels under Varying Panel Orientation. Russian Journal of Nondestructive Testing, 60(7), pp.813–825. doi: https://doi.org/10.1134/s1061830924602022. | Published |

## ACKNOWLEDGEMENTS

First and foremost, I thank God for granting me the strength and endurance to complete this work. I want to express my gratitude to all those who offered their support, both directly and indirectly, during my graduate studies and research at the Cape Peninsula University of Technology.

My deepest appreciation goes to my supervisors, Prof VP Vavilov (Professor and Laboratory Head at the School of Non-Destructive Testing, Tomsk Polytechnic University) and Prof T Ngonda (Department of Mechanical and Mechatronic Engineering at Cape Peninsula University of Technology) for their unwavering guidance and mentorship throughout this project.

I also thank Prof Fester, Assistant Dean in Research, innovation and Partnership in the Faculty of Engineering and the Built Environment, for her logistical and administrative support during my studies.

A special thank you goes to my family and my incredible wife, Zinzi Magoda, for her love, patience, and boundless support at every stage of this journey.

Finally, I acknowledge the Cape Peninsula University of Technology (CPUT) for its invaluable support, which enabled me to undertake and complete this research.

## DEDICATION

This thesis is dedicated to all industries that involve non-destructive evaluation, especially honeycomb panels manufacturers and the aviation industry to efficiently detect and characterise water trapped in the aircraft fuselage.

## ACRONYMS AND ABBREVIATIONS

| | |
|---|---|
| e | Thermal effussivity (Wm$^{0.5}$/(m$^2$ $^0$C ) |
| α | Thermal diffusion coefficient $\left(m^2/s\right)$ |
| $C_m$ | Running contrast |
| k | Thermal conductivity $\left(W/m.k\right)$ |
| q | Heat flux (W/m$^2$) |
| $q_{rad}$ | Radiation heat lost (W/m$^2$): heat escaping from the surface of the specimen to the environment when it is subjected to heat flux |
| $q_{conv}$ | Convection heat lost (W/m$^2$): heat escaping from the surface of the specimen to the environment when it is subjected to heat flux |
| ΔT | Differential temperature signals $\left({}^0C\right)$or$\left(K\right)$ |
| $F_0$ | Fourier number (dimensionless): used in the conduction equation when predicting the temperature response of materials undergoing transient conductive heating |
| (x,y,z) | Directions of heat flow |
| Δt | Time change (seconds) |
| $B_i$ | Biot number (dimensionless): ratio of the thermal resistance inside of a body (defect) and at the surface of the body |
| $N_u$ | Nusselt number (dimensionless): the ratio of convective to conductive heat transfer across a boundary (surface) |
| $P_r$ | Prandtl number (dimensionless): a ratio between kinematic viscosity and thermal diffusivity. |
| SNR | Signal to Noise ratio: an average power image to average power noise in the image or sequence. |
| NDE | Non-destructive evaluation: a non-contact technique used for material evaluation |
| NDT | Non-destructive Testing : a technique used to evaluate properties of components without causing damage. |
| TNDT | Thermal Non-destructive Testing : an NDT technique which uses external heat source (heat flux) to excite components. |
| AIRT | Active Infrared thermography: a non-contact and non-destructive technique used for material testing and evaluation with the assistance of the infrared camera and external heat source. |

| | |
|---|---|
| PIRT | Passive Infrared thermography: a non-contact and non-destructive technique used for material testing and evaluation due to temperature difference between the material and the environment. |
| PPT | Phase Pulse thermography: an NDT technique that uses a brief pulse of light to heat a material's surface for testing and evaluation. |
| LPT | Long pulse Thermography: an NDT technique that uses long pulse thermal excitation to heat a material's surface for testing and evaluation |
| GFRP | Glass fibre-reinforced polymer: a composite material made by combining glass fiber sheet/skin with a polymer resin matrix. |
| ThermoCalc-3D | Modelling software for solving Thermal Non-destructive evaluation problems (3D heat transfer problems) |
| SNR | Signal to Noise ratio: the ratio of the signal power to the noise power. |
| TSR | Thermal signal reconstruction: a data processing technique to analyse image sequence captured during thermography experiment. |
| TPU | Tomsk Polytechnic University: A university located in Tomsk, Russia |
| DTT | Dynamic Tomography: an NDT technique that allows capturing a series of images of a moving or changing object or process. |
| UTT | Ultrasonic Stimulated Infrared Thermography: It’s an NDT technique that uses ultrasonic waves to induce vibrations in a material, then infrared thermography detects temperature changes revealing water ingress. |
| Composite material | A material made as a single rigid unit from constituent others that may have different properties |
| Water ingress | Water trapped in the honeycomb cells |

**TABLE OF CONTENTS**

## LIST OF FIGURES

## LIST OF TABLES

# CHAPTER 1:
# INTRODUCTION TO RESEARCH

## 1.1 Introduction

Honeycomb Composite panels are mostly used in aerospace and automotive industries due to their high strength-to-weight ratio and thermal insulation properties. However, water ingress poses a significant threat to their structural integrity and performance (Smith & Jones, 2020). It is for this reason that the characterisation of honeycomb cells filled with water ingress becomes an integral part of the structural integrity of the panels, especially in the aviation industry. Several studies have been developed to investigate the integrity of composite material panels associated with the application in a particular field due to the nature of impact forces and the environment. To avoid the degradation and total failure of the composite panels, it is important to develop a preventative maintenance plan that responds to maintaining the integrity of these panels. Non-destructive testing (NDT) methods can test and evaluate the structural integrity of composite materials.

NDT is among the most commonly used methods to investigate the integrity of material structures (Niccolai *et al.*, 2021). NDT involves the testing of materials for defects without impairing their future usefulness (Deepak *et al.*, 2021). Common NDT methods include acoustic emission, radiography, thermography, ultrasonic testing, eddy current testing, magnetic particle testing, penetrant testing, etc. There is substantial literature on the inspection of composite materials using NDT methods. However, more needs to be done on the inspection of water ingress in honeycomb composite materials using infrared thermography (IR), specifically active pulsed thermography. With the other NDT methods, the need to personalise the inspections is inevitable, which could easily explode costs, leading to financial constraints.

This study explores Active Infrared Thermography (AIRT) as a validation technique for computationally predicted data, given its feasibility. The focus is on its applicability, ease of implementation, and the range of structural sizes on which it can be used. The AIRT provides useful information on the spatial homogeneity or inhomogeneity of a component or structure in the form of thermal distribution (Ruwandi et al., 2019). Two types of IR Thermography exist passive and active thermography. This study will focus on active thermography, where a heating lamp will be used to excite thermal waves into the composite material, and after that, the thermal distribution, temperature contrast, and excess temperature will indicate the presence of defects.

## 1.2 Background of the Problem

Honeycomb panels are preferred for interior aircraft structural panels because they deliver safety, durability, and weight savings. Detecting water ingress in honeycomb panels of aircraft under operation is still challenging. Vavilov, Pan and Nesteruk (2016) used an infrared thermography technique to detect water in aviation honeycomb panels. They discussed the framework of both 1D analytical and 3D numerical models. They also demonstrated the influence of the honeycomb cell structure on the modelling protocol. Optimal test conditions were also formulated theoretically and experimentally in scenarios where the force of gravity causes the water to be against the face sheet at the bottom of the cells or where an air gap separates the water from the top face sheet. Similarly, Vavilov et al. (2017) discussed the use of Infrared thermography and numerical modelling for the quantitative evaluation of water ingress in aviation honeycomb panels. The focus was to develop a correlation between water thicknesses and the surface temperature anomalies and the times of their appearance in active one-sided thermal tests. It was found that quantitative evaluation of water content in honeycomb cells using IR thermography is a challenging task, and the results obtained were not promising. It was suggested to inspect both panel surfaces and use a ratio of respective temperature signals $\Delta T_{front}/\Delta T_{rear}$ or contrasts $C_{front}/C_{rear}$ for water mass calibration. Later, Shrestha, Choi and Kim (2021) inspected water ingress in composite honeycomb sandwich structures. The focus was to do a comparative study among Lock-in thermography algorithms (i.e. Fast Fourier transform, Harmonic approximation, and the principal component analysis) in terms of signal-noise ratio (SNR). Meaningful structural health monitoring techniques by the aviation industry are critical elements in the quality approval process. The emphasis has always been on detecting and characterising water ingress in the cells of honeycomb panels.

Normally, aircraft surveying is done remotely on an aircraft at a distance from 3 to 30 m, with the survey time being at most 1 hour per 1 aircraft. The survey is done when an aircraft lands and reaches a final stop place. The survey may start even when passengers leave the aircraft or after. Therefore, the first hour after landing is the best for water detection, but if there is a lot of water, clear signals may be present for up 6 hours.

The warmer the ambient temperature, the better the detection of water ingress. However, since it is -50 to -60°C at a cruising altitude, any temperature at the ground level is sufficient to produce a necessary gradient. However, Water tends to get at the bottom of the panel cells under gravitation. So, the maximum of water is observed at the bottom sections of the fuselage, rudder, and air intakes. In ailerons, water is concentrated closer to the edges.

If an aircraft is not painted by a darker paint, i.e. is shiny, it is recommended to avoid a very sunny day or take a survey in the early morning or night.

Infrared Thermography is the most popular technique which is employed to characterise sub-surface defects in composite materials, the specific parameters used to accurately characterize the sub-surface defects should be identified. However, the complexity of the relationship between these parameters (depth, lateral size and shape) yields a critical need for a combination of methods to accurately predict the size, depth, and shape.

For this research, the thermographic survey will be done without input heat intensity. The temperature difference between the aircraft fuselage and the ground level temperature after the aircraft has landed will be used to detect water ingress. The surface temperature variation is widely used by researchers in this field as the preferred parameter to be considered. Most researchers have opted for the excess surface temperature, which is the difference between the highest temperature observed above water ingress and that of the adjacent nodes to identify and characterize (depth) the sub-surface water pockets over the temperature variation. For this reason, it is critical to perform an experimental and numerical comparative study between the IR with the surface temperature variation and the IR with the fuselage surface temperature difference to identify a reliable, affordable, and, most importantly, a technique which is practically acceptable in the non-destructive field.

Water's detection and characterisation process in the honeycomb structure is like that of sub-surface defects characterisation. Literature in the recent past has proposed techniques and parameter correlation when characterising sub-surface defects. For instance, Sharat, Menaka and Venkatraman (2013), Manchor, and Di Scalea (2014), Grys. (2018), Wei et al. (2021), Moskovchenko et al. (2021), and Wang et al. (2022) have been focussing on a non-destructive evaluation (NDE) technique known as infrared thermography (IRT) to characterise sub-surface defects in composite materials, focusing on the use of excess temperature directly above the defects (water ingress) to estimate their sizes and depths. Vavilov and Burleigh (2020) discuss defect characterisation techniques, including analysing temperature response over time on a sample heated with a pulse. This technique focuses on describing the surface temperature of a semi-infinite object subjected to direct heating. The Thermal properties of a sample material, such as thermal diffusivity, are independent of time in the case of a non-defected material. Therefore, any deviation of the surface temperature ($T_s$) from a reference value (non-defected area) should be treated as an indication of the presence of sub-surface defects and variations in thermal properties. This technique, generally used by NDE specialists, is considered one of the most trusted techniques for non-destructive inspection. In the past, it was primarily used for the identification of sub-surface defects/voids, mostly for

homogenous materials; however, the detection and characterisation of defects such as delamination in composite structures has become a challenge with IRT in terms of its ability to accurately characterise the defects in terms of their depth and sizes. Estimating a defect's depth from the inspection surface of the defect is an important first step towards preventative maintenance against failure for such materials.

The detection and characterisation of water ingress in the aircraft fuselage, rudder, and air intakes using IRT is influenced by the thermal behaviour of the material, the temperature difference, and complex boundary conditions (convection and radiation heat transfer). Consequently, much effort has been – and continues to be made, to incorporate mathematical or analytical modelling in such a way as to predict the presence of water in the panel accurately.

However, Airbus and Boeing employ a relatively straightforward procedure for detecting water in aircraft components when they are moved to a hangar. This process typically involves placing a warm "blanket" or heating element on the surface of the part for a specific duration to encourage any moisture present to evaporate. This method, while effective for identifying the presence of water, does not include a quantitative evaluation of the amount of moisture or the severity of the issue. The procedure primarily serves as a qualitative measure, relying on the assumption that any residual water will be driven off by the applied heat (Airbus, 2017). However, this approach lacks precision in quantifying moisture levels or determining the impact on the structural integrity of the component, which could be crucial for more rigorous maintenance protocols

### 1.3 Problem Statement

The characterisation of water ingress in terms of the level of water in the cell and the position of water concentration in different parts of the aircraft has been critical for the thermographic survey of aircraft just after landing. Failure to accurately detect and characterise these water pockets means failure of the entire panel, which may result in catastrophic failures in actual applications. To detect and characterise these water pockets, quantitative data should be obtained using specialised modelling software and high-standard equipment for experimental work. In practice, water ingress weakens the aircraft fuselage, and it may lead to a total failure, which is catastrophic due to the operating conditions of an aircraft. This has given this research study purpose, which is to assess the water ingress in aircraft fuselage and other parts using the integration of computational technique (CT) and infrared thermography (IRT). This will subsequently benefit the management of aircraft structures with honeycomb core materials.

However, it should be noted that a temperature gradient between the ground level and a cruising altitude is so high that water, due to its high heat capacity, keeps its low temperature for a reasonably long time after landing. A drawback of passive inspection is the difficulty in evaluating water content. Approximately this can be done by measuring the surface occupied by water. In practice, aircraft engineers often just would like to know is there: "a lot of water", "reasonable amount", "few water", "no water". Quantitative determination of water, whether in an active or passive procedure, is a challenging task.

## 1.4 Research Aims and Objectives

The study aimed to perform qualitative and quantitative investigation of water trapped in a honeycomb structure. Firstly, computational analysis is performed to detect water trapped in honeycomb structures. The cells were to be fully (100%) and partially (25% and 50%) filled with water at various orientations. The key parameters to be recorded and analysed were the signal-to-noise ratio, surface differential temperature, the running contrast and their observation times. Secondly, active and passive IRT NDT will detect water trapped in the honeycomb structures at various orientations. Similar key parameters were recorded and analysed. Data is to be processed for both sets of image sequences (computational and experimental) and the signal-to-noise ratio of each algorithm across all scenarios. It also aimed at quantifying water in the honeycomb cells using experimental data. Lastly, it aimed at performing a 3D normalisation, which is a scientific approach to enhance the visibility of water in the cells of the honeycomb structure.

### 1.4.1 The sub-objectives of this research study are:

- The use of a specimen's surface temperature variation to identify the water level in the honeycomb cell considering their thermal diffusivity.
- The induced positive thermal contrast directly over the water pocket to identify the water levels in the material.
- The use of a finite difference numerical model (ThermCalc-3D) to predict the water ingress in honeycomb cells and validate the predictions with physical experimental work (Active and passive thermography).
- To analyse how a source of heating such as halogen lamps, hot air guns, and flash lamps affects the detection of water ingress. The signal-to-noise ratio to be used as the key parameter
- To determine the most suitable image processing technique to enhance the results.

## 1.5 Research Questions

This research study will seek to address the following research questions:

- How can the TNDT model be used to characterise water ingress (pockets) in the ThermoCalc-3D software?
- How can different heating techniques be used in the finite difference numerical model (ThermCalc-3D) to minimise possible errors when characterising sub-surface water ingress?
- What is the water level range of water ingress that can be detected using infrared thermography?
- How does the emissivity of the aircraft fuselage affect the inspection results?
- Which is/are the most suitable image processing techniques that can be used with pulsed thermography?

## 1.6 Research Impact

This research is based on the very real need for water detection and characterisation in honeycomb composite materials in the fuselage of an aircraft. The honeycomb panels are more favoured materials due to their excellent thermal and physical properties. It is important for researchers to provide techniques which are critical for water detection and characterisation in honeycomb structures after the aircraft has landed for better and safe application.

The output of this research may directly benefit the aviation, composite manufacturing, and non-destructive testing industries.

The method applied in this research study is expected to yield results that are satisfactory to industrial or laboratory applications in the non-destructive testing of composite materials. Including the numerical model will minimise time spent detecting the presence of water and accurately detect sub-surface water in honeycomb structures and identify the water content in cells.

## 1.7 Significance of the Research

This research contributes to the aviation industry as it develops a theoretical framework and experimental techniques to conduct a thermographic survey and implement preventative maintenance to avoid catastrophic damage to the aircraft. Active and passive thermographic techniques have been introduced to inspect the aircraft fuselage. passive technique has posed some challenges to accurately determining water levels(content) in the cells. for accuracy and

simplicity, there is a need to couple the experimental work with the numerical model for the sole purpose of detecting and characterising the water content in a honeycomb structure. The material output of this research may directly benefit the aviation composite manufacturing and non-destructive testing industry

# CHAPTER 2:
# LITERATURE REVIEW

## 2.1 Introduction

This chapter examines recent and pertinent literature on the general use of honeycomb structures and the methods employed to characterise subsurface defects, such as water ingress, within these structures. Specifically, it highlights thermal non-destructive testing (TNDT) techniques for honeycomb structures, with an emphasis on infrared thermography (IRT). Additionally, the chapter addresses the literature related to mathematical modelling formulations and their applicability to analysing subsurface defects. Furthermore, it reviews studies on water ingress analysis in inclined surfaces and the associated data processing techniques.

## 2.2 Honeycomb structures

According to Ku et al. (2011), fibre-reinforced polymers are composite materials which consist of two or more materials with different physical and thermal properties. These materials are bonded together during manufacturing and produce a finished panel or structure. Most of these structures are strong, lightweight, stiff and low-density. It is a material revolution within the advanced manufacturing industry to cater to specific applications in fields such as aviation, marine, automotive, and thermal systems design. A typical fibreglass composite with a Nomex honeycomb core is depicted in Fig. 2.1.

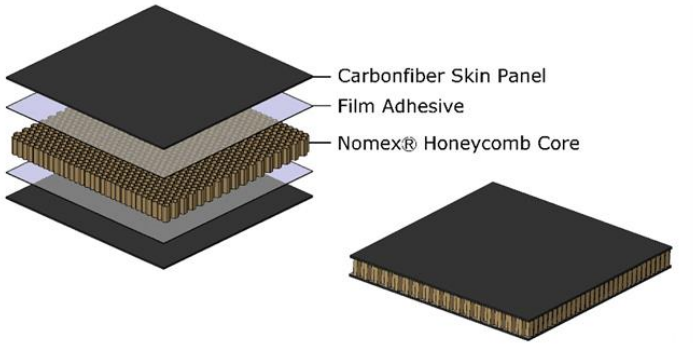


Figure 2.1:Honeycomb Panel assembly( Ku et al,2011)

Ramirez-Vazquez et al. (2016) resonated with the above statement by indicating that composite materials have improved the materials and manufacturing sector; however, proper standards, durability data, and life cycle assessments should be instituted before they become proper alternatives to conventional materials. To date, researchers continue to investigate

some of these composites' thermal and physical properties. In fact, for these materials to be regarded as viable alternatives, they must be structurally and economically feasible.

## 2.3 Infrared Thermography and Thermal Testing

It is a non-contact and non-destructive inspection technique where thermal excitation produces heat flux in the form of pulses. The pulses travel through the specimen. Upon encountering internal heat flow resistance due to defect, void or any form of non-uniformity, the excess temperature is accumulated on top of the defect. This phenomenon takes place when the defect has a lower thermal conductivity (k) than the parent material. It forms a either a positive or negative differential temperature signal ($\Delta T_m$) and the running contrast ($C_m^{run}$). On the contrary, the specimen consisting of higher thermal conductivity (k), such as water in honeycomb cells, forms negative differential temperature signals ($\Delta T_m$) and the running contrast ($C_m^{run}$) (Maldague, 2001)

Umar et al. (2019) introduced ultrasonic-stimulated Infrared Thermography (UIT) as an innovative method for detecting damage in carbon-carbon composites. This technique applies a short ultrasonic pulse to the material, and an infrared camera records the resulting surface temperature variations. UIT can detect subsurface, low-energy impact damages in the material. However, a practical challenge arises in on-site aircraft fuselage inspections, as the ultrasonic transducer must be in direct contact with the specimen, unlike thermal non-destructive infrared testing, which uses a non-contact excitation source. So, for this reason, the active and passive IR are adopted in this study

In principle, the IRT uses an infrared camera that can detect and measure small temperature differences on the surface of the material, resulting from differences in radiation emission captured by the camera. The temperature difference is caused by the heat flux as is transmitted through the thickness of the material induced by an external heat source such as halogen lamps. The surface temperature history on the surface over time is generated in forms of thermograms. The thermograms can be downloaded from the infrared camera and analysed. According to Marquez et al. (2020), infrared thermography inspection can be conducted either as an active infrared thermography or passive infrared thermography.

Figure 2.2 gives an overview of the various IRT techniques.

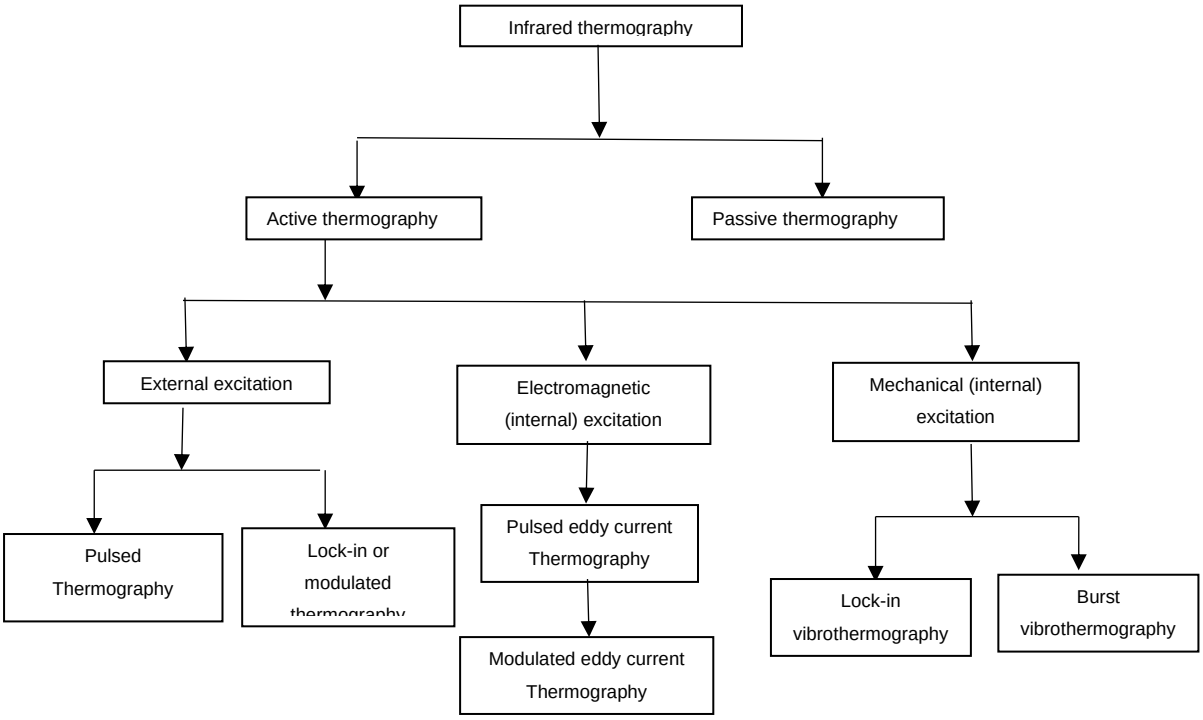


Figure 2.2: Classification of Infrared thermography techniques

Active infrared thermography (AIRT) uses an external heat source that excites the specimen by applying flux to the surface. The temperature gradient is developed in the specimen due to heat conduction. The common types of this technique include pulse thermography, lock-in thermography, long-pulsed (transient) thermography, and vibrothermography.

In pulsed thermography, a body is externally heated with a heat pulse from sources such as a heating gun, halogen lamps or flashes. The thermal images which record temperature data are captured during cooling. Lock-in thermography uses lock-in frequency to pulse sample material, where a thermal diffusion is propagated into the sample material. The surface temperature variation is monitored by the IR camera, which captures the amplitude and phase of local responses provided by pixels using an image processing protocol. The algorithms are embedded in the data analysis software. The long-pulse (transient) thermography uses an external heat source for a relatively long-time increment to aid better heat penetration for thicker materials with low thermal and can be used to evaluate the heating and cooling processes. Vibrothermography is another commonly used technique where mechanical energy due to vibration(friction) is converted to thermal energy, and hot spots are generated and detected in the defective areas.

Passive infrared thermography (PIRT) does not require an external source. The object under investigation should be at a different temperature, and the infrared radiation emitted by the sample material should be captured and analysed. The PIRT is mostly used for the

thermographic investigation of subsurface defects on panels on site and during phase change of water trapped in honeycomb cells (Magoda et al., 2024). It is more effective if the temperature difference between the panel and the environment is relatively big. For instance, the presence of frozen water ingress in the cells of the honeycomb panel.

There are other well-established NDT techniques, such as ultrasonic testing, that are capable of detecting the presence of defects but still, the challenge is to be able to characterise them, particularly with materials that attenuate the ultrasound waves.

The advantages of the IRT technique include the ability to record temperature changes with time, that the setup is portable and non-contact, it is simple to record data, has the ability to inspect/evaluate large areas. It is mostly used to evaluate sandwich panels, carbon/epoxy composites, spot welds, adhesive bonds and delamination in composites. However, this technique also has a few shortcomings, such as a need for specific training to interpret properly the infrared images and the fact that it should be used under a controlled environment (temperature, airflow, and humidity). It requires a special chamber (covered by black cloth) to prevent interference from the environmental radiation during data capturing process.

Genest and Martinez (2009) indicated that pulsed thermography has widely been used for various applications, such as detecting and monitoring debond growth in bonded graphite repairs. Ishikawa et al. (2013) indicated that for a one-dimensional heat transfer, when the heat flux is applied to the top surface of the specimen, the surface temperature variation over time is given by:

$$T(t) = \frac{2Q}{\rho c H} \sum_{n=1}^{\infty} \frac{{\mu_n}^2}{B_i + 2B_i + {\mu_n}^2} e^{-{\mu_n}^2 F_0} \qquad 2.1$$

Where t is the time after heating [s], H is the defect's depth, ρ and c respectively denote the density [kg/m$^3$] and specific heat [J/(kg K)] of the specimen. $B_i$ is the Biot number defined by $B_i = \frac{hH}{k}$, where h is surface heat exchange coefficient [W/(m$^2$ K)] and k is the thermal conductivity [W/(m K)] of the material, and $F_0$ is Fourier number defined by $F_0 = \frac{\alpha t}{H^2}$, in which α represents thermal diffusivity [m$^2$/s], $\mu_n$ is a dimensionless variable, which is determined from Equation 2.2.

$$\tan(\mu) = \frac{2\frac{\mu h}{Hk}}{\left(\frac{\mu}{H}\right)^2 - \left(\frac{h}{k}\right)^2} \qquad 2.2$$

Almond and Pickering (2014) gave experimental insight into the significance of thermographic non-destructive testing (TNDT). The TNDT involves the flash heating of a component under inspection by a high optical intensity flash lamp and the monitoring of the transient surface temperature with an infrared camera. The technique is generally considered suitable for detecting and imaging near-surface, in-plane delamination, such as those found in composite material components, or delamination between coatings and their substrates caused by a failure in adhesion. Inspection of composite components and thermal barrier-coated components has become the main field of industrial application of TNDT.

Maldague and Marinetti (1996) specified the application of the TNDT in composite materials. They indicated that the defect within the material (composites) can be detected by using either flash or long pulse excitation TNDT technique.

The short pulse phase thermography (PPT) uses pulse excitation, which is evaluated in the frequency domain. Fourier transformation of the pixel temperature change is adopted to define thermal waves. The records of variation of phases of these waves (thermal waves) are critical because they penetrate the sample specimen to exhibit failures in the material at different depths.

Wrobel, Pawlak and Muzia (2011) indicated that when conducting an IRT NDT experiment, it was observed that the time dependence of the magnitude of a disturbance over a defect is such that the temperature differences near the defect increases with time, reaches a maximum, and subsequently decreases. This is strictly a function of the thermal diffusivity of the material.

Due to the relatively low thermal diffusivity of the composite materials, a long-pulse thermal excitation approach is recommended and was used in the work of Tewary, et al (2009).

Vollmer et al. (2018) explained that thermography is a measurement technique which is able to quantitatively measure the surface temperatures of objects. To use this technique correctly, the user must know exactly what the camera does and how the useful information from the images can be extracted. It is also indicated that the correctness of the IR images can be

affected by a number of factors, such as radiation from the specimen, the emission from the atmosphere due to its temperature and the presence of warm or hot objects from the surroundings. Table 2.1 indicates several parameters and factors affecting the quality and correctness of the thermograms.

Table 2.1 Parameters and factors affecting images recorded with modern IR Cameras system.

| | |
|---|---|
| Parameters affecting IR images generated from the camera. They can be adjusted using Camera software | • Emissivity of sample material<br>• Distance of Camera and its position (should be perpendicular to the sample material)<br>• Size of specimen<br>• Relative humidity<br>• Surrounding temperature<br>• Interference from nearby objects |
| Parameters affecting data analysis and processing | • Thermograms (IR images) visualization.<br>• IR Image colour patterns and temperature span<br>• Temperature range and level |

### 2.3.1 The insight of Infrared and Thermal Non-destructive Testing protocol

The technique of Infrared thermography consists of three main elements: an infrared camera, a heat flux source, and an image or data processing system. This technique has been widely used for structural monitoring and evaluation. Kylili et al. (2014) reviewed the application of IRT technique for building diagnostics and indicated that the principle of passive IRT is applicable where thermal radiation from the walls is recorded by the Infrared Camera. The wall materials absorb heat from the environment and emit radiation because of temperature difference.

They concluded that while IRT is a useful tool for characterising defects in the building sector, there is a great prospect for developing more advanced, effective and accurate approaches that will employ a combination of thermography approaches or thermography and mathematical modelling.

The latter statement was supported by Vavilov and Burleigh (2015), who indicated that mathematical models can be applied to evaluate parameters of materials and defects when analysing heat transfer in the material. They also suggested that lateral dimensions of sub-

surface defects can be determined directly (or using some simple procedures) by surface temperature footprints of sub-surface defects with accuracy better than 5-10%, and the defect's depth can be evaluated with an accuracy of 20-30%. Furthermore, the determination of the defect's thickness or thermal resistance is characterised with an accuracy of 30-60%.

In practice, there are two groups of methods intended for solving thermal non-destructive testing.

i)Using the inversion formula

ii)Applying an iteration least-square process to match experimental and theoretical data.

A typical IRT NDT set-up is shown in Figure 2.3.

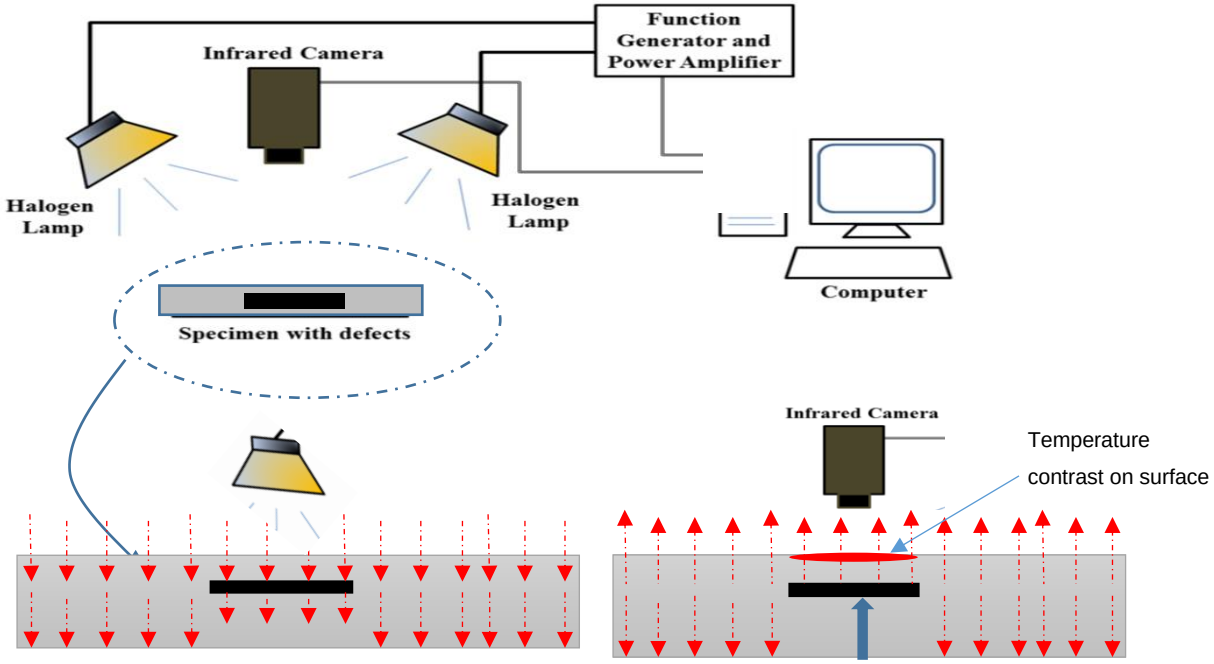


The influence of the void on the thermal process. Externally excited

The influence of radiation on the specimen's surface. Caused by the change in thermal process inside the

Figure 2.3: The setup and scheme of active Infrared thermography technique, adopted for the thermal process (source: Tewary (2009))

## 2.4 Infrared Thermography Inspection of Composite Materials

Composite materials have good mechanical properties and thermal insulation behaviour and are lightweight. For this reason, their application rapidly grows in structures for which these qualities are vital, such as aerospace structures. Typical defects of composite materials are due to the manufacturing process (delaminating and lack of adhesion) or during exploitation

(concentrations, deformations and water ingress). With the development of technology for producing composite materials, the requirements for the assessment of their quality are growing. For this purpose, non-destructive testing (NDT) techniques such as Infrared thermography is used (Maldague,2001). Recently, Wei et al. (2024) employed long pulse thermography (LPT) as the primary method for identifying debonding or delamination defects in composites due to its full-field imaging capabilities and high detection efficiency. The study showed that, when paired with thermal signal processing algorithms, this technique effectively identifies debonding defects in rubber-to-metal bond plates. Furthermore, it was noted that LPT outperforms shearography in quantitatively assessing defect sizes. The relationship between the defective and non-defected areas in the composite material is normally depicted in the log temperature and log time graph as indicated in Figure 2.4.

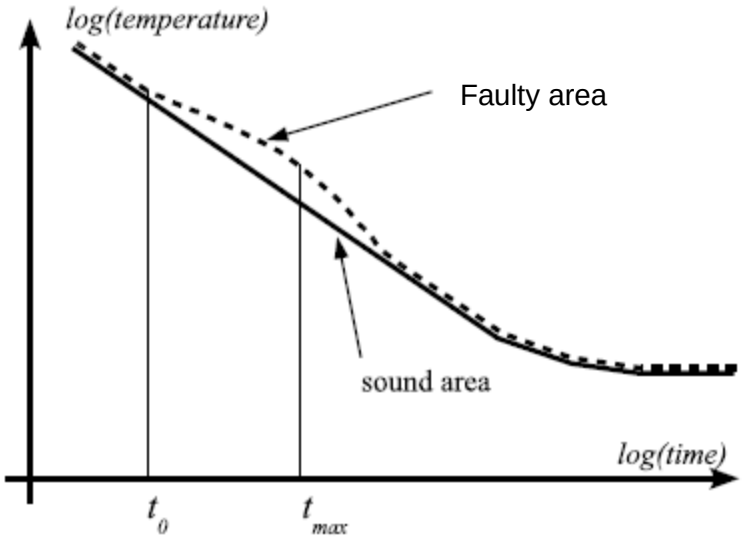


Figure 2.4: Principle of stimulated Infrared thermography (Source: Prakash,2012)

IRT testing is an effective non-destructive technique that is broadly used for inspecting composite materials. The presence of defects such as water ingress in the honeycomb cells may change an effective thermal conductivity of a panel. The thermal radiation emitted by a surface of a panel is recorded by means of an infrared camera to create images that reveal temperature variations, which indicates the presence of defects such as water ingress within the material (Mulaveesala & Tuli, 2008).

In a similar vein, Rani and Mulaveesala (2022) propose novel pulse compression excitation schemes to enhance the effectiveness of infrared (IR) non-destructive testing (NDT) for glass fibre-reinforced polymer (GFRP) materials. The study focuses on improving the sensitivity and resolution of thermal wave imaging techniques used to detect defects or inhomogeneities within GFRP composites. By optimising the pulse compression method, the authors

demonstrate how these advanced excitation schemes can reduce signal distortion and improve the overall accuracy of NDT inspections. Their findings offer valuable insights for enhancing the reliability and efficiency of IR-based NDT methods in composite material evaluation.

The IRT technique can accurately assess any damage within the composite structure provided that the sub-surface defect is within the infrared range which is 2 to 3 mm from the thermal excited surface. IRT is critical to prevent premature failure and extend the service life of the structures. Infrared thermography among others has been used in the evaluation of composite and conventional materials as an effective technique that is quick and precise in detecting of sub-surface defects. In principle, heat excitation on the surface of the structure is allowed to go through the layers of the structure with materials of different conductivities (k) and diffusivities (α). The presence of either delamination or a defect in the layer causes an irreversible degradation of mechanical properties, which will provide a resistance to the heat flow and cause a temperature increase (a hot spot) on the surface due to slow heat transfer around the defect. However, a flat bottom hole provides cold spot on the surface due to the circulation of air underneath the object, which facilitates the natural cooling of the material.

Based on the complexity posed by the presence of layers with different thermal properties, Springer and Tsai (1967) assume a one-dimensional heat flow model through the material to determine the effective thermal conductivity of the composite material. They integrate across a layer of the material and arrive at an expression for effective thermal conductivity. For a cylindrical fibre and a square packing array with heat flow transverse to all fibres, the equation is as follows:

$$\frac{K_T}{K_m} = 1 - 2\sqrt{\frac{V_f}{\pi}} + \frac{1}{\beta}\left[\pi - \frac{4}{\sqrt{1-\frac{\beta^2 V_f}{\pi}}}\tan^{-1}\left(\frac{\sqrt{1-\frac{\beta^2 V_f}{\pi}}}{1+\frac{\sqrt{\beta^2 V_f}}{\pi}}\right)\right] \qquad 2.3$$

$$\beta = 2\left(\frac{K_T}{K_f} - 1\right),$$

where $k_T$ is the thermal conductivity in transverse direction, $k_m$ is the thermal conductivity of the matrix, $k_f$ is the thermal conductivity of the skin (fibre), $V_f$ is the fibre volume fraction.

Equation 2.3 was later simplified by Behrens (1968) which incorporates volume ratio and fibre geometry information but no packing geometry. For circular fibres, the equation is:

$$\frac{K_{eff}}{K_m} = \frac{1+V\left(\frac{\beta-1}{\beta+1}\right)}{1-V\left(\frac{\beta-1}{\beta+1}\right)} \quad 2.4$$

Upon obtaining effective thermal conductivity, the heat transfer in the composite material can easily be determined. It is also possible to analyse heat transfer through layers if the heat conductivities of the individual layer materials are known.

## 2.5 Introduction to Active and Passive Infrared Thermography

### 2.5.1 Active infrared thermography

In this work, two thermographic experimental techniques were used, namely active infrared thermography (AIRT) and passive infrared thermography (PIRT).

The AIRT is a non-destructive and non-contact thermographic technique for water ingress detection and characterisation. During the experimental work of this research, various heating sources such as halogen lamps, flash lamps, and hot air guns were used. This process aimed to identify a better heating technique. Critical heating parameters such as heating time (s), time step (s), total time (s) and pulse time (s) were set in the software controlling the heating source and the infrared camera. The image sequences were recorded at various heating times (s), i.e. 5s,3s,1s. These external heat sources produce heat flux (W/m2) and reach the surface of the specimen. Only the effective heat flux is conducted into the specimen. Water is considered to be a heat-resistive defect with high heat capacity (kJ/kg.K) compared to air in the neighbouring cells and the cell wall (Nomex paper). It is due to this reason that cells filled with water demonstrate a cold environment during heat conduction (negative delta temperatures). It is easier to detect this water, especially when water in cells is in contact with skin.

In this technique, Dirac thermal pulses travel in the specimen at low or high frequency and amplitude. The fluctuation of these thermal pulses depends on the resistance they encounter in the specimen. Pulses with high frequency and short wavelengths detect deeper defects, and those with low frequency and long wavelengths are used to detect shallow defects. When the Dirac pulse is absorbed into a semi-infinite medium, the surface temperature decay conforms to $\Delta T = Q/(e\sqrt{\pi t})$, where $\Delta T$ is the temperature increase of the surface, Q is the quantity of energy absorbed, and $e=\sqrt{K\rho C}$ is the thermal effusivity of the material with K being the thermal conductivity, ρ is the density, and C is the specific heat capacity and t the time (Carslaw and Jaeger,1959).

The Infrared Camera records/ captures the temporal evolution of the specimen surface temperature and pulse history over time, allowing sub-surface defects to be revealed.

According to Maldague (1993), the temperature of the material changes rapidly after the initial thermal perturbation because the thermal front propagates by diffusion under the surface and also because of radiation and convection losses. The presence of a defect reduces the diffusion rate so that when observing the surface temperature, defects appear as areas of different temperatures with respect to surrounding undamaged areas once the thermal front has reached them. As a result, deeper defects will appear later with reduced contrast.

Cielo et al. (1987 and Allport and McHugh (1988) provided a parameter correlation between the observation time (t), thermal diffusivity (α) and the defect's depth (z), whereby

$t \approx z^2/(\propto)$ and $c \approx 1/z^3$

where c is a loss of contrast

Based on the above correlation, the observable defects will be shallow, and the contrasts will be weak. An empirical rule, according to Vavilov and Taylor (1982), says that the smallest detectable defect should be at least one to two times larger than its depth under the surface.

This technique was used to detect and characterise water ingress in honeycomb cells at various orientations when heated on front and rear surfaces.

### 2.5.2 Passive infrared thermography

This study used the PIRTR to detect water ingress in the solid phase (ice) in honeycomb cells. The sample specimens were filled with water and stored in a freezer overnight. No external heating source was used; in a steady state, the specimens were heated by the ambient temperature in the thermographic unit. This phenomenon was done because water and ice have different heat capacities which animates to different s delta temperatures ($\Delta T$), thermal contrast (Cm), Signal to Noise ratio (SNR), and the optimum observation times for both $\Delta T$ and Cm. In fact, this technique relies on capturing thermal emissions from the surface of the material, allowing for the identification of temperature variations that indicate the presence of ice. The ice alters the thermal conductivity and surface temperature of the honeycomb cell, creating discernible thermal patterns. By employing infrared cameras, operators can visualise these patterns and assess the structural integrity of the honeycomb, ensuring early detection of potentially hazardous conditions.

The application of passive thermography in ice detection offers several advantages over traditional methods. It allows for real-time monitoring without direct contact with the material, reducing the risk of damage during inspections. Furthermore, this method can be used in various environmental conditions, making it versatile for different operational settings. By integrating passive thermography with advanced image processing techniques, operators can enhance the accuracy of ice detection, thereby improving safety and reliability in structures where honeycomb cells are utilised. This proactive approach not only aids in maintenance but also extends the lifespan of critical components by addressing ice-related issues before they escalate.

## 2.6 Equipment for Thermal Non-Destructive Testing

TNDT involves the excitation sources, data recording equipment, and image processing algorithms to detect defects, measure material properties, and ensure structural integrity. Normally, the TNDT experimental setup includes the environmental chamber to avoid interference from the environment in order to obtain credible results. The heating source must be chosen carefully to ensure an effective heating process and to prevent any potential areas of non-heating. According to Vavilov et al. (2016), techniques like infrared thermography can be utilised to characterise water ingress in honeycomb panels. Normally, infrared thermography experiments are carried out using the active mode of heating in the lab or a passive mode of heating in the lab or on-site.

### 2.6.1 External Thermal Stimulation Techniques in Infrared Thermography

There are active and passive heating modes in infrared thermography. Active heating involves applying an external heat source to the inspected object to induce a thermal response. Pulsed thermography forms part of active heating, which involves applying a brief, intense heat pulse to the object and observing the subsequent thermal response. The common heating technique involves hot air blowers, which deliver a stream of hot air to raise the object's temperature; heat lamps, using infrared or halogen lamps to heat the surface of the object; and flash lamps, using high-intensity flash lamps to deliver a rapid thermal pulse. on the object’s surface (Vavilov et al., 2016).

As indicated above, there are several applicable thermal excitation sources in the TNDT experiments. These thermal sources provide heat flux on the surface of the sample specimen. The sample surface exchanges some of this heat with the environment and the rest is conducted in the material. Upon encountering heat resistance in the material due to the presence of sub-surface defects, the fluctuation in temperature signals is revealed on the

surface of the sample. The next section outlines some of the common thermal excitation sources.

#### 2.6.1.1 Thermal lamps and hot air blowers

Thermal lamps, such as flashbulb-based lamps or halogen lamps with specific capacity (power) are used to apply localised or controlled thermal loads to test specimens. Similarly, hot air blowers are also used as an active heating source. However, the use of hot air blowers may cause uneven heating on the specimen's surface. Normally, pulsed thermal waves at a specific heating time ($t_h$) and frequency (Hz) are applied to the test specimen, and the temperature signals are monitored and recorded by the infrared camera. The flash lamps and halogen lamps are shown in Figures 2.5 (a), (b), (c), and (d).


(a) (b)

(c) (d)

Figure 2.5: Active IRT heat sources a) Flash lamps b) halogen lamps c) flash lamp d) Hot air blower (Source: Tomsk Polytechnic University, laboratory for thermal testing)

## 2.7 Thermal Measurement and Data Processing Systems

A standard pulsed TNDT procedure generates a series of infrared images that capture the temperature changes over time: T(x,y,t). This sequence can be mathematically represented

as a 3D matrix of temperature: T(i,j,k,t), where i and j denote surface coordinates and k indicates discrete time. In TNDT, data processing algorithms are typically either 1D, focusing on pixel-based temperature changes over time T(t), or 2D, analysing individual images T(x,y). To minimise random noise or to examine the geometrical features of areas of interest, single infrared images are often filtered or segmented. Analysing the time evolution of temperature provides significantly more insights into defect parameters. As a result, most TNDT processing algorithms utilise pixel-based T(t) functions (Vavilov and Burleigh,2015).

Omar and Zhou, (2008) in their work offers a comprehensive analysis of various processing techniques used in flash thermography for non-destructive testing (NDT) applications. The review focused on three prominent flash thermography routines which are thermal signal reconstruction TSR, dynamic thermal tomography DTT, and pulse phase thermography PPT imaging. Through experiments in an analytical domain, it was observed that the PPT is found to be least sensitive to anisotropy variations, while the signal time-delay in TSR is shown to be dependent on defect aspect ratio and not on its depth.

According to the laboratory for thermal testing in TPU (2022), the infrared Camera ThermoCam (Optris PI 450) captures thermal images of the specimen's surface, allowing for the visualisation of temperature distribution and identification of defects. The data recording system is embedded with the image processing software. However, TPU has developed a special data processing software (ThermoFit Pro) with quite a few algorithms.

### 2.7.1 Filters used in the IR images processing and the thermogram analysis.

In this study, pre-processing steps such as noise reduction through Gaussian filtering, which is widely used to minimize noise while preserving critical structural details in thermal images, and calibration for emissivity variations, play a vital role in enhancing image quality, as discussed in section 4.7.1. Similarly, the image processing software employed in this research includes several algorithms. However, the primary focus is on Fourier phase, Principal Component Analysis (PCA), Time gram, Tomogram, Correlogram, and Tomography (negative time gram, upper threshold). The resulting images from these algorithms are compared and analysed. in section 4.7.1. In infrared (IR) image processing and thermogram analysis, filters are key tools used to improve image quality and extract meaningful, reliable data. Specifically, spatial filters are applied in this study to reduce noise, sharpen edges, and enhance water ingress detection within the thermal images (Thermogram).

For thermogram analysis, the above-mentioned image processing algorithms and Signal-to-Noise ratio are utilized to analyse the temperature distribution captured in IR images, aiming to detect water ingress. In this context, filters are employed to isolate thermal patterns of interest, particularly distinguishing between empty cells and those partially or fully filled with water. When combined with other image processing techniques such as thresholding, histogram equalization, and contrast enhancement, filters help to provide a more accurate interpretation of thermographic data, thereby improving the precision of water ingress detection in honeycomb panels.

### 2.7.2 Controlled environment during data recording in Therma Non-Destructive Testing

The accuracy of measurements and data recording in a laboratory environment depends on a few parameters, including emissivity, ambient temperature, and distance from the investigated object that could potentially result in false readings. This is more evident in passive thermography, which is more applicable to recording data on site. However, Emissivity is a common obstacle to IRT. According to Avdelidis and Moropoulou (2003), Non-metallic surfaces that have high emissivity (>0.8) are easily detected by an IR camera and metallic surfaces of low emissivity act as reflectors and do not emit energy efficiently. This makes measuring their temperature very difficult since radiation of nearby surfaces biases the readings. For this reason, the test samples used in this work were covered with high-emissivity black cloth. Furthermore, during the transmittance of energy from the investigated object to the IR thermal imager, some energy may be scattered or absorbed by large atmospheric particles, limiting the measurements. Tomsk Polytechnic University laboratory for thermal testing has a customized environmental chamber made from an aluminium frame covered with black cloth, as indicated in Figure 2.7.


Figure 2.7: Environmental Chamber (Source: Tomsk Polytechnic University, laboratory for thermal testing)

## 2.8 TNDT of Inclined Honeycomb Panels with Water Ingress

This chapter previously indicated that TNDT is a technique used to inspect and evaluate materials and structures for defects or anomalies without causing any damage. This method uses thermal imaging and other thermal measurement techniques to assess the integrity of materials, especially oriented surfaces with specific directional properties (Vavilov et al., 2016).

The inclined surfaces represent samples with water ingress set at an angle. This is a crucial factor since aircraft panels can be oriented in multiple ways—vertically, horizontally, and at various angles. However, initial research by Vavilov et al. (2017) primarily focused on horizontal aviation honeycomb panels. It demonstrated that the angle of inclination has a minimal effect on both heat conduction properties and the detectability of water within the cells.

### 2.8.1 Challenges with Oriented Surfaces

According to Ladd (1999), oriented surfaces, such as those in composite materials or layered structures, present unique challenges when analysing their heat conduction. The thermal properties are direction-dependent, which affects how heat spreads through the material. The other is the Irregularities and complex geometries which can complicate the analysis of thermal responses.

### 2.8.2 Applications of TNDT on Oriented Surfaces

TNDT is used in various fields to inspect oriented surfaces for structural integrity. According to O'Brien (2001), the aircraft design involves surfaces at various orientation aircraft wings and fuselage. Similarly, Silva J.B (2009) indicated that the TNDT can be used to evaluate the condition of bridges and other structures for maintenance needs. These bridges consist of composite slabs oriented at various angles. The other area of application is to assess the quality of composite parts in vehicles (EI-Atab,2004)

TNDT is a versatile and effective method for inspecting oriented surfaces. By applying advanced thermal techniques and overcoming challenges associated with anisotropic materials and complex geometries, TNDT can provide valuable insights into the condition of materials and structures.

## 2.9 Modelling for Thermal Non-Destructive Testing

TNDT is a powerful technique for evaluating the integrity of materials and structures without causing any damage. This testing method relies on thermal principles to detect flaws, assess material properties, and ensure the safety and reliability of various components. To model TNDT effectively, it is essential to understand the underlying principles, methodologies, and applications.

Vavilov and Pawar (2015) presented a novel approach for one-sided thermal nondestructive testing of composites by using infrared thermography. A one-dimensional classical plate sample (model) was introduced and the temperature responses from both surfaces were recorded. In the book authored by Vavilov and Burleigh, 2020, numerical modelling provides accurate solutes as opposed to analytical methods. They also indicated that commercial software packages designed for heat transfer problems are available. However, there are some limitations associated with these packages. For this reason, Tomsk Polytechnic University (Russia) developed the specialized TNDT software to provide a numerical solution for heating a 2D three-layer disk body and a 3D six-layer parallelepiped-like body up to 40 parallelepiped-like defects.

## 2.10 Thermal Non-destructive Testing (TNDT) of Honeycomb Panels with Water Ingress

Thermal Non-Destructive Testing (NDT) of honeycomb panels with water ingress involves complex modelling to assess the integrity and condition of these structures. Honeycomb panels are widely used in aerospace, automotive, and civil engineering applications due to their high strength-to-weight ratio. Water ingress can significantly degrade the structural performance of these panels, making effective NDT methods crucial.

In fact, modelling water ingress in honeycomb panels for thermal NDT requires understanding both the thermal properties of the materials and the effects of defects. However, according to Chen and Lu (2012), Liao and Cline (2013) and Lee and Chang (2014), the finite element analysis (FEA), Analytical models (AM) and finite difference methods (FDM) are Key approaches in estimating thermal responses in 3D heat transfer problems. In the FEA, the panel is divided into discrete elements, and the heat transfer equations are solved numerically. Water can be modeled as a defect with different thermal properties compared to the dry core. The FDM provides discrete solutions, while FEM provides a continuous solution.

According to Magoda et al. (2024), there are several non-destructive testing (NDT) techniques which were suggested by previous researchers to successfully detect water ingress and

assess water content in the cells of aircraft panels. Such techniques include ultrasonic, magnetic resonance (MR), the introduction of argano-ceramicscomposite and the near-field microwave NDT. These techniques are contact and cover a small area of inspection. Therefore, active and passive infrared (IR) thermography has proven to be the most popular and widely used technique to evaluate sub-surface defects, including water ingress. The introduction of advanced infrared cameras, numerical modelling software and image processing software have enhanced the reliability of the obtained data for application in various industries such as aviation.

According to Vavilov (2010), around 1980, there were quite a few researchers such as Balageas, Vavilov and Taylor, MacLaughlin and Mirchandani, Popov and Karpelson and others who extensively developed a thermal-physical approach to TNDT and introduced one-dimensional (1D), two-dimensional (2D) and three-dimensional (3D) models of defects.

Later, in the work of Ishikawa et al. (2013), it was suggested that pulse phase thermography provides an appropriate data acquisition technique, whereby the applied discrete Fourier transformation leads to phase as a function of frequency. Based on the phase-frequency relation, defect depths were examined.

It was further simplified by Vavilov and Burleigh (2015) that pulsed Infrared thermography produces thermograms (IR images) which are the true reflection of the surface temperature variation over time. The heat in the sample material is conducted in three dimensions (x, y, z, t), where z, x, and z are nodal coordinates and t is the time. However, the surface temperature is presented in two dimensions and recorded based on pixel intensity variation with time. The thermograms are normally filtered to eliminate or reduce noise level as part of the image processing protocol. In fact, the IR technique uses pixel-based temperature variation function as part of processing algorithms. One practical concern when using this technique is that only point data is recorded, therefore it is a time-consuming process.

Classification and a short description of these TNDT algorithms are presented in Figure 2.8.

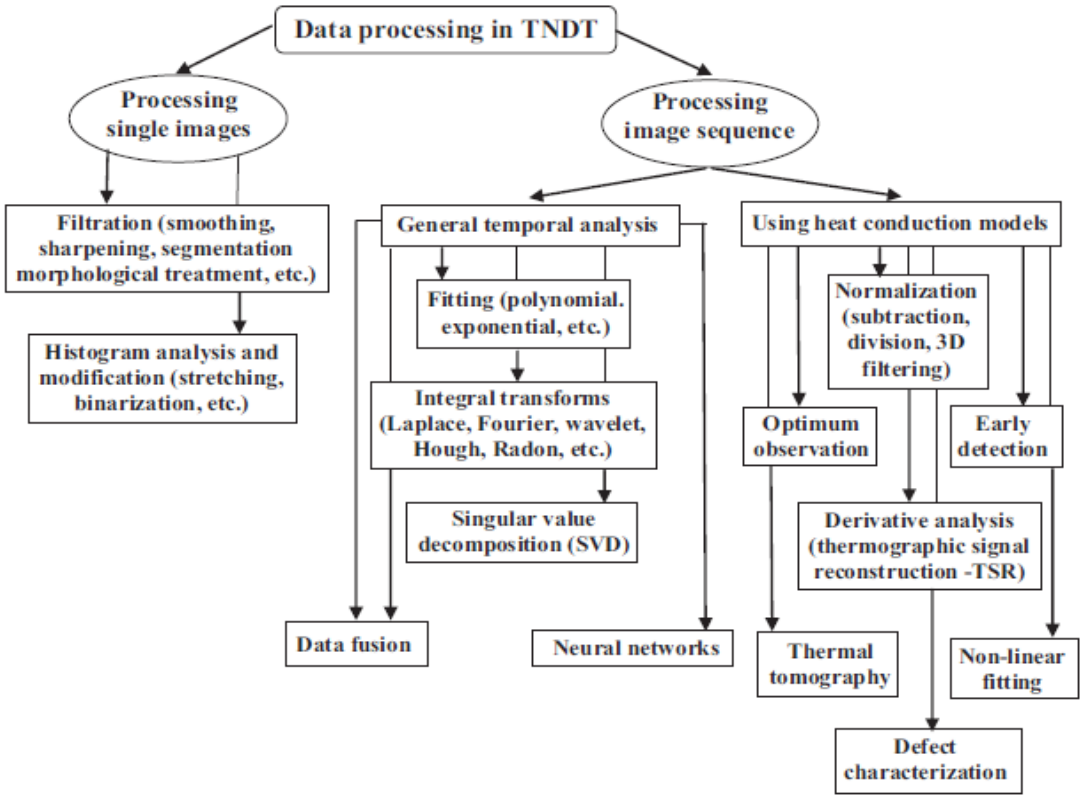


Figure 2.8: Illustrating data processing algorithms in a non-destructive technique (source: Vavilov and Burleigh (2015:43))

### 2.10.1 Noise in Infrared Thermography

Noise refers to unwanted variations in the thermal image data that can obscure or distort the actual thermal signals being measured. It can come from various sources and manifest as random fluctuations or consistent errors in the thermal measurements. There are a few sources of noise during the infrared thermography experiments such as sensor noise, thermal noise, electronic noise, background noise and operational noise. According to the specialised software (ThermoCalc-3D) from TPU, there are two categories of noise: additive noise and multiplicative noise. The noise induces nonuniformities in the image or a sequence of images, which affects the visibility of the sub-surface defects. Therefore, image processing is critical to eliminate the noise effect by removing the background of the image through filtering.

### 2.10.2 Managing and Mitigating Noise in Infrared Thermography

Eliminating noise from the image sequence of thermal infrared thermography is critical to achieve better detectability of sub-surface defects (water ingress). It is recommended that the thermal camera to be calibrated more regularly to ensure accuracy. This includes checking the emissivity settings and conducting routine maintenance to keep the camera in good condition. Ensure stable environmental conditions during testing to minimize ambient

temperature fluctuations and avoid reflective surfaces (Ibarra-Castanedo, Tarpani & Maldague, 2013). In fact, managing noise in Infrared Thermography requires a combination of proper equipment handling, understanding environmental impacts, and employing advanced data analysis techniques.

## 2.11 Conclusion

In this chapter, a brief review of literature is presented as relevant background knowledge for the work that follows in Chapters 3 and 4.

The first section covers the theoretical foundations of composite materials, especially fibre-reinforced composites. The second part of this chapter deals with non-destructive evaluation techniques, in particular infrared thermography (IRT). The application principles of IRT in evaluating the composite materials, as well as the data processing procedures, are presented. It also presents the accuracy of data recording and processing.

The third section presents the numerical method, especially the numerical software (ThermoCalc-3D) and the image processing software (ThermoFit Pro), with a focus on the 3D model with water ingress at various levels and orientations.

Finally, the principles of experimental validation of the numerical solutions, formulated for the purpose of characterising the water ingress in honeycomb composites, will be employed in this work.

# CHAPTER 3:
# NUMERICAL MODELLING

## 3.1 Introduction

This chapter is devoted to the three-dimensional heat conduction mathematical modelling of honeycomb structures with cells partially or fully filled with water. A honeycomb is a porous structure consisting of cells with a hexagonal prismatic configuration. The modelling of a honeycomb structure is a challenging task due to its structural complexity. Honeycomb cells filled with water at different levels, as well as cells containing air, are modeled using ThermoCalc-3D software, with image processing algorithms applied to enhance visibility. The models are at a horizontal, vertical, and inclined orientation. The ThermoCalc-3D is the thermal modelling software (designed at Tomsk Polytechnic University) which can solve a three-dimensional heat conduction problem of heating a 36-layer solid body containing up to 40 parallelepiped-like defects. It implements the finite difference method, which provides better accuracy than the Finite Element method when solving Thermal NDT problems. Therefore, the primary objective of this chapter is to predict water ingress levels (depth of defect), perform 3D normalisation, investigate the effect of radiation and convection heat transfer in detecting cells with water and provide a parameter correlation to estimate water content (mass) in honeycomb cells when the model is placed in a different orientation. A critical concept of signal-to-noise ratio (SNR) and the optimum observation time is used to accurately detect water ingress in cells. In addition, the analysis of surface thermal contrast and delta temperature variation over time of the model orientated at various angles is presented.

## 3.2 General TNDT Models to Analyse Sub-Surface Defects in Composite Panels

Most proposed 3D models are for composite materials with induced sub-surface defects, such as flat bottom holes. However, a similar approach is adopted to characterise water ingress (defects) in honeycomb panels. Several researchers have proposed and developed models in 1D and 3D for composites with flat bottom defects. For instance, Maillet et al. (2000) proposed a solution for a 3D Transient Non-destructive Testing problem of heating a composite material with flat bottom holes (defects). A similar solution was later introduced by Vavilov (2022) for the active TNDT problems with enclosed subsurface defects. The solution was obtained by applying the Fourier transform to two lateral spatial coordinates and the Laplace transform to time. In general, the TNDT model of the anisotropic non-adiabatic panel with subsurface defects is based on heat diffusion mathematical formulation, which is a parabolic differential equation of heat conduction as follows.

$$\frac{\partial T_i(x,y,z,t)}{\partial t} = \alpha_x \frac{\partial^2 T_i(x,y,z,t)}{\partial x^2} + \alpha_y \frac{\partial^2 T_i(x,y,z,t)}{\partial y^2} + \alpha_z \frac{\partial^2 T_i(x,y,z,t)}{\partial z^2}; i = 1 \dots (layers + defects); \quad 3.1$$

i) Initial conditions

$$T_i(t=0) = T_{in} \quad 3.2$$

ii) Boundary condition (top surface)

$$-k_1^z \frac{\partial T_i(x,y,z=0,t)}{\partial z} = Q(x,y,t) - h_F[T_1(x,y,z,t) - T_a] \quad \text{heating and cooling} \quad 3.3$$

iii) Boundary condition (bottom surface) in case of a 3 layered composite (skin, core, skin)

$$-k_3^z \frac{\partial T_i(x,y,z=0,t)}{\partial z} = -h_R[T_3(x,y,z,t) - T_a] \quad \text{cooling only} \quad 3.4$$

iv) Specific temperature boundary conditions on the side surfaces

$$\frac{\partial T_i(x,y,z,t=0)}{\partial x} = T_a \; at \; x = 0, y \ldots L_y ; \quad x = L_x, \; y..L_y; \quad 3.5$$

$$\frac{\partial T_i(x,y,z,t=0)}{\partial y} = T_a \; at \; y = 0, x = 0 \ldots L_x ; \quad y = L_y, \; x \ldots L_x; \quad 3.6$$

v) At the defect boundaries

$$T_i(x,y,z,t) = T_{i\pm1}(x,y,z,t) \; and \; k_i^{qj} \frac{\partial T_i(x,y,z,t)}{\partial t} = k_{i\pm1}^{qj} \frac{\partial T_{i\pm1}(x,y,z,t)}{\partial q_j} \quad 3.7$$

Where $\alpha_x, \alpha_y, and \; \alpha_z$ are thermal diffusivities of the material along coordinates x, y, and z. $T_i$ . $T_a$ are the material initial and ambient temperatures. $k_i^{qj}, \alpha_i^{qj}$ are the thermal conductivity and thermal diffusivity in the i-th area (material's layers and sub-surface defects) along $q_j, x, y, z$.which are the cartesian coordinates. $(i = 1-3)$corresponds to sample layers and $(i = 4 - M + M)$ corresponds to M defects).The $h_F$ and $h_R$ are the coefficients of heat exchange on the front and rear surfaces respectively. $L_x L_y, and \; L_z$ are the lateral dimensions of a sample. Equation 3.7 represents the continuity of temperatures and heat fluxes at defect boundaries.

It should be noted that in modelling anisotropic solids, it is assumed that only thermal conductivity is anisotropic, and both specific heat (heat capacity) C and ρ are constant by all coordinates. The concept is illustrated in Figure 3.1.

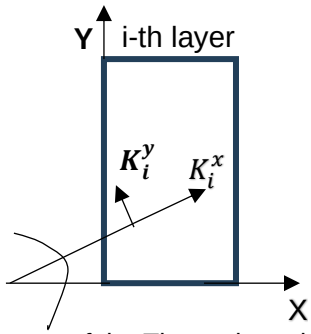

Figure 3.1: Components of the Thermal conductivity (TPU,2018)

The flat bottom holes have widely been used in classical mathematical models as defects. However, internal defects such as delamination have also been used to represent the practical or possible actual defects found in composite panels.

There are several critical parameters to be considered when modelling sub-surface defects. In fact, the thermal and physical properties of the host material and the defects are important.

The temperature contrast over defects depends on the thermal conductivity and diffusivity of the defects. The heat conduction phenomena around the defect are critical to characterising it accurately. The heat capacity and the thermal resistance ($R_d$) are the specific parameters used in the model's defect characterisation. In the case of water ingress, the "negative" temperature contrast is expected due to water's higher thermal diffusion than that of host material. The detectability of water ingress is also influenced by the contact between water and the skin surface.

In general, computer simulations such as ThermoCalc-3D, COMSOL, ANSYS, ABAQUS, and MATLAB have been used to characterise sub-surface defects. These software can be combined to increase the results' accuracy rate. For instance, temperature data can be exported from COMSOL to perform apparent effusivity reconstruction with the algorithm implemented in MATLAB. However, ThermoCalc-3D has been tailored to solve 3D heat conduction problems (models) with many layers and defects. It is user-friendly with high accuracy.

### 3.3 Approaches to Modelling Composite Materials

In Chapter 2, the discovery of the existence of the defect within composite materials has been presented. However, determining the depth of these defects is an area of further investigation; hence, the purpose of this work. Chrysafi et al. (2017) used spatial mathematical methods to determine the presence of defects in composite materials. These methods include the depiction of the norm of the first and second spatial derivative of temperature, the Discrete Fourier transform, and the Wavelet transform on the overall heat domain.

The interest of this work focuses on the depiction of the norm of spatial derivatives of the thermal field for 3D image processing because it uses the finite difference method presented as follows:

$$D_3T(x,y,z,t) = \sqrt{\left(\frac{\partial^2 T}{\partial^2 x}\right)^2 + \left(\frac{\partial^2 T}{\partial^2 y}\right)^2 + \left(\frac{\partial^2 T}{\partial^2 z}\right)^2} \tag{3.8}$$

Based on Equation 3.1, the spatial derivative of the temperature changes abruptly around the defect, and to identify this change at the specific region, the depiction of the temperature derivative norm distribution is presented by the equation at various instants. The finite difference method (central difference) expression for the spatial derivatives of temperature is deployed and gives as follows:

$$D_3T_{i,j,k}^n = \sqrt{\left[\frac{T_{i-1,j,k}^n - 2T_{i,j,k}^n + T_{i+1,j,k}^n}{(\Delta x)^2}\right]^2 + \left[\frac{T_{i,j-1,k}^n - 2T_{i,j,k}^n + T_{i,j+1,k}^n}{(\Delta y)^2}\right]^2 + \left[\frac{T_{i,j,k-1}^n - 2T_{i,j,k}^n + T_{i,j,k+1}^n}{(\Delta z)^2}\right]^2} \tag{3.9}$$

The solutions of this model were obtained because of the steps shown in Figure 3.2. As indicated, the development of the model is an iterative process of postulates formulation, validation and refinement. This model is fashioned using information from three major areas: the material's properties, the process of heat transfer, and the finite difference mathematical technique.

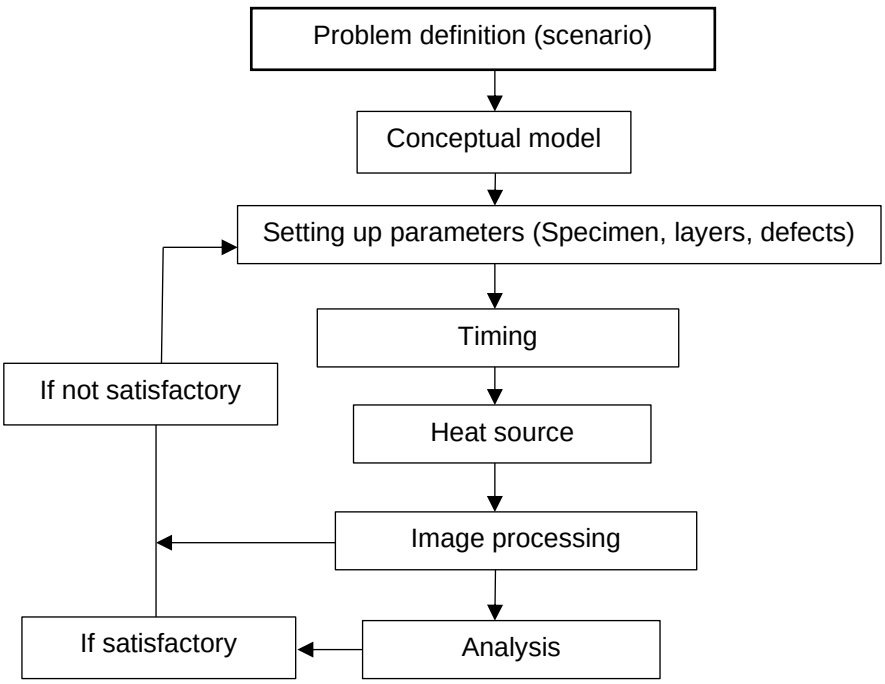


Figure 3.2: Different steps in model development

## 3.4 Thermal Non-destructive Testing Models for Water Ingress in Honeycomb Panels

Analytical methods and (TNDT) models have been used to detect and characterise the hidden defects (water ingress) in honeycomb panels but do not provide accurate solutions, especially in the case of the water content in the cells of honeycomb panels. Numerical methods are more reliable for regular-shaped defect characterisation. Two numerical methods are used for solving heat diffusion in composite materials: the finite element method and the finite difference method.

Vavilov et al. (2017) analysed the 3D model of a honeycomb panel where water can fully or partially occupy cells. The mathematical formulation of the model is executed in the ThermoCalc-3D software.

The model consists of a honeycomb with square cells (10 mm high) made of Nomex paper and the panel skin (0.5 mm thick) made of glass or carbon fibre-reinforced plastic. It was found that the most important relationships between sample parameters and temperature signals can be obtained by analysing a simple 1D model of heat conduction in a three-layer plate. Still, the analysis of some more elusive phenomena requires 3D numerical modelling. It was observed that it is difficult to quantitatively evaluate water content in the cells unless the inspection is performed on both panel surfaces and a ratio of respective temperature signals $\Delta T_{front}/\Delta T_{rear}$ or contrasts $C_{front}/C_{rear}$ for water mass calibration.

In fact, there are two parameters that are critical in thermal NDT. The differential temperature signals $\Delta T = T_d - T_{nd}$ and the running contrast $C=\Delta T/T_{nd}$, along with their observation times t ($\Delta T$) and t (C). The $T_d$ and $T_{nd}$ are the temperatures on the defected and non-defected areas. it was also noted that in the theory of thermal NDT, a defect detection limit is provided by the noise contrast $C_{n,}$ which is a characteristic of a material and surface conditions.

## 3.5 Critical Output Parameters

The parameters such as the surface temperature, contrast, and observation time which are obtained from the temperature images of the model are critical to effectively characterise water

ingress in honeycomb panels. However, understanding the other physical and thermal properties of the material is critical. For instance, how quickly the panel absorbs water (in mass or volume), the rate of water ingress, time to saturation, and the height to which water rises in the honeycomb cells, which is influenced by the geometry and size of the cells. The critical thermal properties of the model material include thermal conductivity (k), and thermal diffusivity (α). These parameters provide a comprehensive understanding of water ingress behaviour in honeycomb panels.

### 3.5.1 The Differential Temperature Signals (∆T)

Water ingress in honeycomb structure compromises the integrity of the structure and its detection is necessary. However, in water ingress models, differential temperature signals can provide valuable insights into moisture behaviour within honeycomb panels. Monitoring temperature differences can help identify areas of increased moisture, as water has a higher specific heat capacity than air.

Temperature gradients can indicate how heat moves through the panel. Water ingress can slow down heat transfer, leading to observable temperature differences in thermographic measurements. By analysing differential temperature readings over time, the moisture migration paths can be traced. Areas with higher moisture levels will exhibit different thermal responses compared to drier sections.

Most importantly, by establishing baseline temperature differentials in undamaged panels and monitoring for changes over time, predictive maintenance strategies based on identified thresholds can be implemented.

### 3.5.2 Lateral size of water cell

The water ingress model of a honeycomb structure consists of layers and defects. The water cells are separated by fixed boundaries known as defects. Water which penetrates the cell will occupy the cell's space. It was shown in the work of Magoda et al. (2024) that an increase in water in the x and y directions has little or no impact on differential surface temperature or contrast. However, water ingress in lateral size is also described as the shape of a defect which is visible to the operator's eye. Vavilov (2022) summarised the specific proposed processing techniques for the estimation of the 2D geometrical sizes ($d_x$ and $d_y$) of the defects. Such techniques include the Full Width Half Maximum (FWHM) technique, analysis of temperature spatial derivatives and a non-linear fitting technique. Each technique has its specific application to achieve estimation at minimum errors. For instance, the FWHM is

suitable for noisy temperature profiles but at times, may lead to both under and overestimation of defect size. In the case of the derivative technique, it is suitable and well related to heat conduction around defects, which indicates that the maximum lateral heat fluxes occur at defect borders but are subject to temperature fluctuations.

It was also mentioned that the defect's true size and shape can be underlined by using simple algorithms of gradient filtering and binarization.

### 3.5.3 The Depth of Defect (Water Level)

The non-linear fitting technique is proposed as the preferred processing technique to determine defect depth and thermal resistance but is not accurate for smaller and deeper defects producing lower temperature signals.

Based on the principle that when the heat flux is applied on the surface, the sub-surface defects affect thermal diffusion and produce a corresponding thermal contrast on the surface directly over defect/void, the analysis of either thermal contrasts on the surface or excess surface temperature of the material is important. Manchor and Di Scalea (2014) modelled a 3D heat flow in composite materials with flat bottom holes (defects). They assumed that the thermal conductivity of the material in the x and y directions are the same and different in the z direction. The model was reduced from anisotropic heat conduction problem to the isotropic problem. The excess surface temperature equation was developed.

$$T_e = \frac{ab\delta}{h_1 h_2 d} T_0 \left(1 + \sum_{n=1}^{\infty} \frac{2h_1}{n\pi a} sin\left(\frac{n\pi a}{h_1}\right) e^{-t\alpha(n\pi/h_1)^2}\right) \times \left(1 + \sum_{m=1}^{\infty} \frac{2h_2}{m\pi b} sin\left(\frac{m\pi b}{h_2}\right) e^{-t\alpha(m\pi/h_2)^2}\right) \times \left(1 + \sum_{k=1}^{\infty} 2(-1)^k e^{-t\alpha(k\pi/d)^2}\right) \quad (3.10)$$

The most common experimental techniques are the use of early detection times, apparent effussivity method (Dirac Pulse Heating), Contrast difference, and the surface temperature difference. The term early detection is when the evolving ΔT(τ) signal starts to exceed noise. At this time, the signal-to-noise ratio is lower than at optimum observation time, but defect shape is better reproduced due to weaker lateral heat diffusion. Besides, defect thermal resistance (defect thickness) scarcely influences surface temperature in defect areas at earlier times. Therefore, the early detection technique can be used for determining defect depth l independently of defect thickness. In fact, according to Vavilov and Burleigh, there are four techniques normally used for the depth detection of the sub-surface defects and the thermal resistance: the apparent effusivity, early detection (characteristic time form peak contrast), artificial neural networks, the instant of maximum thermal contrast ($T_{c\text{-}max}$), and the excess surface temperature. The apparent effusivity method uses two dimensionless parameters to

obtain the excess surface temperature of the sample to describe the effusivity (e), the Biot number ($B_i$) and the Fourier number ($F_O$). These dimensionless parameters are presented as

$$Bi_d = l/(\lambda R_d) \tag{3.11}$$

$$Fo_d = \alpha\tau/l^2 \tag{3.12}$$

Where *l* is the depth of the defect from the surface of the sample, $R_d$ is the size (radius) of the defect, $\alpha$ is the material's thermal diffusivity and $\tau$ is the heating time increment.

This method was adopted by Manchor and Di Scalea (2014), who found that the excess surface temperature ($T_e = T_{def} - T_{undef}$) is proportional to the size and depth of defects.

In a similar vein, when using an instant of maximum thermal contrast method, Fang and Maldague (2020) found that the maximum or peak thermal contrast is proportional to the square of the defect's depth.

$$T_{c-max} = \alpha Z^2 \tag{3.13}$$

Where Z is the defect's depth and $\alpha$ is the thermal diffusivity of the material.

Man-made defects will be produced on selected specimens, and their effect on thermal diffusion based on their depths will be analysed.

### 3.6 Description of the Model

This model consists of honeycomb Nomex with fibre glass reinforced plastics skin. This type of composite panel is common in the construction of fuselage. When the aircraft is under use, water ingress (atmospheric water) penetrates the fuselage and settles in the honeycomb cells. Due to low temperatures at high altitudes, the water in the cells freezes and may cause either temporary or permanent damage to the panel. Therefore, it is critical to model the panel with water content. This model focuses on the detection of water ingress at different levels and orientation. The impact of different heating methods on the visibility of water ingress using a signal-to-noise ratio (SNR) concept is analysed. The appropriate technique or procedure for water mass determination is suggested. The models in Fig. 3.3 have been analysed numerically using the ThermoCalc-3D software.

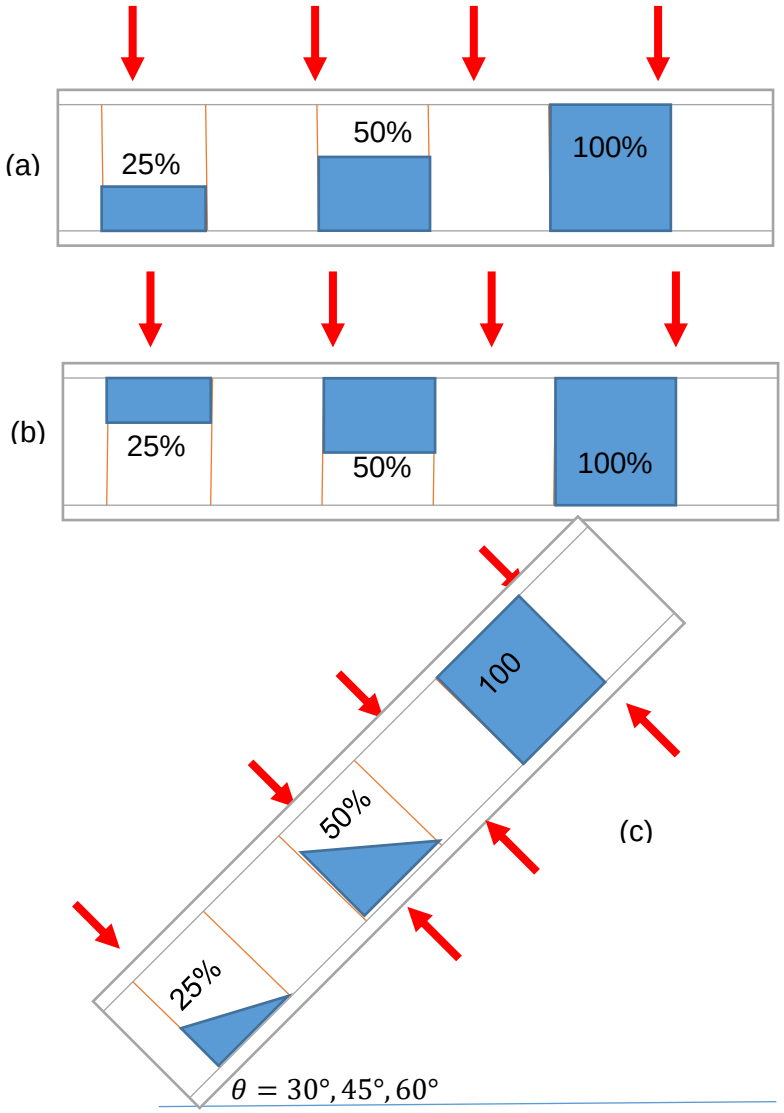


Figure 3.3: 3D numerical models (ThermoCalc 3D-software) of water ingress test cases: a) horizontal heating from top b) horizontal heating from bottom, c) water in inclined position

### 3.6.1 Description of the material used during modelling

The parameters of the model in all scenarios were: 0.5 mm-thick fibreglass skin, Nomex paper made cells, cell is 10x10x10 mm, heating power 50kW/m$^2$, heating time step 0.1s, heating time 0.5s, and total process time 20 s. The additive noise of 3% and additive noise standard deviation of 10%, and the multiplicative noise of 1%-5% were introduced to the vertical and inclined scenarios. The non-uniform heating was also applied to the latter scenarios. The examples of the evolutions of delta temperature (ΔT) and contrast (C) in time are presented in fig.3 indicating all scenarios (horizontal v=100%, 50%, vertical (v=50%), inclined (v=50%), and non-uniform heating).In all scenarios, defect and non-defect points for horizontal panels are chosen over the centres of water-filled and ‘dry’ cells respectively as indicated in fig.1 (a). However, the defect points for inclined and vertical are chosen over the centroids and the

centre of water filled respectively as shown in Figure. 1(d), and (e). The maximum values of these parameters and their observation times calculated for several test scenarios are presented in Table 3.3.

Material thermal properties such as thermal conductivity, density and specific heat capacity used during modelling were of fibreglass skin composite panels with the Nomex honeycomb. The specific material properties and dimensions are illustrated in Table 3.1.

Table 3.1 Material thermal properties

| **Material** | **Thermal conductivity (W/m. K)** | **Density (kg/m^3)** | **Heat flux ($W/m^2$)** | **Specific heat capacity (J/kg. K)** | **Thermal diffusivity $\alpha$, $m^2/s$** | **Thermal effusivity $e$, $Wm^{0.5}/(m^2\ ^0C)$** |
|---|---|---|---|---|---|---|
| **Glass fibre reinforced Plastic (GFRP)** | 1.1 | 1300 | | 1775 | $1.30x10^{-7}$ | 832 |
| **Water** | 0.61 | 1000 | 50000 | 1005 | $1.41x10^{-7}$ | 1573 |
| **Honeycomb (Nomex)** | 0.17 | 128 | | 830 | $1.82x10^{-7}$ | 769 |
| **Air** | 0.07 | 27.3 | | 928 | $5.8x10^{-5}$ | 9.192 |

This is a three-dimensional heat conduction model analysed using ThermoCalc-3D (Tomsk Polytechnic University, Russia) software. The ThermoCalc-3D implements an implicit finite difference scheme in which the numerical grid inside defect areas is created automatically by considering both the specified defect thickness and spatial step.

Figure 3.4 presents the model created in ThermoCalc-3D software with cells filled with water at 25%, 50% and 100%.

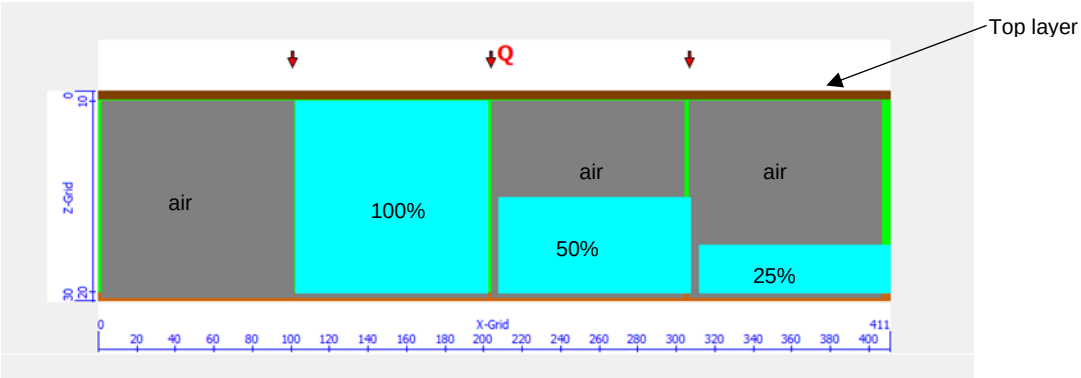


Figure 3.4: ThermoCalc-3D model

After the application of a uniform heat flux of 50kW/m$^2$ as depicted in Figure 3.4, the space, time and delta-T profiles were drawn in Figures 3.5 (a), (b), (c), (d), and (e) to demonstrate the effect of water content to the temperature variation over each cell.

### 3.6.2 Heating of the model

At first, the model will be heated using a periodic square pulse with the inputs time step (1s), heating time (5s), total time (20s), and pulse time (5s). The surfaces are subjected to convection +Radiation heat transfer. The same procedure is repeated using arbitrary heating, and thermal waves (hot air). The exponential heating source with a maximum heat pulse density of 10kW/m$^2$ is used. The coefficients of the spatial distribution of heat pulse in x and y

This software allows the modelling of uneven heating or cooling by specifying a Gaussian heat source, as indicated in Figure 3.5.

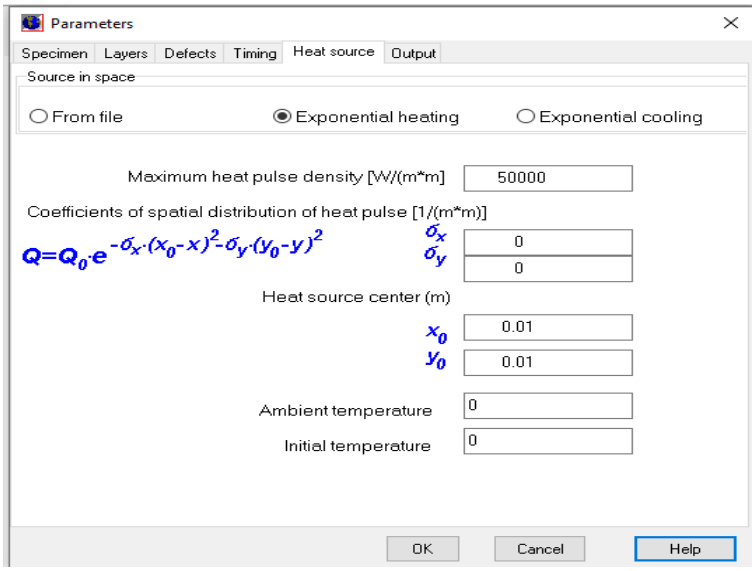


Figure 3.5. Gaussian heat source (uniform heating)

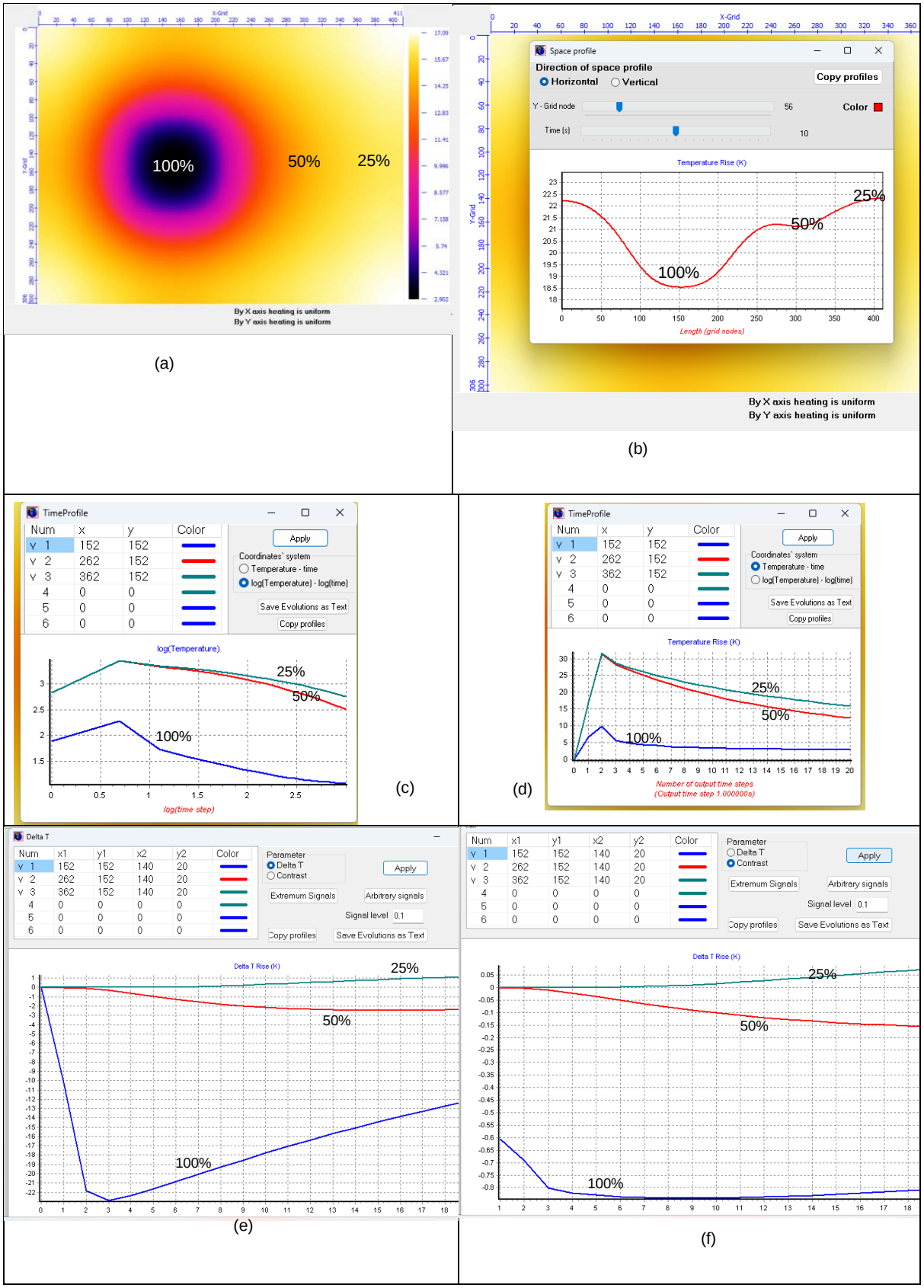


Figure 3.6: ThermoCalc-3D results (a) temperature image, (b) space profile, (c) time profile -Logtemperature-logtime, (d)time profile-temperature-time, (e) DeltaT -

The ThermoCalc-3D has specific surface heat exchange conditions for front and rear surfaces, as indicated in equations 3.3 and 3.4, respectively. The following conditions are applicable for the front heating on the model. A model is heated by a heat pulse $Q(x,y,t) = 50kW$ that operates during the time ($t_h = 5s$) and the heat pulse is square. This model is treated as adiabatic on the sides (h=0). However, the combined heat transfer exchange ( $\alpha_r + \alpha_{conv}$) are considered during modeling. The heating is uniform with an exponential heating option and the parameters of the Gaussian function ($\sigma_{xy}$) are set zero to model as indicated in figure 3.6. The introduction of noisy levels on the model presents a practical analysis when comparing to the experimental results. The most common noises are additive and multiplicative which are random and specified in the custom under output option by choosing X, Y, Z coordinates of outputting surface. Figure 3.7 depicts the introduction of noise onto the model.

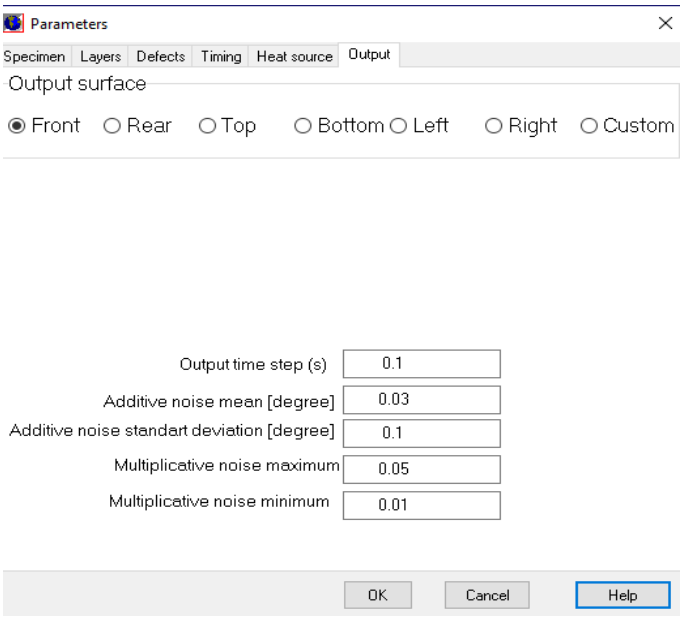


Figure 3.7: Additive and Multiplicative noise

The image processing algorithms form part of theThermoCalc-3D software. Although a separate software (ThermoFit Pro) is specialized in processing the temperature images for better visibility by eliminating noise and other unwanted background intrusions. For demonstration processes, the above model was induced with noise and two different image processing were applied. The results are shown in Figures 3.8 (a), (b), and (c).

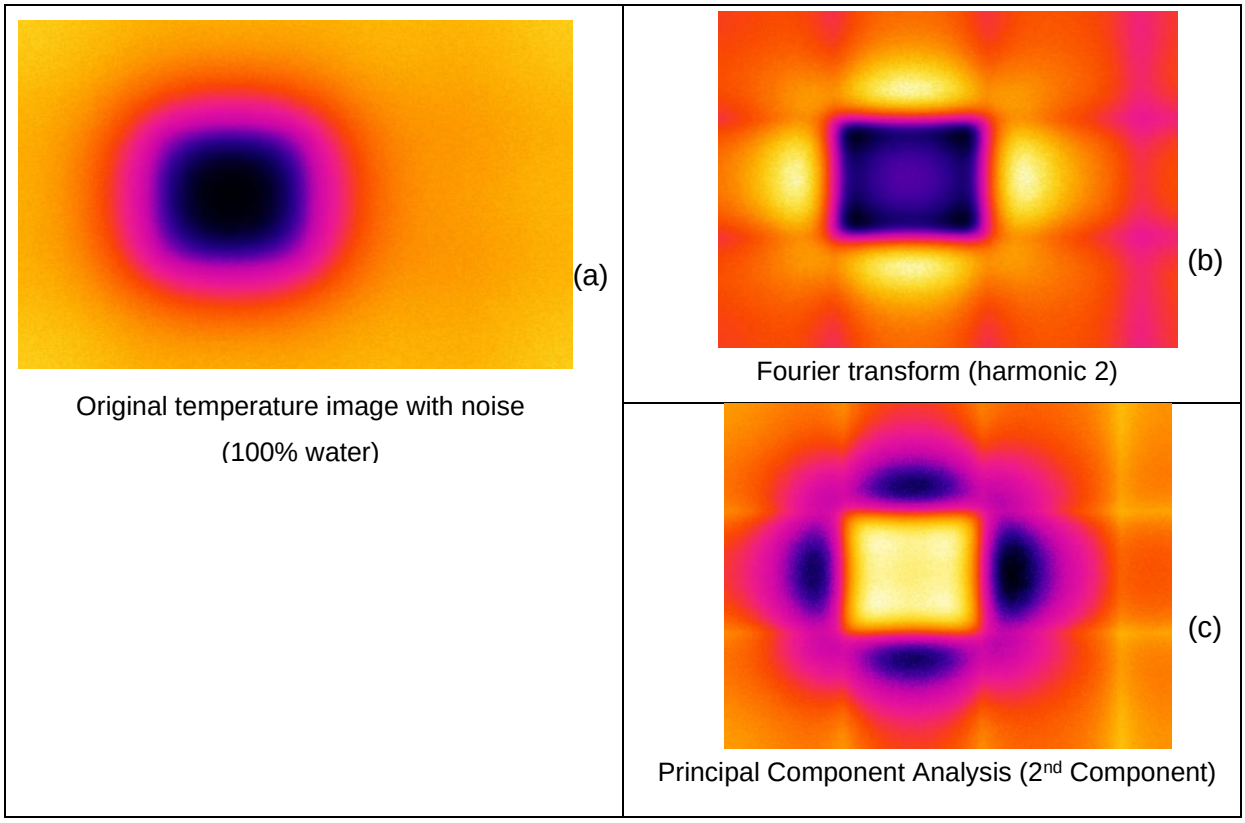


Figure 3.8: Sample of image processing (a) original temperature image, (b) Fourier transform, (c) PCA

Based on the above images, the cell with 100 % water is better seen when the Fourier transform algorithm is applied. It should also be noted that water in the cell should be in contact with top layer where the heat flux is applied on. It can be observed that an air gap between the layer and the water, in the case of 50% or 25%, causes limited or no visibility of water in the cells. As indicated in the previous work by Vavilov et al. (2020) that water should be in contact with skin (layer) for better detection.

### 3.7 Details on Numerical Image Processing (ThermoFit software)

The image processing is an integral part of data analysis in Infrared thermography to achieve a better defect's characterisation and visibility. It is achieved by applying image processing algorithms to reduce pixel's noise levels. According to Herby (1998), at the pixel level, the noise is additive, of Gaussian nature and of high frequency with respect to the useful signals. Several techniques are used to characterise the noise content present in infrared images. Such techniques include the use of image processing algorithms installed in software such as ThermoFit ™ Pro. The most useful parameter when performing image processing is to compute the signal-to-noise ratio (SNR), which is determined using equations 1.1 and 1.2

In light of the above introduction, the section below details the image processing techniques and algorithms used in this research work. The numerical modelling software (ThermoCalc-3D Pro) has incorporated two image processing algorithms (Fourier transformation, and the principal component analysis-PCA). Figure 3.9 shows the key features of the software.

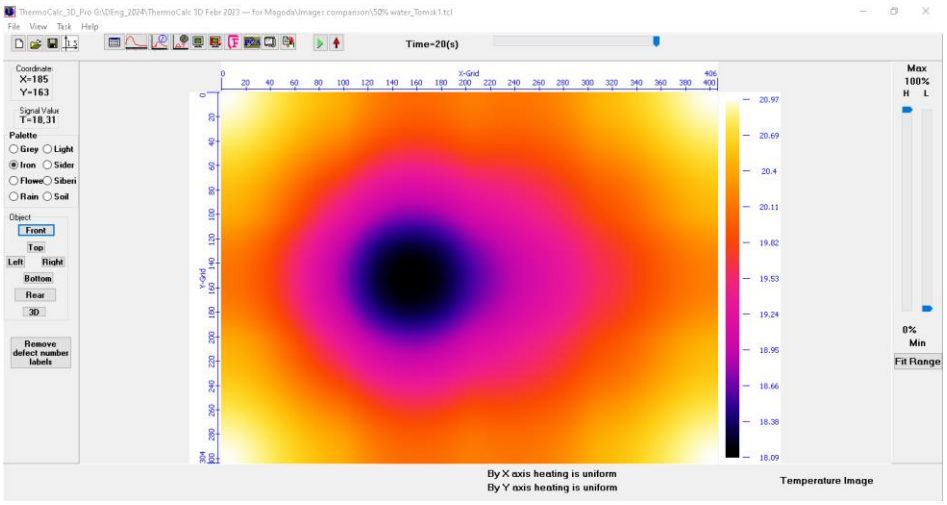


Figure 3.9: Fourier transform and PCA embedded in ThermoCalc-3D Software

This work uses the ThermoFit TM Pro (Tomsk Polytech University, Russia) for image processing. It processes images recorded from the infrared (IR) camera due to pulsed TNDT. The Program allows for enhancing defect visibility, evaluating material loss, determining material thermal properties, and processing IR images statistically using processing algorithms such as Background, Normalization, Fitting, Fourier transform, Derivative, Maxigram and Tomography, Statistics, 1D and 3D Defect characterisation, Corrosion, Material properties, Correction Point distance, Principal Component Analysis (PCA), and Wavelet Analysis. Most of these algorithms are suited for solid homogenous materials. However, in this research, the analysis is done on the honeycomb material filled with water. This non-homogenous material consists of air, water, epoxy, fibreglass, and Nomex paper. For this reason, Fitting, Fourier transform, and Principal Component Analysis (PCA) are the preferred algorithms for this study.

### 3.7.1 Polynomial fitting

This is one of the popular and most effective technique of image processing in which the logarithm reduces a sequence of arbitrary length to few images of polynomial coefficients. The stored image sequence is free of high frequency noise which enable such mathematical algorithms as differentiation. There are three fitting algorithms available/installed in this program.

The first fitting function (Fit 1) follows the classical solution for heating a semi-infinite adiabatic body with a square pulse and is applied to decaying temperature signals. In the case of a water defect, a cooling phase is more important than a heating one because of a vast difference in heat capacity and diffusivity of air and water.

$$T(t) = A_0 + A_1\theta + A_2\theta^2 + A_3\theta^3 + A_4\theta^4 + A_5\theta^5; \quad (3.14)$$

$$\theta = \sqrt{\frac{t}{t_h}} - \sqrt{\frac{t}{t_h} - 1}; t \geq t_h \quad (3.15)$$

This option is limited to the following conditions

$\text{The time step } (\Delta t) > 0\ ;\ \text{heating time } (t_h)\ > 0; \text{Time corresponds to k} - \text{th image } (t_k) \geq t_h,$
$k \geq 2$

Where $A_0,\ A_1,\ A_2,\ A_3,\ A_4, and\ A_5$ are polynomial coefficients

The *second fitting function (Fit 2)* is general and independent on the physics of the analysed process. It is applied for arbitrary temperature signals.

$$T(t) = A_0 + A_1 t + A_2 t^2 + A_3 t^3 + A_4 t^4 + A_5 t^5 \quad (3.16)$$

This option is limited to the following conditions$\text{The time step } (\Delta t) > 0\ ;\ \text{Time corresponds to k} - \text{th image } (t_k) \geq 0,\ \ k \geq 2$

The *third fitting function (Fit 3)* follows the classical solution for heating a semi-infinite adiabatic body with a Dirac (flash) pulse. It is applied to decaying temperature signals

$$Ln[T(t)] = A_0 + A_1\Theta + A_2\Theta^2 + A_3\Theta^3 + A_4\Theta^4 + A_5\Theta^5 \quad (3.17)$$

$$\theta = \sqrt{\frac{t}{t_h}} - \sqrt{\frac{t}{t_h} - 1}; t \geq t_h$$

This option is limited to the following conditions

$\text{The time step } (\Delta t) > 0\ ;\ \text{Time corresponds to k} - \text{th image } (t_k) \geq 0,\ \ k \geq 2$

### 3.7.2 Fourier transform (FT)

The FT is a fundamental tool in image processing. It extends the Fourier transform to signals, breaking them down into a sum of complex oscillations, or more precisely, complex exponentials. In the context of image processing, the Fourier transform decomposes an image into oscillations that vary in frequency, phase, and orientation. It's important to note that these oscillations are not complex exponentials when the pixel values are real numbers.

In essence, the Fourier transform reveals the frequency content of an image, showing how the intensity values are distributed across different frequencies.

FT normally performs a 1D or 2D Fourier transform through a sequence in time. It is a pixel-based temporal evolutions of temperature signal to produce images of both magnitude and phase at different Fourier frequencies. Normally, images of phase are preferred compared to images of magnitude. It is because phasegrams can underline the subtlest differences between the temperatures in a defect and non-effected area. Low frequency Fourier images reveal better results. In fact, the interpretation of Fourier images is done qualitatively. The Fourier transform is applied to a whole image sequence (N images in a sequence) except the Image No.1. if $T(i,j,k)$is the temporal evolution in the pixel $[i,j]$, where $k = 2 \div N$, the images of phase and Magnitude are produced according to

$$Magnitude = \sqrt{[Re(T)]^2 + [Im(T)]^2}; \tag{3.18}$$

$$Phase = ArcTan\left[\frac{Re(T)}{Im(T)}\right]; \tag{3.19}$$

where $Re(T)$ and $Im(T)$ represent the real and imaginary part of the Fourier transform applied to the $T(i,j,k)$ function.

Below are the Fourier transform images for the honeycomb cell filled with water (50%) in an inclined panel.

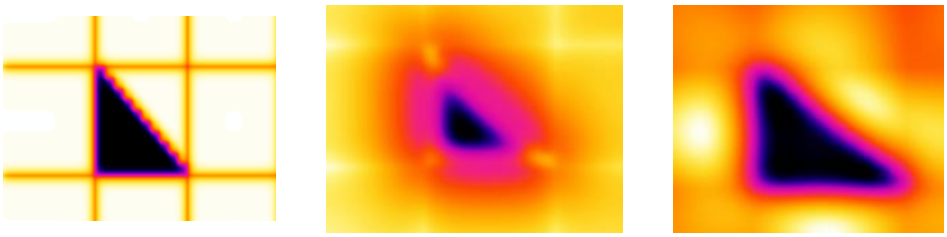

(a) (b) (c)

Figure 3.10: “Standard” Fourier transform image processing in ThermoFit™ Pro of hidden water in an inclined honeycomb panel reference sample (0.5 mm fiberglass skin, 20 x20x 23 mm cell, 50kW/m$^2$ heating flux, 0.5s heating stage, 20s total time: (a) raw image (c) Fourier phase image

### 3.7.3 Principal Component Analysis (PCA)

Principal Component Analysis (PCA) is a linear transformation method rooted in statistical techniques. It serves as a powerful tool for data analysis and pattern recognition, frequently applied in signal and image processing for tasks such as data compression, dimensionality reduction, and decorrelation. In fact, in this research, the PCA is used as a tool for image enhancement and analysis.

In the context of this research, PCA is an image processing technique in ThermoFit which converts image sequences into the corresponding sequence known as Principal components (PC). The PC reveals important statistical relationships between images in the analysed sequence. It does not require any preliminary knowledge. Typically, the visibility of related physics can apply to any image sequence. The visibility of defects (and other image features) is enhanced in the first 3-5 images of the PC. In the ThermoFit, PC can be determined by Correlation, Covariance or square sums. Below are the PCA images for the honeycomb cell filled with water (50%) in an inclined panel

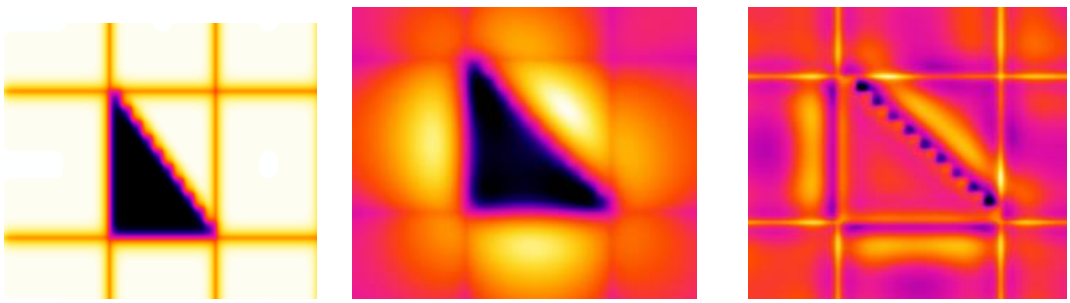

(a) (b) (c)

Figure 3.11: PCA image processing with sigma normalization and correlation option (a) raw image (b) image number 3 (c) image number 6

### 3.7.4 Correlation

This is an image processing algorithm which intends to correct pixel values by a sample shape. It also allows to calculate the correlation coefficient between temporal evolutions in a chosen reference point and other pixels. There are a few correlation modes during a cooling process such as reference point, average, model front, model rear and self-correlation. The reference point is applied in the models of this work. Below are the correlation images for the honeycomb cell filled with water (50%) in an inclined panel and uniform heating.

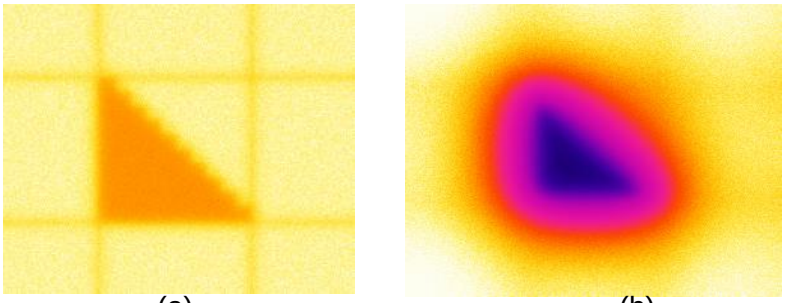

(a) (b)

Fig. 3.12: Correlation image processing with reference point correlation mode (a) raw image (b) image number 3

### 3.7.5 Thermographic signal reconstruction (TSR)

Generally, TSR analyses the time-dependent temperature changes (or thermal evolution) of each pixel in a thermographic image sequence. It fits a low-order polynomial function to the logarithmic time evolution of each pixel. This polynomial function is then transformed back to the linear domain, resulting in a reconstructed temperature-time curve that is less noisy than the original raw signal. The reconstructed data has now a higher signal-to-noise ratio, making it more suitable for signal analysis. TSR effectively reduces temporal noise, leading to clearer and more interpretable thermographic images which can reveal water ingress in the honeycomb cells. The clear (noise free) thermograms with the help of Signal -to-Noise ratio, the level of water in the cells can easily be determined.

It is a special data processing (algorithm) technique either installed in the equipment or within the data processing software such as ThermoFit Pro. Its main objective is to enhance thermographic images and improve the SNR. Basically, the TSR consists of the fitting of the experimental log-log plot thermograms by the following logarithmic polynomial

$$\log_{10}(\Delta T) = a_0 + a_1 \log_{10}(t) + a_2[\log_{10}(t)]^2 + \cdots .. a_n[\log_{10}(t)]^n \quad (3.20)$$

$\Delta$T is the temperature increase as a function as a function of time t (thermograms) for each pixel (i,j).

It also consists of the computation of the first and second logarithmic derivatives of the thermograms, which provide better SNR and sharpness than the raw thermographic images.

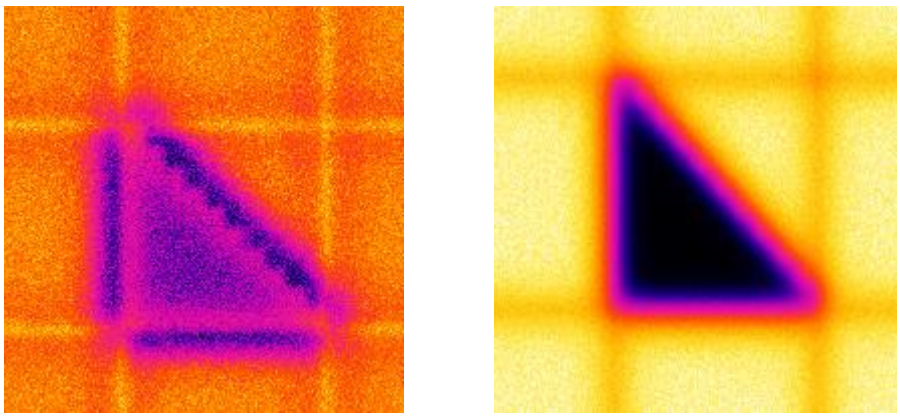

(a) (b)

Figure 3.13: TSR image processing (a) raw image (b)

### 3.8 Introducing Noise into Image Processing (ThermoFit Pro)

Numerical modelling is an ideal (theoretical) approach with almost perfect data input for the desired ideal output. However, in the experimental work, the data output is affected by several factors, such as noise from the camera and the sample's manufacturing quality, such as surface roughness. In this section, both additive and multiplicative noises are applied to the models using image processing algorithms to improve visibility and the SNR. The outputs from these models are validated experimentally using an active pulse thermography.

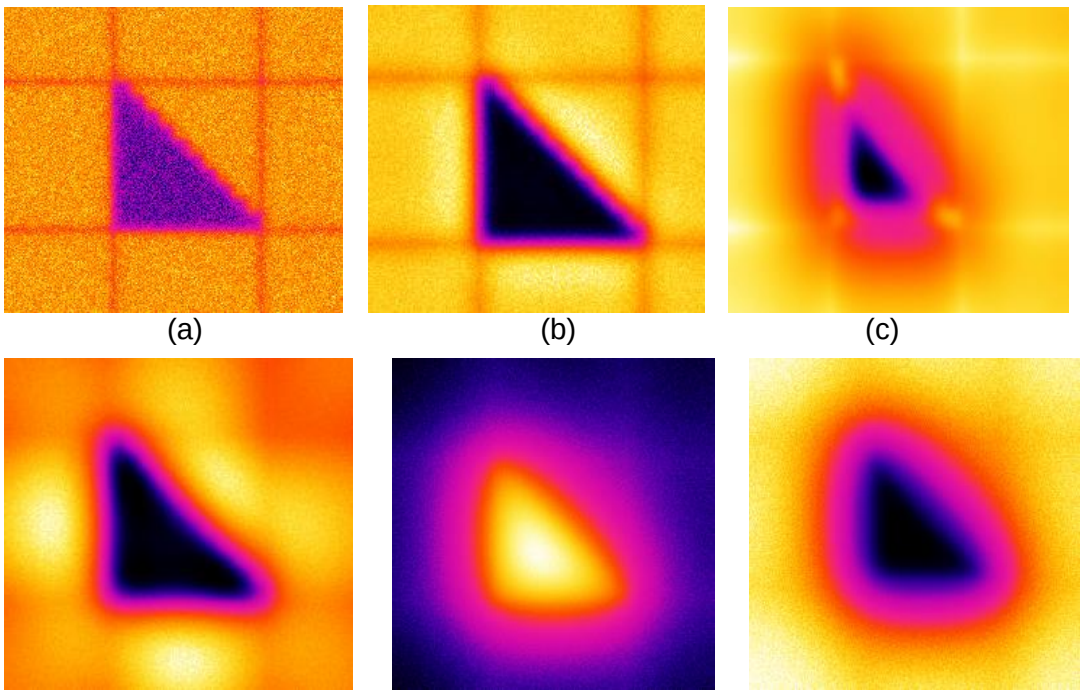

(a) (b) (c)

(d) (e) (f)

Figure 3.14: Image (with noise) processing (a) raw image (b) fitting algorithm (c) Fourier (phase) (d) Fourier (magnitude) (e) PCA with sigma normalization and correlation option (f) Self correlation

### 3.8.1 Signal-to-Noise Ratio Analysis

The SNR analysis was conducted on the scenarios of 50% water in an inclined panel, 50% water in a vertical plate and 100% water in a horizontal panel and the results are presented in Table 3.2. All three models are induced with noise (3% of additive noise and 1%-5% of multiplicative noise). It is shown that under similar parameters, the principal component analysis algorithm has a high SNR value in the first and second scenarios. In contrast, in the third scenario, the Fourier Phase (2 harmonic) shows a high SNR value. It shows that there is no one best image processing algorithm across the board. The preferred algorithm depends on the size of the selected areas for defected and non-defected areas on the images in the ThermoFit. Generally, the SNR values presented below are high, it is because the skin of the model is very thin (0.0005 m), and water has a very high heat capacity compared to other materials of the panel, which leads to being sensed very well. It was also noticed from the histograms in the ThermoFit that the defected and non-defected areas were well separated, which indicates that the SNR values are high.

Table 3.2 Results of several SNR image processing algorithms

| Scenario | Algorithm | Option | SNR |
|---|---|---|---|
| **50% water in an inclined panel with uniform heating** | Fitting | | 11.6 |
| | Fourier | Amplitude(2 Harmonic) | 21.7 |
| | | Amplitude(3 Harmonic) | 18.4 |
| | | Phase (2 Harmonic) | 41.4 |
| | | Phase (3 Harmonic) | 42.9 |
| | PCA( 2nd component) | | 52.2 |
| | Self-correlation | | 15.3 |
| **50% water in a vertical panel with uniform heating** | Fitting | | 39.06 |
| | Fourier | Amplitude(2 Harmonic) | 34.3 |
| | | Amplitude(3 Harmonic) | 35.4 |
| | | Phase (2 Harmonic) | 42 |

| | | | |
|---|---|---|---|
| | | Phase (3 Harmonic) | 19.3 |
| | PCA( 2nd component) | | 55.6 |
| | correlation | | 51.7 |
| | Fitting | | 27.9 |
| | Fourier | Amplitude(2 Harmonic) | 9.3 |
| **50% water in a vertical panel with non-uniform heating** | | Phase (2 Harmonic) | 120.3 |
| | PCA( 3rd component) | | 52.2 |
| | correlation | | 13.3 |
| | Fitting | | 28.5 |
| | Fourier | Amplitude(2 Harmonic) | 19.03 |
| | | Amplitude(3 Harmonic) | 18.6 |
| | | Amplitude(4 Harmonic) | 13.9 |
| **100% water in a horizontal panel** | | Phase (2 Harmonic) | 45.6 |
| | | Phase (3 Harmonic) | 35.5 |
| | | Phase (4 Harmonic) | 42.3 |
| | PCA ( 2nd component) | | 16.6 |
| | Self-correlation | | 29.6 |

### 3.9 Modelling Results and Discussion

Initially, the evolution of excess temperature in water-filled cells was analysed. This evolution is influenced by the panel orientation (scenario), water content, and the surface to which the heat flux ($W/m^2$) is applied. When water is in contact with the skin, the area over the defect (water cell) displays relatively low temperatures compared to cells with an air gap. This is because air significantly hinders heat flux propagation, while water, with its high heat capacity, resists rapid heating. A cell filled with 100% water (with water in contact on both surfaces)

generates higher maximum ∆T_m signals and shorter observation times (t_m). A similar pattern is observed in the vertical panel scenario, where both surfaces are in contact with water, albeit with less mass than cells containing 100% water. Previous research indicated that observation time decreases with lower water content, and the presence of air gaps between water and skin renders both C_m and t_m values highly dependent on water content. When water is in direct contact with the skin, temperature signals show minimal dependence on the thickness of the water layer (Ibarra-Castanedo et al., 2012).

Figure 3.14 illustrates the ΔT and C over time for all scenarios, while Figures 3.15 (a) and (b) present 3D temperature distributions on the sample surface for selected scenarios (vertical and inclined panels). It is important to note that due to the specific test parameters, both the differential temperature signals and contrasts are negative, indicating that the temperature over water-filled cells is lower than that in defect-free areas; the minus sign is therefore omitted.

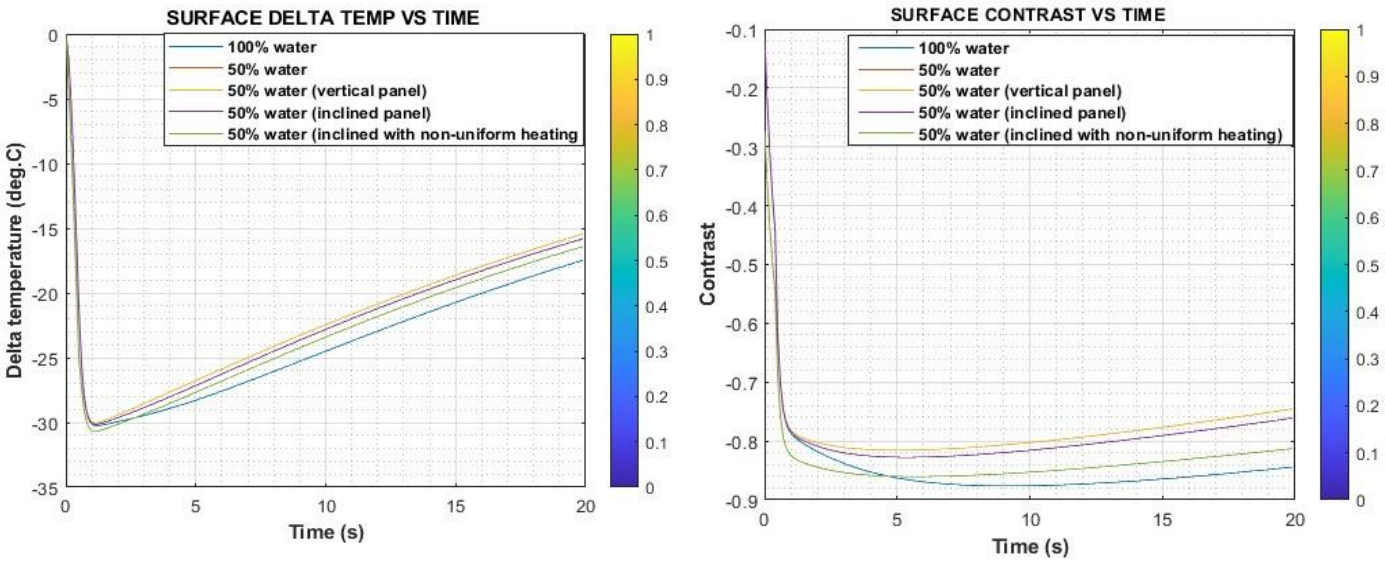


a)

Figure 3.15. *Evolution of surface temperature parameters in time:*
a - $\Delta T$ *vs. t,*
b - C *vs. t*

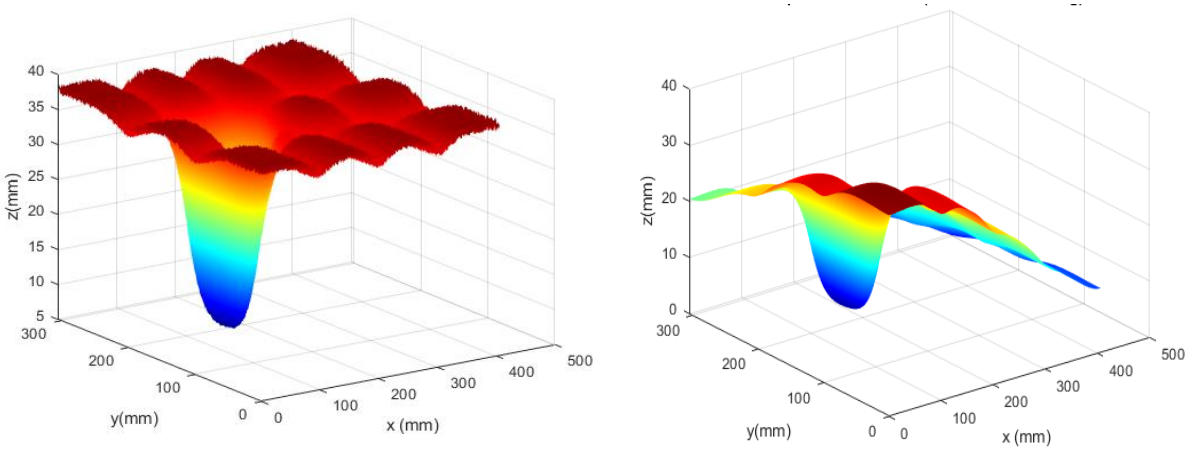


a) b)

Figure 3.16: 3D temperature distributions at the time of maximal $\Delta T_m$ (50% water in inclined panel): a) uniform heating, b) non-uniform heating

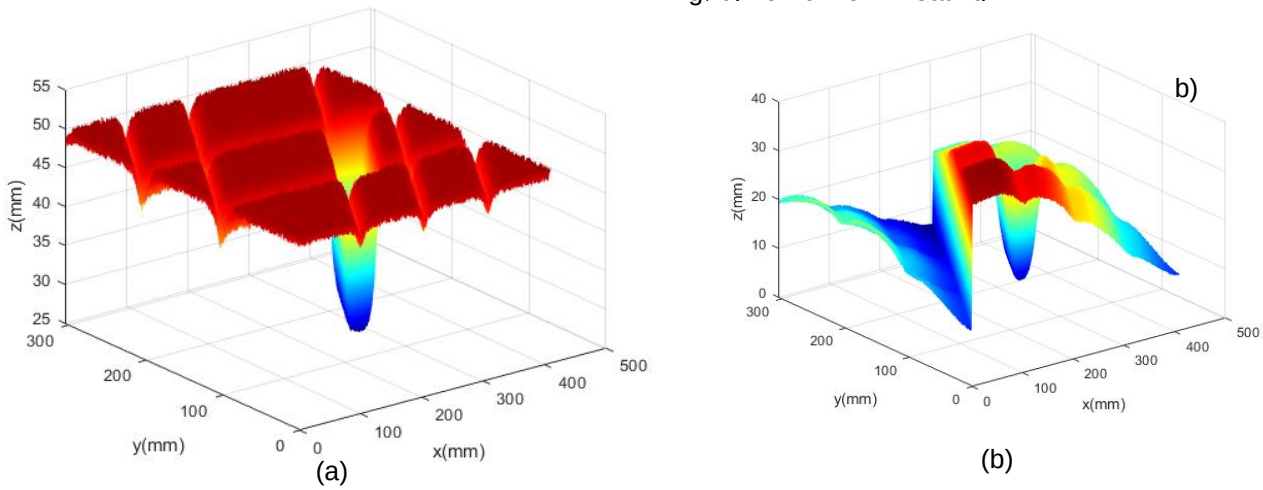


(a) (b)

Figure 3.17: 3D temperature distributions (50% water in vertical panel)
a) uniform heating, b) non-uniform heating

The modeling results presented above are considered "ideal" due to the precisely defined input parameters. They show that water-filled cells remain cooler than those without water. Typically, the differential temperature signals, $\Delta T\_m$, reach their maximum values at specific times, $t\_m$. These $\Delta T\_m$ values occur earlier than the $C\_m$ values, and both are higher in cells with greater water content. Notably, in all scenarios, if the inspection occurs on the surface where water is in direct contact with the skin, the ΔT signals appear and peak more quickly. The vertical panel reflects a similar observation time of 5.1 seconds, as expected. However, when the inspection is conducted on a surface where an air gap separates the water from the skin, the ΔT signals appear later and are of lower magnitude. Overall, it seems that the presence of water in the cells could be detected through air gaps, but the thicker the air gap, the greater its thermal resistance, resulting in a weaker temperature signal on the surface.

Table 3.3 presents the modelling results for all critical parameters related to water ingress detection in honeycomb panels subjected to flash heating (0.1 seconds). When examining data from the front surface, the cell filled with 100% water exhibits the highest temperature differential signal (-30.3°C) and thermal contrast (-88%). This scenario also has the shortest observation time of 1.2 seconds, making it the most favourable for detection. In contrast, the lowest temperature signal (-30°C) and contrast (-14%) occur on the surface of the horizontal panel with 50% water due to the presence of an air gap.

Regarding the temporal behaviour of thermal contrast, the inclined and vertical panels with 50% water show shorter observation times (5.1 and 5.5 seconds) compared to the 100% water scenario (9.3 seconds). When water is in direct contact with the skin, it is generally observed that thermal contrasts can reach as high as 1 (or 100%) at brief observation times. Consequently, cells with water can be detected earlier than those with air gaps. This significant contrast is attributed to the high heat capacity of water, which allows water-filled areas to retain thermal energy (and temperature) for extended periods, even after being heated for a shorter duration

Table 3.3. Optimum water detection parameters (fibreglass honeycomb panel, modelling results, $t_h = 0.1$ s, Q=50 kW·m$^{-2}$)

| | Scenario | $\Delta T_m$, ℃ | $t_m(\Delta T_m), s$ | $C_m$ | $t_m(C_m), s$ |
|---|---|---|---|---|---|
| | Cell filled with water (100%) in horizontal panel | 30.3 * | 1.2 | 0.88 | 9.3 |
| **Front surface water (separated by air gap)** | Cell filled with water (50%) in horizontal panel | 27.0 | 13.5 | 0.14 | 20 |
| | Cell filled with water (50 %) in vertical panel | 30.0 | 1.4 | 0.82 | 5.1 |
| | Cell filled with water (50 %) in inclined panel | 30.1 | 1.8 | 0.83 | 5.5 |
| | Cell filled with water (50 %) in inclined panel under non-uniform heating. | 28.1 | 1.5 | 0.86 | 5.8 |
| **Rear surface water (water is in contact with skin)** | Cell filled with water (50%) in horizontal panel. | 2.9 | 20 | 1 | 1.3 |
| | Cell filled with water (50 %) in vertical panel | 30.0 | 1.4 | 0.82 | 5.1 |
| | Cell filled with water (50 %) in inclined panel. | 2.8 | 20 | 1.0 | 1.3 |
| | Cell filled with water (50 %) in inclined panel under non-uniform heating. | 1.4 | 20 | 1.0 | 1.4 |

* The minus sign of $\Delta$T and *C* is omitted.

## 3.10 Surface Heat Transfer (Convection and Radiation) to be Replaced with Convective Heat Transfer only

This section provides clarity on a scientific phenomenon that in thermal NDT if temperatures are close to the ambient, the non-linear radiation heat exchange can be neglected. It is achieved by performing a modelling analysis using a ThermoCalc-3D radiation program (software) to obtain surface temperature when Convective heat exchange is applied and when Adaptive heating is applied on the front surface and Rear surface (Figure 3.18). This phenomenon demonstrates the impact of environmental conditions in detecting water ingress in the honeycomb panel. In this analysis, the convection heat transfer is assumed to be under natural conditions, such as when the experimental work is done in a controlled lab environment.

The convective heat transfer coefficient (h) or the heat exchange coefficient (α) is critical when analysing the heat transfer rate between the model's surface and the environment. It varies based on flow velocity, surface roughness, and temperature difference.

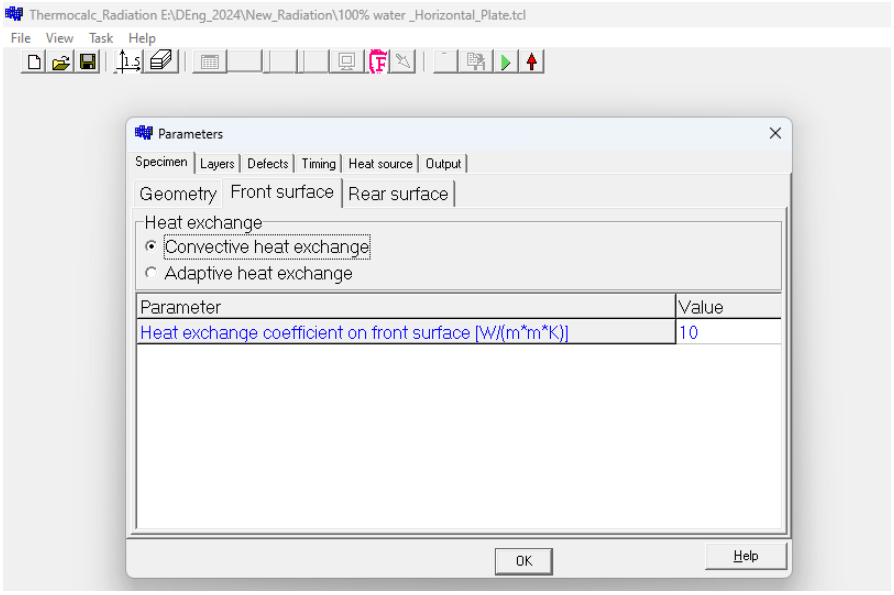


Figure 3.18: Convective heat exchange set up in the ThermoCalc-3D_Radiation software

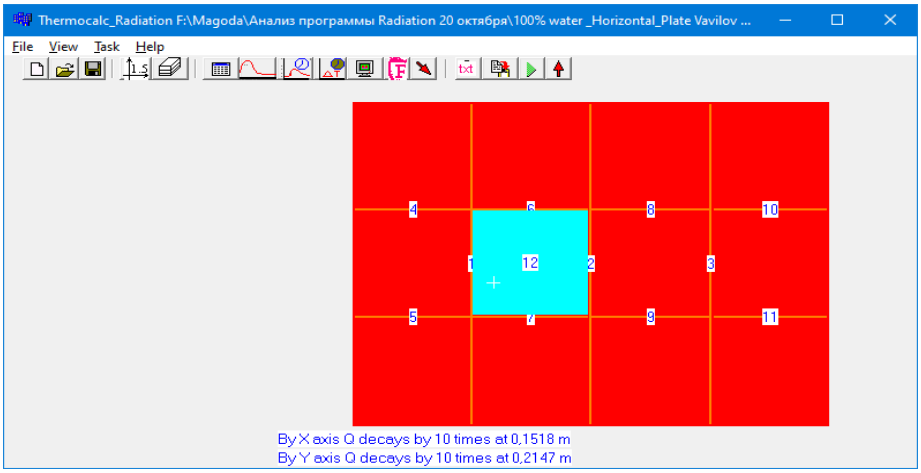


Figure 3.19: 3D Model (scheme) in ThermoCalc-3D_Radiation software

The results are presented in Figures 3.20 and 3.21.

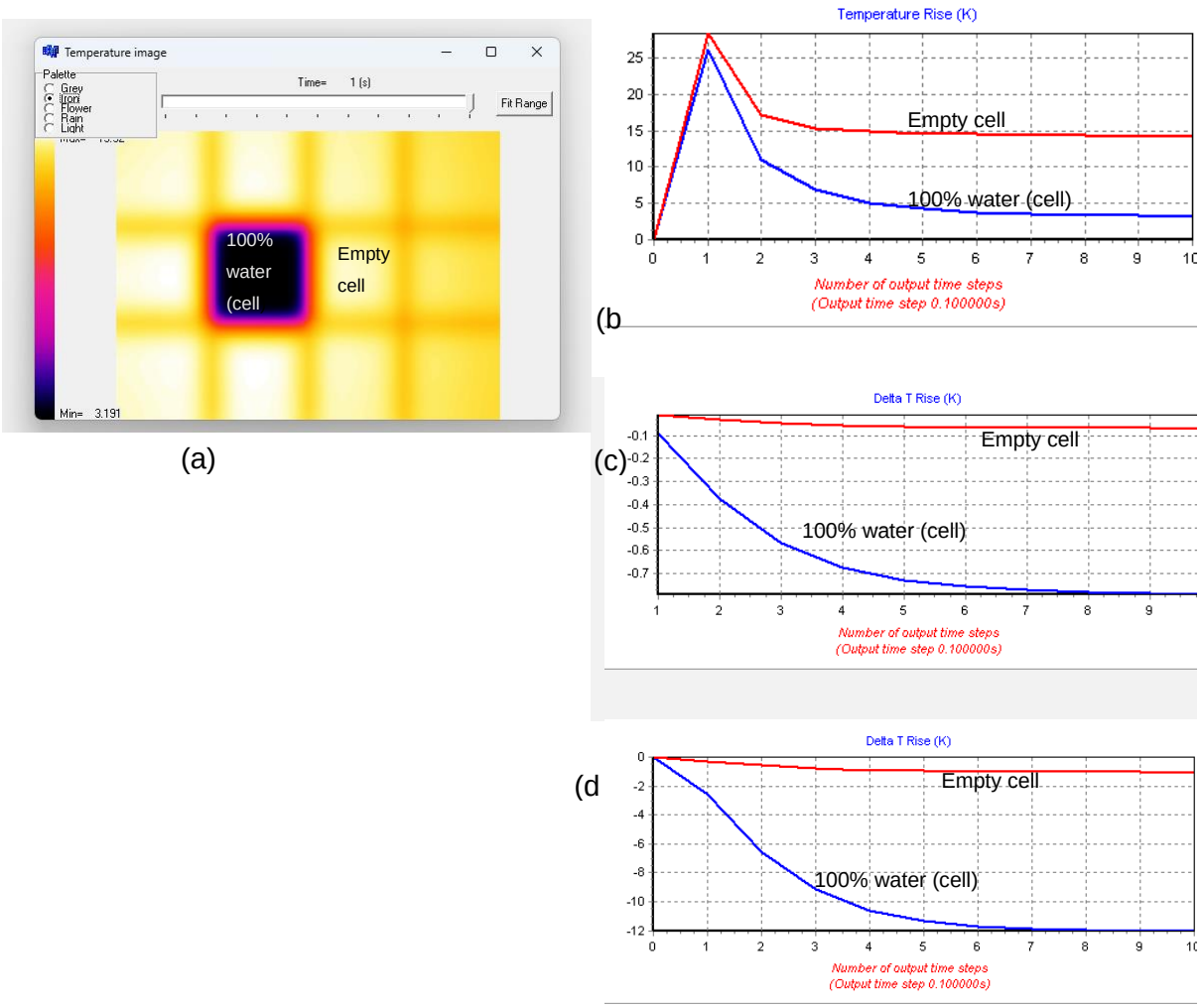


Figure 3.20: Results for Convectiive heat exchange: a –Temperature image; b-Time profile; c- Delta T profile; d- temperature contrast profile

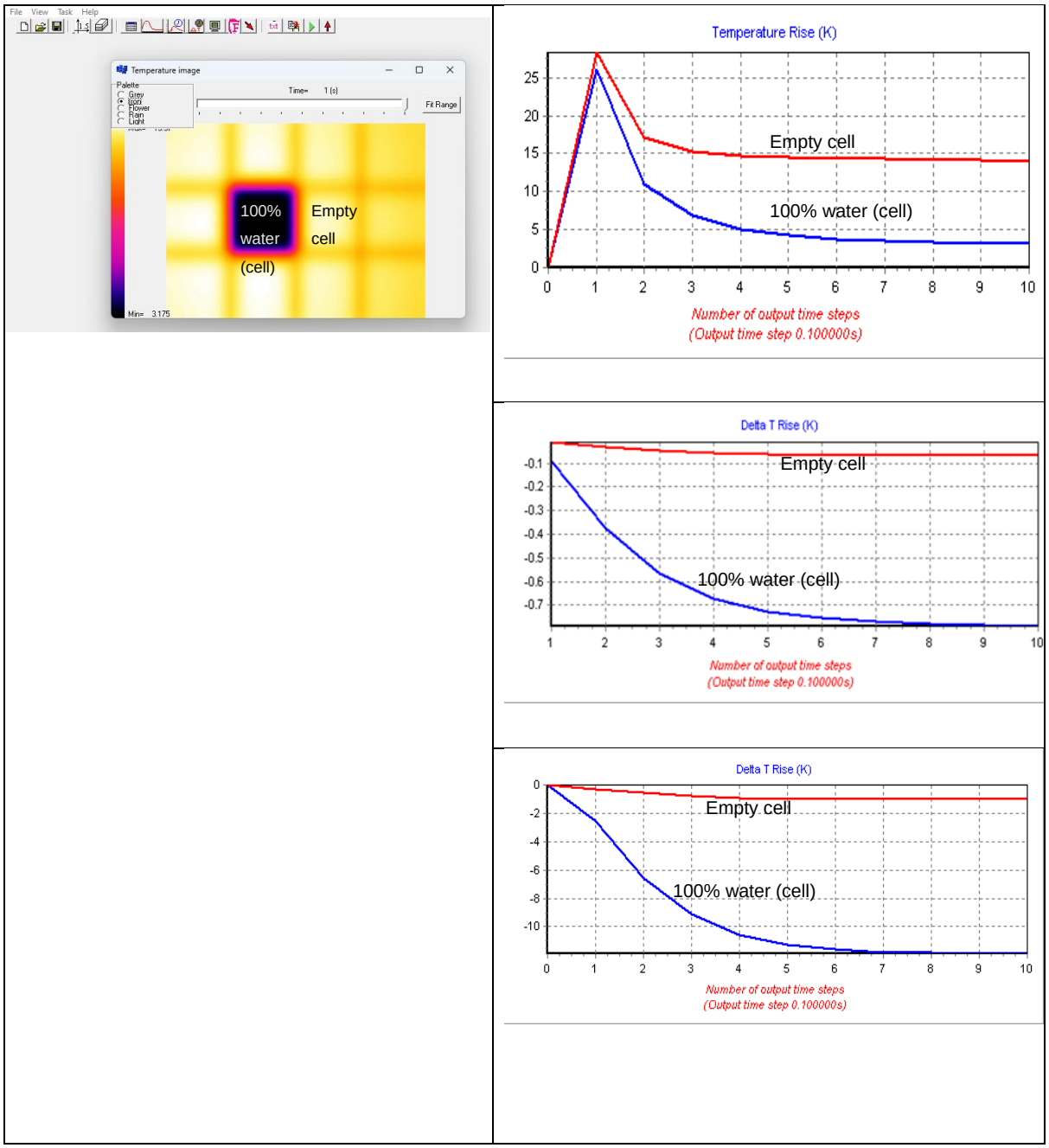


Figure 3.21. Results for adaptive heat exchange: a –Temperature image; b-Time profile; c- Delta T profile; d- temperature contrast profile

It can be observed that the results for convective and adaptive heat exchange are identical, which proves that in thermal NDT, if temperatures are close to the ambient, the non-linear radiation heat exchange can be neglected.

### 3.10.2 Heat Exchange Ecoefficiency

The general heat exchange coefficient (α) between the model's surface and the environment depends on both time and temperature (eqn. 3.11) and is derived from the combination of convective and radiative heat exchange coefficients (eqn. 3.12):

$$\alpha_{general=f\ (Time\ and\ Temp)} \tag{3.21}$$

$$\alpha_{general} = \alpha_{conv} + \alpha_{rad} \tag{3.22}$$

In an environment where natural convection occurs, the convection heat exchange coefficient (α) is approximately 10. In case of unnatural conditions, the exchange coefficient ranges between 50 and 100 W/m$^2$·°C. For an adiabatic model, there will be no change if the following condition is satisfied:

$$Bi = \frac{\alpha L}{\lambda} < 0.1 \tag{3.23}$$

## 3.11 ThermoCalc- 3D Normalisation

This section focuses on a new scientific procedure for the 3D normalisation of experimental data, specifically image sequences. It is worthwhile to note that 3D normalisation is supposed to consider lateral diffusion of heat in surface clutters, such as spots, and areas of uneven heating, because the pairs of images taken at the same times of heat conduction are to be normalised. While common normalisation involves division of images taken at different times by the image taken at one time moment. The latter is the focus of this section, which employs ThermoDouble software in conjunction with both the experimental image sequence and the mask image calculated sequence to obtain a normalised sequence. By utilising this approach, we aim to improve the analysis of 3D images, ensuring that regions of interest are effectively isolated and artefacts are minimised, leading to more precise interpretations of the experimental results.

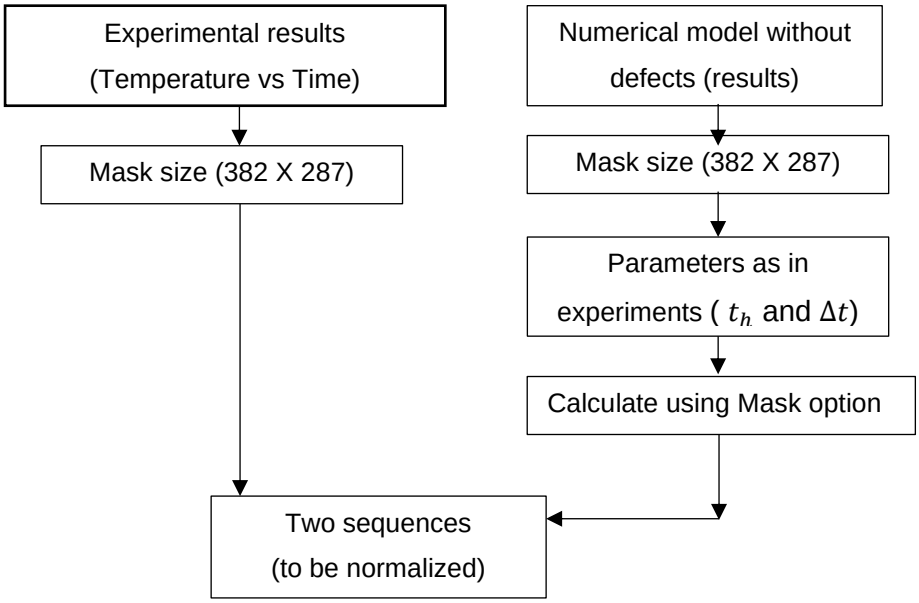


Figure 3.22. A mask imaging in ThermoCalc for 3D normalization

In this study, the sequence of experimental images captured at 3 seconds using a halogen light source at 16 Hz, consisting of 500 images, was chosen for the normalization process. The image corresponding to the end of the heating cycle was selected for this analysis,

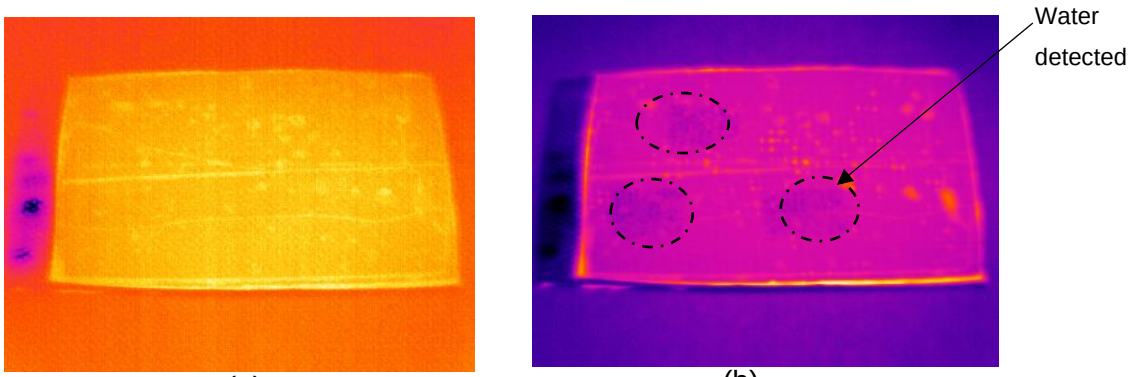


(a) (b)

Figure 3.23: Mask images (a) image #7 (b) image #48 (end of heating)

specifically identified as image #48. However, this image faintly reveals water in the sample. Therefore, image #7 (figure 3.22) was selected as a mask image.

A new sequence was created, including the following images: #7(mask image), #48 (3s), #98 (6s), #144 (9s), #192 (12s), #240 (15s), #288 (18s), #336 (21s), #384 (24s), #432 (27s), and

#480 (30s). These images are uniformly spaced, with intervals of 48 frames, corresponding to 3 seconds each.

From this newly created sequence, images #7 and #48 were selected as the masks for normalization in ThermoCalc-3D, as they represent the data point at 3 seconds. A new scenario for ThermoCalc-3D utilizing these mask images were developed. The intention was to make a meaningful comparison between the mask image with no detected water (#7) and with detected water (#48) which the end of heating.

For successful normalization, it is essential that the dimensions of the mask image align closely with the numerical mesh used in ThermoCalc-3D. In this case, the mask image has dimensions of 382 x 287 pixels, while the numerical mesh comprises 381 x 286 spatial steps. The sample size utilised for the experiment measures 200 x 150 mm, ensuring compatibility between the mask and the numerical mesh for effective normalisation.

Figure 3.23 is the ThermoDouble window, which shows that all other files are located in the same folder, and the sequences are divided.

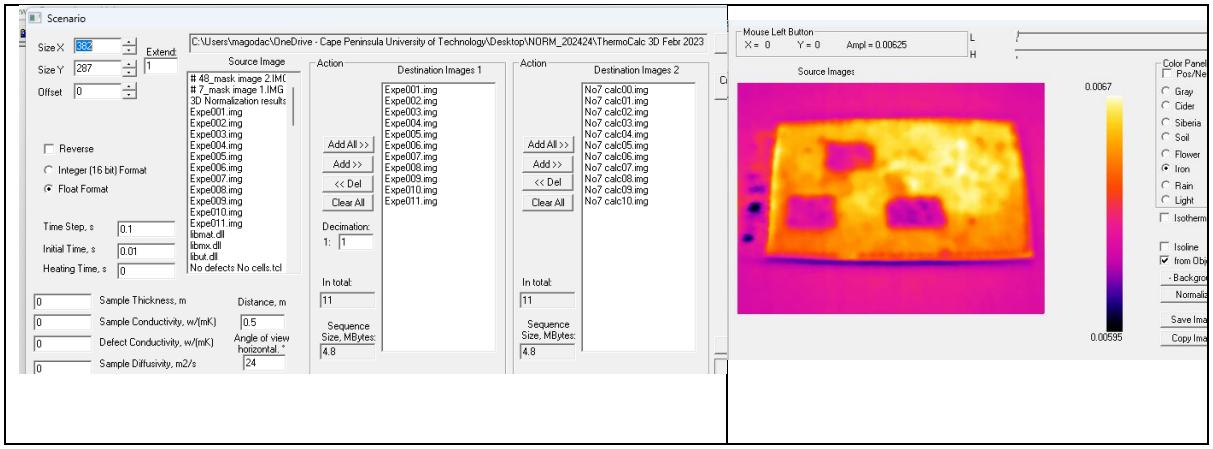


(a) (b)

Figure 3.24: (a) ThermoDouble window (b) normalized image

Figures 3.24 and 3.25 present the 3D normalisation results when using image #7 as a mask and when using image #48 as a mask.

| | Experimental imagines(3s) | Calculated images with image #7 | 3D normalization images (ThermoDouble) |
|---|---|---|---|
| 3s | 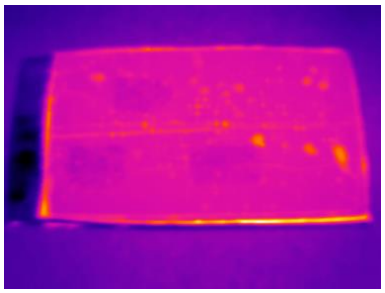 | 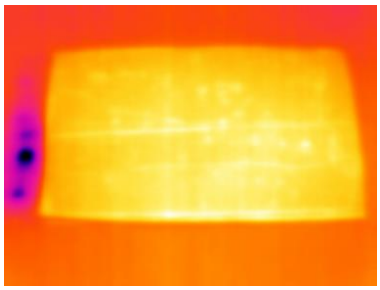 | 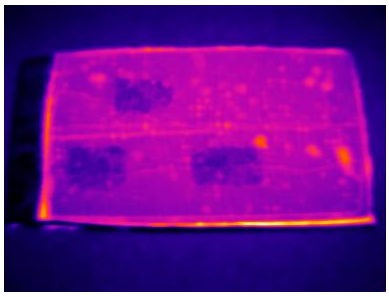 |
| 6s | 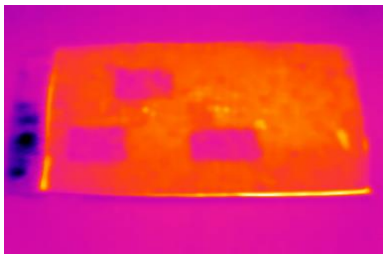 | 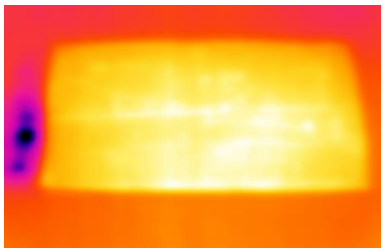 | 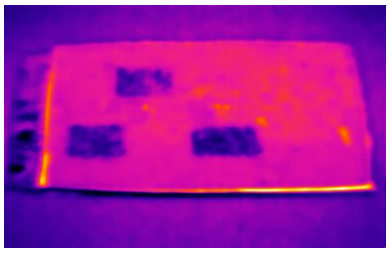 |
| 9s | 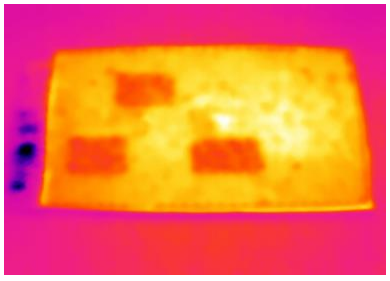 | 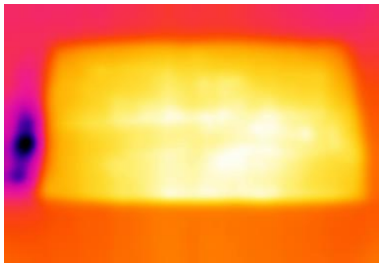 | 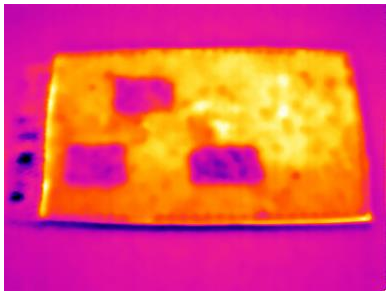 |
| 12s | 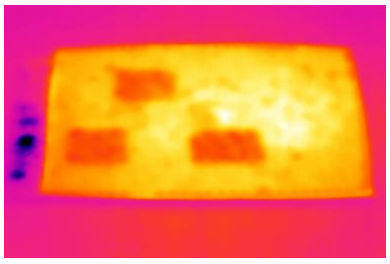 | 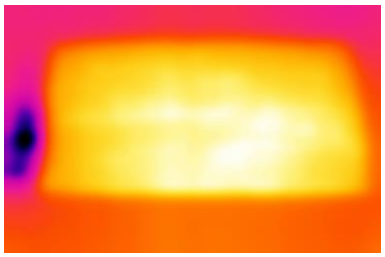 | 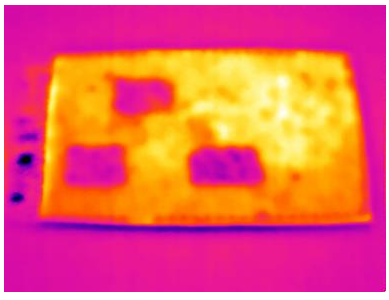 |

15s

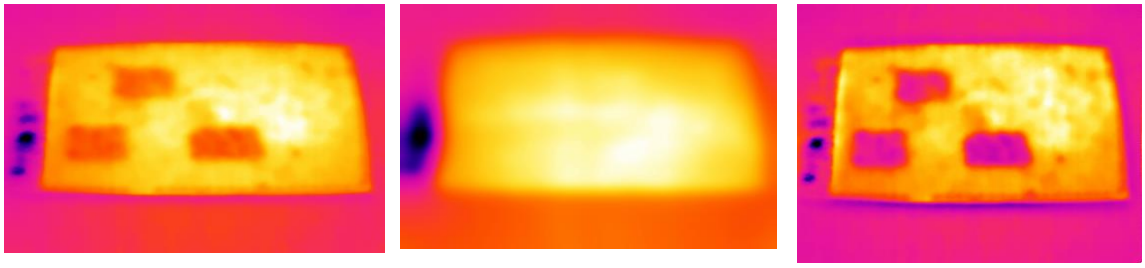

18s

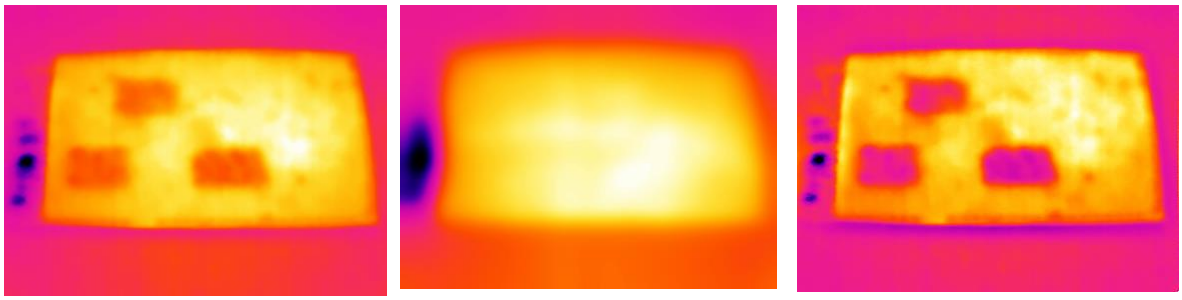

21s

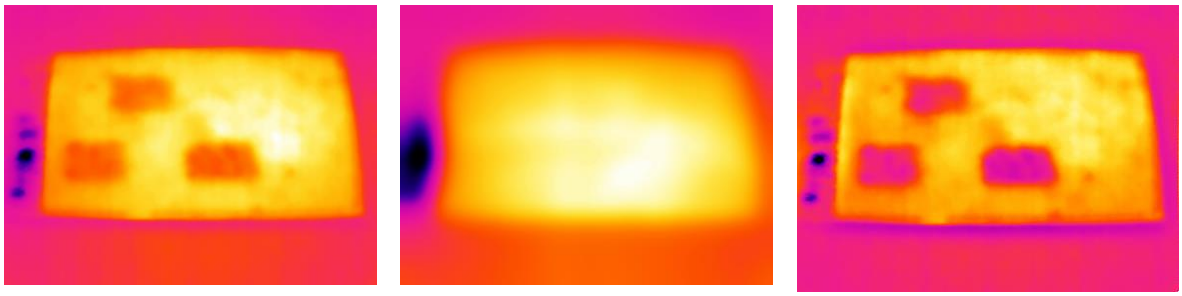

24s

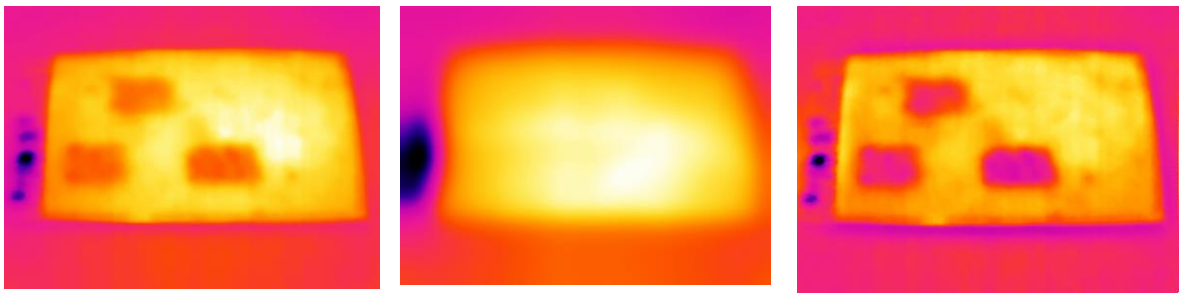

27s

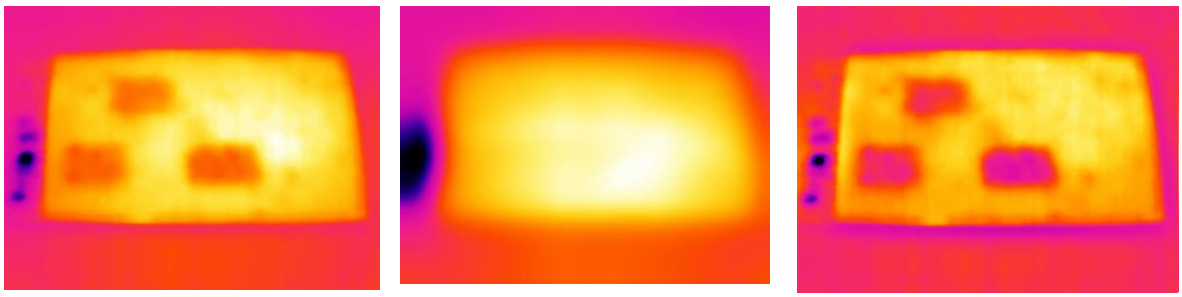

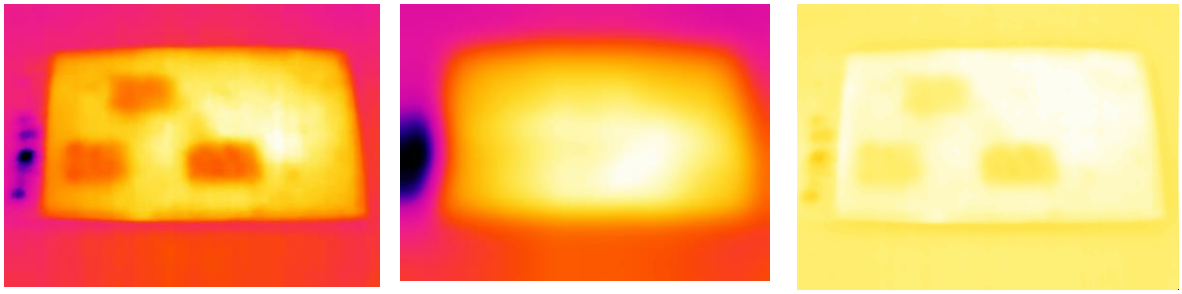


Figure 3.25: A mask image #7 calculation in ThermoCalc for 3D normalization

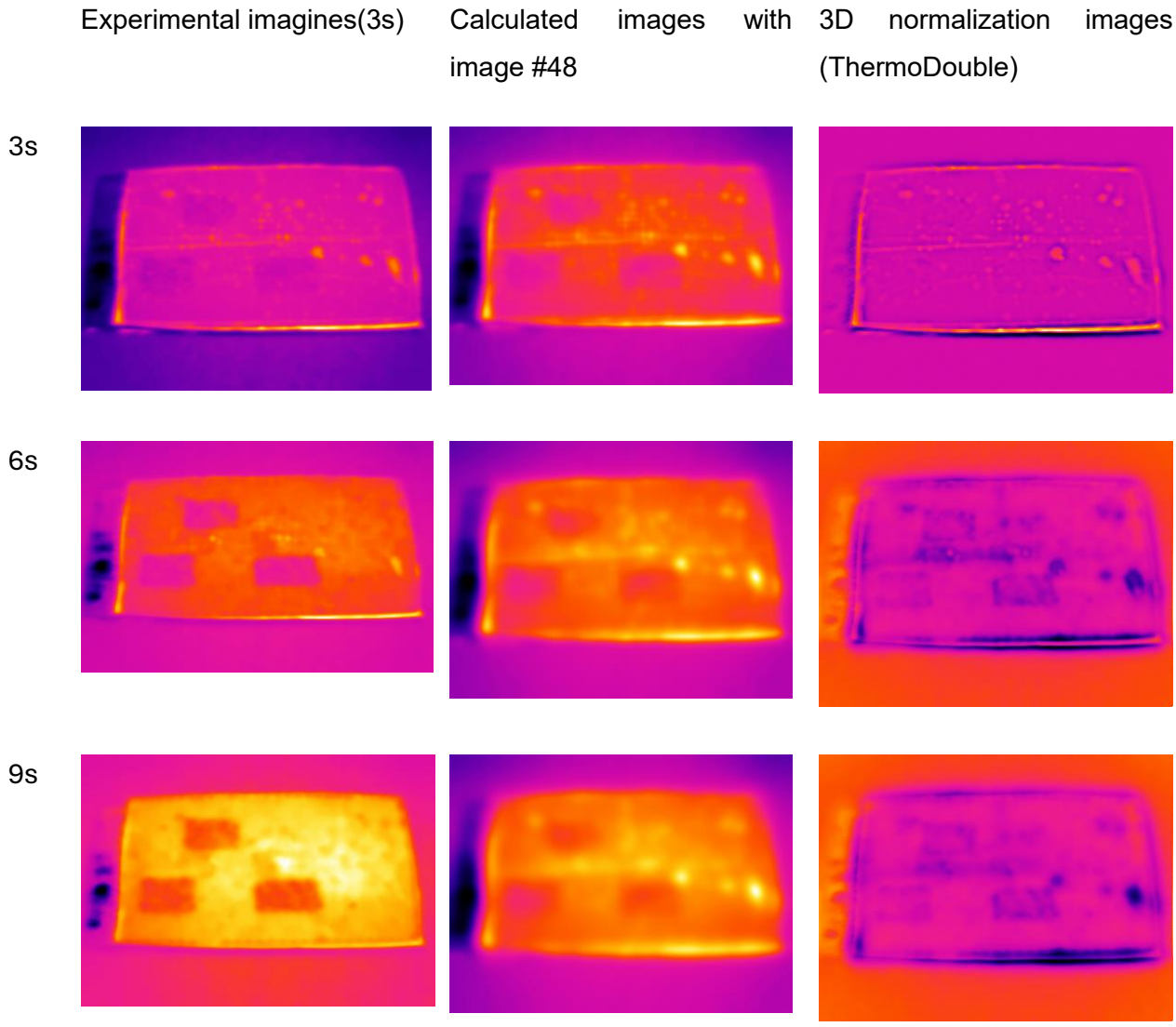

12s

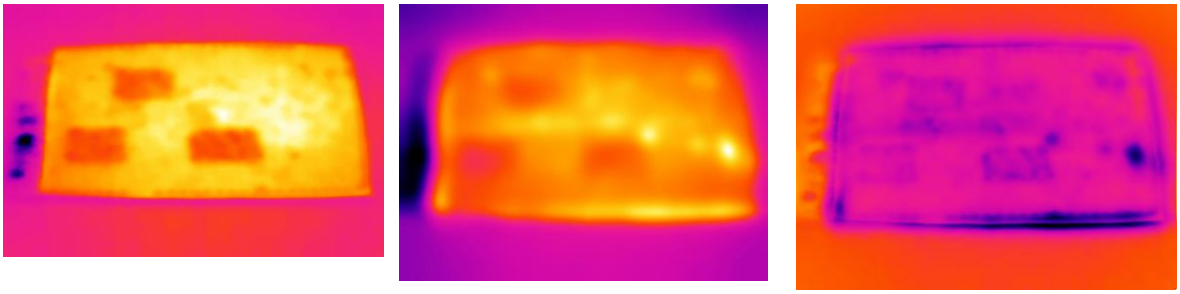

15s

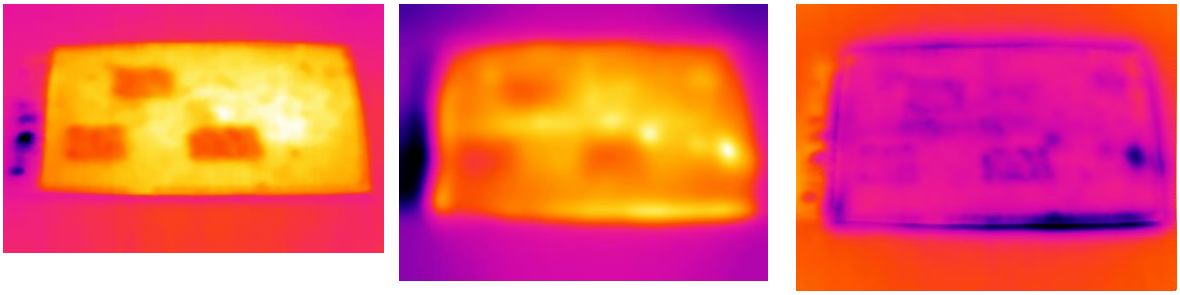

18s

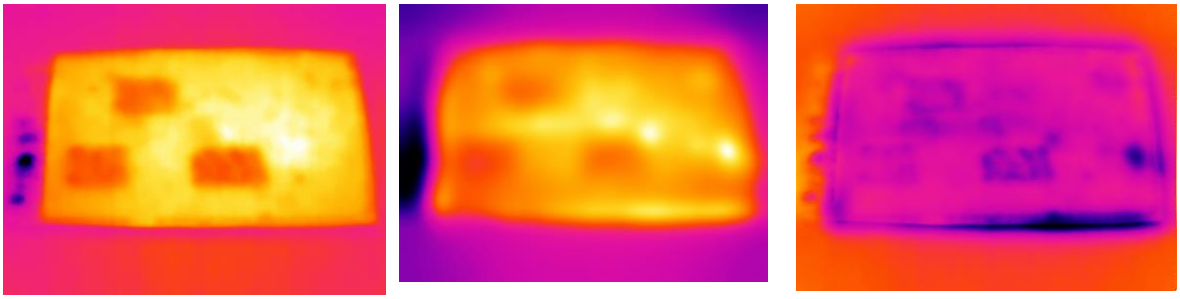

21s

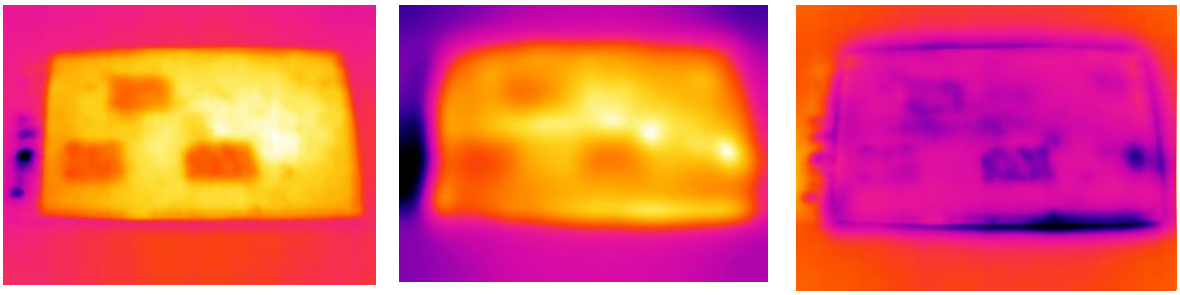

24s

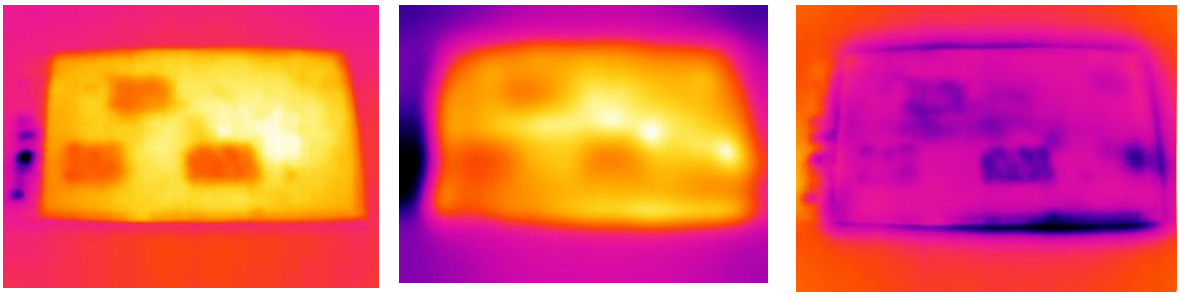

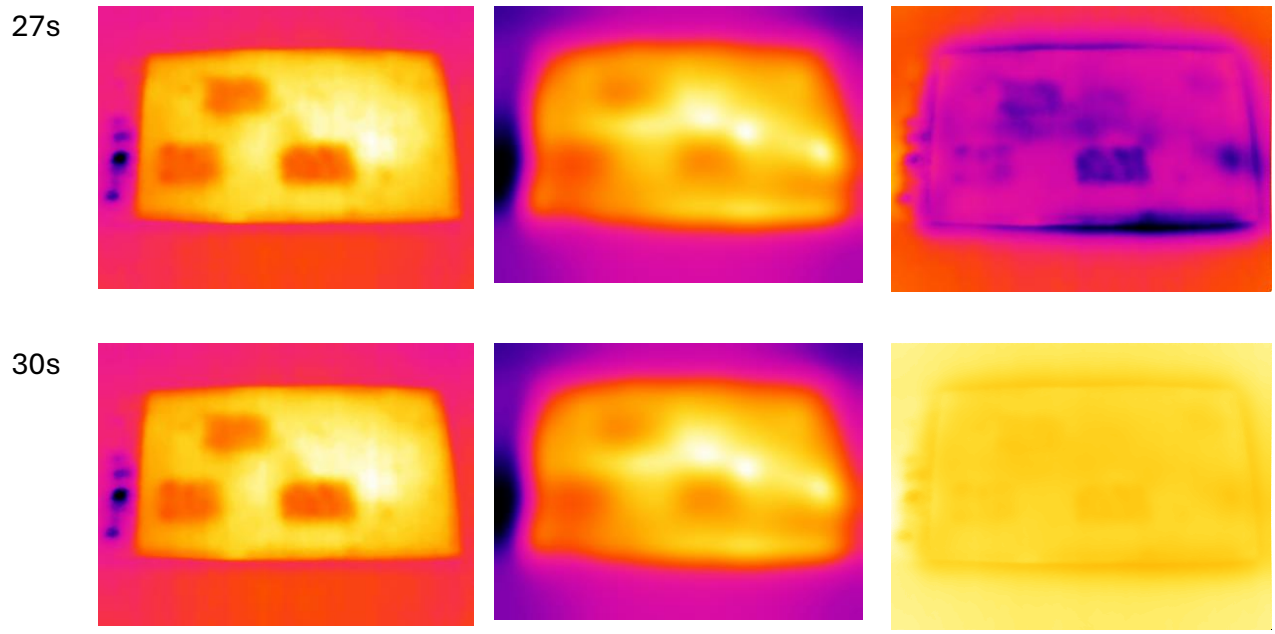


Figure 3.26: A mask image #48 calculation in ThermoCalc for 3D

The following observations emanated from the above results

a) Indeed, normalization enhances water ingress detection (reference to figure 3.24 results from a mask image #7)
b) In Figure 3.24, perfect results are obtained from 9s to 27s heating period
c) Figure 3.25 (mask image #48) presents bad results because this mask image (end of heating) reveals water present in cells. It can be seen from the calculated images (figure 3.25)

## 3.12 Accuracy and Possible Errors

Accurately modelling water ingress in honeycomb panels ensures the structural integrity and longevity of composite materials used in various applications, including aerospace. Honeycomb panels are designed for lightweight strength and durability but are inherently vulnerable to moisture infiltration, which can lead to significant damage over time. By effectively simulating water ingress, engineers can predict how moisture affects the mechanical properties of the panels, identify potential failure points, and develop more effective mitigation strategies. This helps maintain performance standards and reduces the risk of catastrophic failures that could arise from undetected moisture damage.

Furthermore, precise modelling of water ingress is essential for compliance with industry standards and regulations. As manufacturers strive to create safer and more reliable products, understanding the moisture dynamics within honeycomb structures becomes increasingly important. Advanced modelling techniques, such as finite element analysis and computational fluid dynamics, allow for a detailed investigation of moisture pathways and accumulation patterns within the panels. This knowledge not only aids in designing better materials but also enhances maintenance strategies, ensuring that honeycomb panels can withstand harsh environmental conditions without compromising safety or performance. Overall, accurately modelling water ingress plays a vital role in advancing material science and engineering practices.

This section identifies factors influencing accuracy and potential errors in modelling.

### 3.12.1 Model Assumptions

#### 3.12.1.1 Simplified Geometry

Simplifying the geometry of a honeycomb structure when modelling water ingress can lead to significant inaccuracies in predictions of moisture behaviour and its subsequent effects on material integrity. Honeycomb panels possess intricate internal features that influence how water penetrates and distributes within the material; oversimplifying these geometries may overlook critical pathways for moisture ingress or misrepresent the flow dynamics. Such reductions can result in underestimating potential damage, leading to unforeseen failures or compromised structural performance in real-world applications. Ultimately, while simplified models may facilitate quicker computations and analyses, they can misguide design decisions and maintenance protocols, potentially compromising safety and reliability in critical applications.

#### 3.12.1.2 Material Homogeneity

Considering the heterogeneity of materials in honeycomb structures is vital when modelling water ingress, as these panels often exhibit variable properties due to differences in material composition, cell geometry, and manufacturing processes. Assuming uniform properties can lead to significant inaccuracies in predictions of moisture behaviour, as it overlooks how localised variations can affect permeability and moisture retention. This can result in misestimations of the rate and extent of water infiltration, ultimately compromising the structural integrity and performance of the panel. Such oversights can lead to premature failure or degradation, posing serious safety risks and increasing maintenance costs. By acknowledging the heterogeneous nature of materials, engineers can create more accurate models that better reflect real-world conditions, enabling more effective design and preventative measures against moisture-related issues.

### 3.12.2 Input Parameters

#### 3.12.2.1 Water Content

Accurate characterisation of water content is essential when modelling water ingress in honeycomb structures, as it directly influences the material’s mechanical properties and overall performance. Variability in water distribution within the panel can significantly impact model outcomes; uneven moisture accumulation can lead to localised weakening, increased risk of delamination, and unexpected failure modes. If models fail to capture this variability, they may produce misleading predictions regarding the panel's structural integrity, potentially resulting in insufficiently informed design choices and maintenance strategies. Consequently, understanding and quantifying water content and its distribution is critical for developing reliable predictive models, ensuring that the structural performance of honeycomb panels is maintained even in challenging environmental conditions.

#### 3.12.2.2 Boundary Conditions

Boundary conditions are critical parameters that define how a model interacts with its environment, significantly influencing the accuracy of simulations related to water ingress in honeycomb structures. These conditions determine factors such as moisture entry rates, environmental pressures, and temperature gradients, which can drastically affect how water permeates through the material. Common boundary condition assumptions, such as treating the surface as perfectly impermeable or assuming uniform moisture exposure, can lead to inaccuracies by failing to account for real-world complexities like varying environmental conditions or localized protective coatings. Such oversights may result in an inaccurate

depiction of moisture dynamics, potentially leading to flawed predictions about the material's durability and performance. Ultimately, precise definition and realistic representation of boundary conditions are essential for developing reliable models that reflect actual operational environments, ensuring the safety and longevity of honeycomb structures.

### 3.12.3 Thermal Properties

#### 3.12.3.1 Heat Transfer Coefficients

The variability of convective and radiative heat transfer coefficients plays a crucial role in accurately modelling water ingress in honeycomb structures, as these coefficients directly influence temperature gradients and moisture transport mechanisms. In real-world applications, factors such as airflow patterns, surface roughness, and surrounding environmental conditions can cause significant fluctuations in these coefficients, leading to variations in heat transfer rates. If thermal models rely on fixed or averaged values for these coefficients, they may fail to capture the dynamic interactions between heat and moisture, resulting in inaccurate predictions of moisture behaviour and potential structural impacts. Such inaccuracies can compromise the effectiveness of design and maintenance strategies, as they may underestimate the risks of thermal-induced moisture ingress or overestimate the material's resilience under fluctuating conditions. Consequently, incorporating realistic variations in convective and radiative heat transfer coefficients is essential for developing robust thermal models that reflect the complexities of real-life environments and enhance the reliability of honeycomb structures.

#### 3.12.3.2 Heat Capacity of Water

Water's heat capacity, which measures the heat required to change its temperature, is a critical factor in modelling water ingress in honeycomb structures, as it directly influences how moisture interacts with the surrounding material. Accurate estimation of heat capacity is essential for predicting thermal behaviour, particularly during exposure to varying temperatures, as it affects the rate of heat transfer and the subsequent evaporation or condensation of moisture within the structure. Errors in estimating water's heat capacity can lead to significant discrepancies in thermal models, resulting in flawed predictions of moisture dynamics and potentially underestimating the thermal stresses that may cause material degradation. Such inaccuracies can compromise the integrity of the honeycomb panels, leading to unexpected failures and increased maintenance costs. Therefore, precise characterization of water's heat capacity is vital for developing reliable models that ensure the structural performance and longevity of honeycomb materials in real-world conditions.

### 3.12.4 Air gap effects

Air gaps play a significant role in enhancing the thermal resistance of honeycomb structures, as they provide an insulating effect that reduces heat transfer between layers. These gaps can influence moisture dynamics by affecting how heat is distributed across the material, thereby impacting evaporation and condensation processes. Neglecting the effects of air gaps in thermal modelling can lead to substantial inaccuracies, as it may result in an overestimation of heat transfer rates and an underestimation of moisture retention within the structure. This oversight can misguide engineers in their assessments of thermal performance and moisture ingress risks, potentially leading to premature material failure or inadequate design responses to environmental conditions. Therefore, accurately accounting for air gaps is essential for developing reliable models that reflect the true thermal behaviour of honeycomb panels and ensure their durability in challenging environments.

### 3.12.6 Comparison with experimental data

Validating models against experimental results is essential when modelling water ingress in honeycomb structures, as it ensures that theoretical predictions accurately reflect real-world behaviour. This validation process helps identify discrepancies between model outputs and actual performance, allowing engineers to refine their simulations and improve their predictive capabilities. Without this crucial step, models may produce misleading results that overlook critical factors influencing moisture dynamics, leading to design flaws and safety concerns. Furthermore, experimental validation fosters confidence in the modelling approach, facilitating better decision-making in material selection and maintenance strategies. Ultimately, this iterative process of model validation enhances the reliability and effectiveness of simulations, ensuring that honeycomb structures can withstand environmental challenges while maintaining their structural integrity.

## 3.13 Conclusions

Detecting water in honeycomb sandwich airframes is a crucial inspection task in the aviation industry. 3D modelling appears to be the most effective method for obtaining quantitative data on water presence in honeycomb cells. This study quantitatively compares key parameters such as signal-to-noise ratio, differential temperature signals, contrasts, and their observation times across various test scenarios (horizontal, inclined, and vertical panels), as indicated in Table 2. The findings from the numerical modelling suggest the following:

- Panel orientation does not significantly impact the SNR values observed during modelling; in other words, the visibility of water trapped in the honeycomb cells is largely unaffected by panel orientation.
- No single post-processing algorithm yields optimal inspection results across all model scenarios.
- The results align with previous studies, confirming that the most effective detection occurs when water or ice is in contact with the skin surface.

# CHAPTER 4:
# EXPERIMENTAL WORK

## 4.1 Introduction

This chapter details the experimental protocol (Pulse Phase Thermography) used to validate the predicted results from the mathematical model (ThermoCalc-3D) presented in Chapter 3. It starts by introducing the two experimental techniques used in this work. The chapter describes the materials used for the specimens, the procedure or experimental protocol used in characterising the water ingress induced in the honeycomb panel (specimen), and the image processing techniques. It also presents experimental results, mainly focusing on the visual thermographic images (thermograms) and the raw data regarding delta temperatures, thermal contrast, signal-to-noise ratio, and the optimum observation times for both $\Delta T$ and $C_m$. Different heating techniques (flash, halogen lamps, and hot air) were used during experiments, and the results of various parameters were analysed. In addition, it presents the phenomenon of water quantity determination in terms of parameter correlation. The quantitative results are compared based on the techniques mentioned above.

## 4.2 Experimental Protocol

### 4.2.1 Description of sample material

The sample materials in this work were the Nomex honeycomb core with fibreglass skin. The fibreglass skin was made from the fibreglass (FG) plies (sheets) with a stacking sequence of 0° /90°. Table 4.1 lists typical features of the materials. Three sets of seventy cells were filled with water at 100%, 50%, and 25%

**Table 4.1 Description of the specimens**

| Material | Skin thickness (mm) | Type of the defect | Number of specimens | Area of cell ($m^2$) | Total covered area ($m^2$) | At a depth from top surface (mm) |
|---|---|---|---|---|---|---|
| Fibreglass with Nomex honeycomb core (4x4 mm cell (6 mm deep) size) composite | 0.5 | 127 cells filled with 25% water | 2 | $1.6x10^{-5}$ | $4.32x10^{-5}$ | 5 |
| Fibreglass with Nomex honeycomb core (4x4 mm cell (6 mm deep) size) composite | 0.5 | 127 cells filled with 50% water | 2 | $1.6x10^{-5}$ | $4.32x10^{-5}$ | 3 |
| Fibreglass with Nomex honeycomb core (4x4 mm cell (6 mm deep) size) composite | 0.5 | 127 cells filled with 100% water | ~~2~~ | $1.6x10^{-5}$ | $4.32x10^{-4}$ | 0.5 |

### 4.2.2 Selection of a heating mechanism

Three different heating modes were applied to sample material. 1) a flash lamp producing a 1.5 kJ square pulse for a duration of 5 ms, 2) one (0.5 kW) halogen lamp, and 3) a 3-kW hot air blower for a duration of 10 s.

The first experimental session was performed to evaluate a suitable heating mode. Based on the data indicated in Table 4.2, it was observed that the Halogen lamp revealed higher signal–to-noise ratio (SNR) of 39.56 and delta temperature signal (-4.38℃). The thermal contrast is relatively lower (69%) compared to Flash and hot airgun heating. It is for this reason that the halogen lamp was a preferred heating technique.

Table 4.2. Optimum water detection parameters (heating techniques).

| Heating technique/Test scenario | Signal-to-Noise Ratio (SNR) | $\Delta T_m$ (℃) | $C_m$ |
|---|---|---|---|
| **Halogen lamp heating** | 39.56 | -4.38 | -0.69 |
| **Flash lamp heating** | 21.71 | -1.34 | -0.81 |
| **Hot air heating** | 22.49 | -1.26 | -0.87 |

### 4.2.3 Experimental protocol (AIRT)

Three sets of seventy (70) cells in a 100×200 mm specimen were filled with water according to the indicated scenarios (100%, 50%, and 25%). Twenty specimen cells were opened and filled with 50% and 25% water to analyse the effect of capillary forces on the internal surfaces of the cells subjected to rotation. Most experiments were conducted by using the halogen lamps for thermally stimulating the specimens (Figure 4.1b). As in Table 4.2, the hot air gun and the flash lamp provided weaker temperature signals, especially for cells with low water content (25%) under non-uniform heating.

The shiny glass fibre skin has a low emissivity of about 0.6, being slightly transparent toward both IR radiation and visible light. A self-adhesive PVC film was applied to experimental samples to enhance material emissivity. The stimulation was fulfilled using a single halogen lamp, 1 kW, and the heating duration was 2, 3 and 5 seconds in all scenarios. The results presented in the work are those of the 5s heating period. The thermal response was collected by an Optris PI 450i IR Camera (image format 382 × 288, temperature resolution 40 mK, spectral range 7.5-13 μm). A series of 1000 digitised images with 382 × 288 pixels with 12-bit

resolution collected by the camera with a sampling rate of 1 Hz were processed using the ThermoFit Pro software from TPU.

#### 4.2.3.1 Experimental protocol for horizontally oriented structure.

The schematic diagram and the actual experimental set-up for the horizontal structure are shown in the Figures. 4.1 and 4.2, the specimen was covered with black adhesive tape to minimize reflection and increase emissivity. The correct water volume using a syringe (25%, 50%, and 100%) was injected in cells through the rear surface of the specimen. The adhesive tape was used to protect water from exiting cells during orientation.

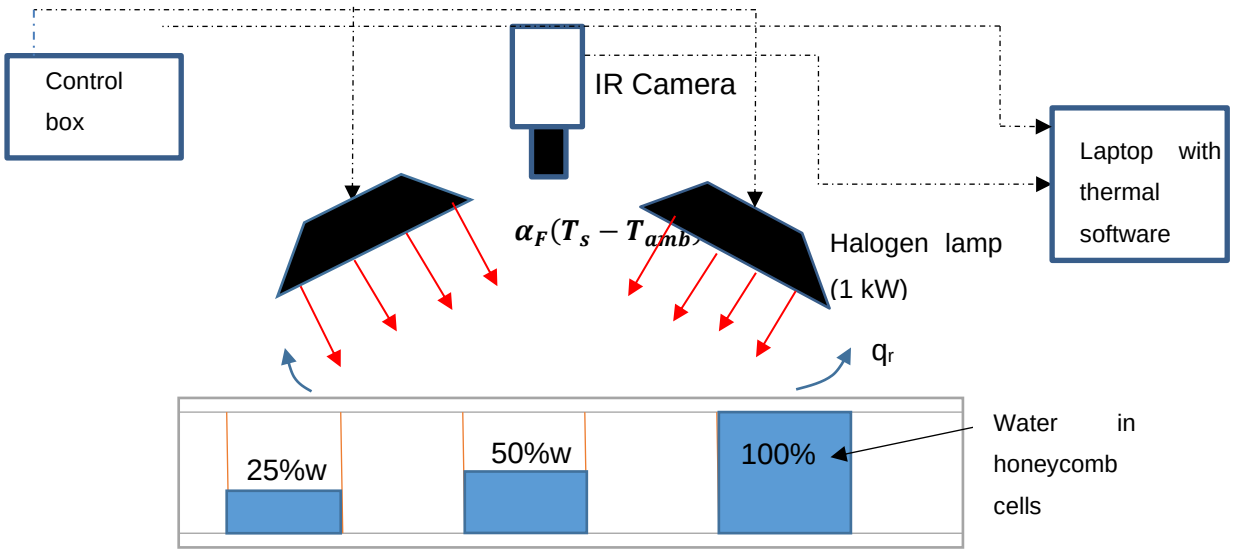


Figure 4.1: Schematic diagram of the experimental set up for the infrared thermography testing

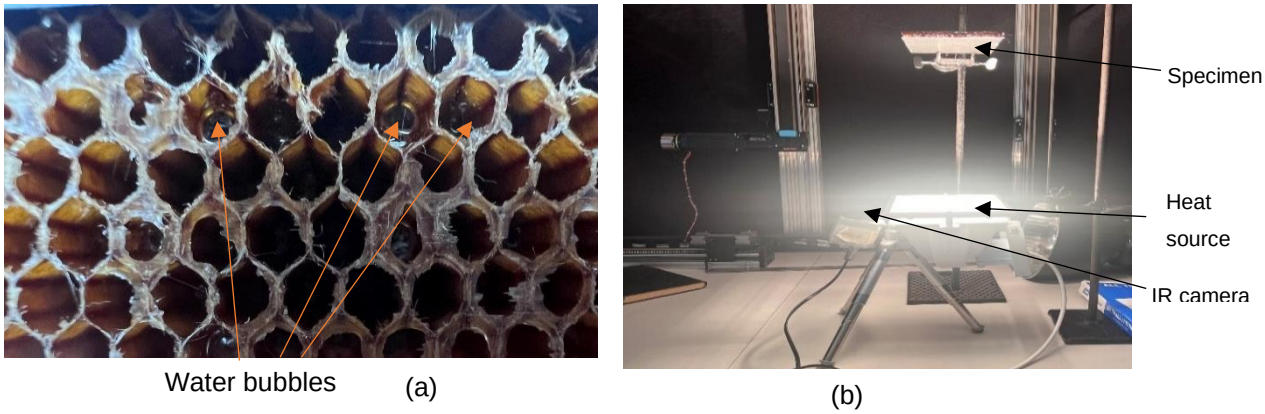


Figure 4.2: Honeycomb cells (a) and experimental setup (b)

After a comparison in terms of Signal-to-Noise ratio (SNR) between different heating techniques (source), i.e. 300 kW halogen lamps, hot air gun (300W-50Hz-220V), and flash lamp (1.4 kJ), the halogen lamp heating revealed relatively high SNR under similar experimental conditions. So, the experiments were carried out using the halogen lamps.

The heating took place on both surfaces. The top surface heating was used to investigate the influence of air gaps (25% and 50%) in the detectability of water in cells. The SNR, the differential temperature signals on the surface ($\Delta T$), the surface temperature contrast (($C_m$), and observation time ($t_c$ and $t_{\Delta T}$) were used to differentiate between cells filled with water at different levels.

The data were obtained as image sequences recorded using thermal lab software. Each pixel is representing the phase at fixed frequency. In this case, 1Hz sampling rate frequency and 16Hz fixed phase frequency was used.

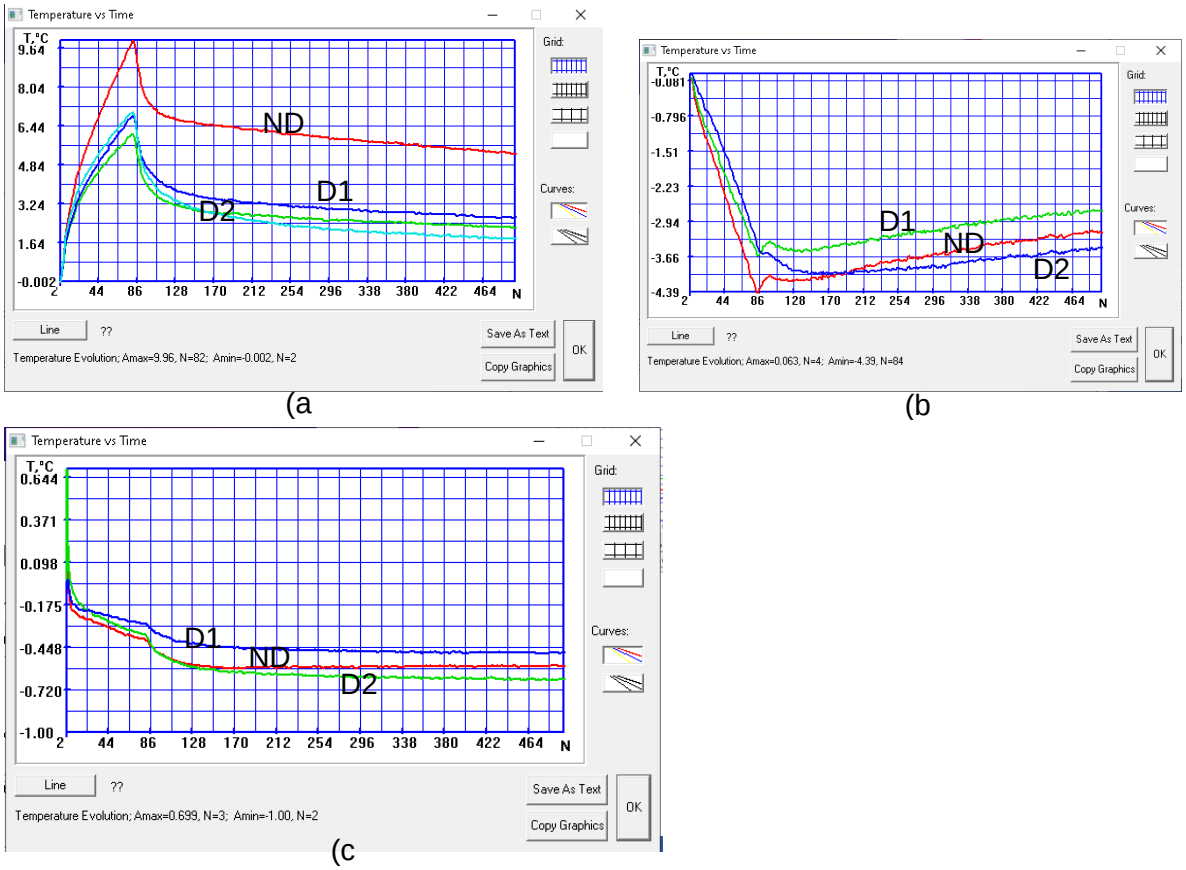


Figure 4.3: Temperature evolutions on front of cells filled with water at 25 %(D1), 50% (D2) and 100% (D3) in a 8 mm thick honeycomb structure: (a) front surface temperature versus time; (b) differential temperature signals versus time; (c) running contrast versus time

The results of the image sequence of the horizontally oriented structure are presented by images in Figure 4.4. The sequence had a total number of 500 images. In this case, images 185 and 224 were selected for analysis because they produce maximum and minimum parameters ($\Delta T$, $C_m$, $t_{\Delta T}$, $t_{Cm}$, SNR). It can be observed that based on the heating power, the temperature at the end of heating in a non-defect area (224,185 – a spot between D2 and D3) is 8.7$^{o}$C

<table>
<tr>
<td> 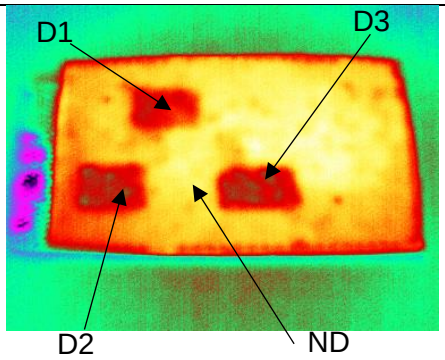
</td>
<td> 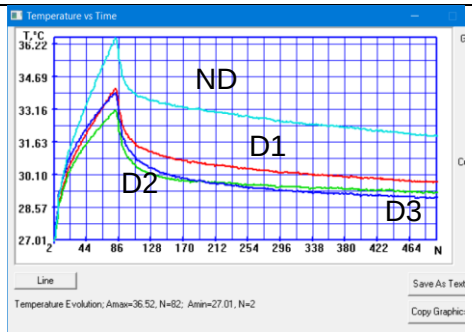
</td>
</tr>
<tr>
<td></td>
<td>All point data obtained with averaging 5x5</td>
</tr>
<tr>
<td> 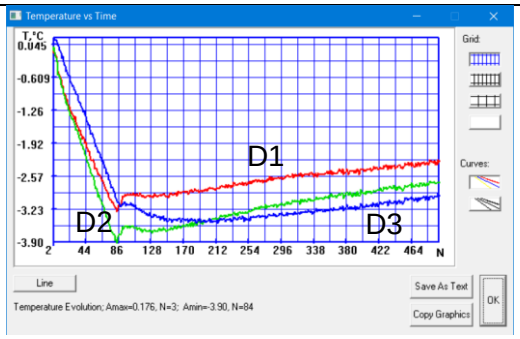
</td>
<td> 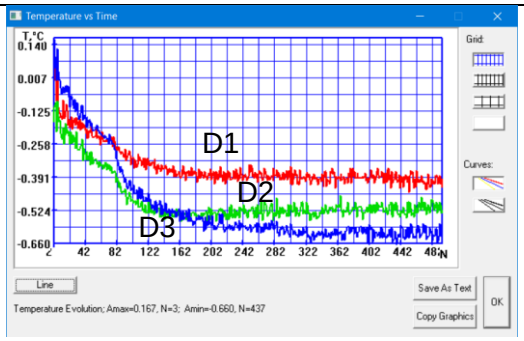
</td>
</tr>
<tr>
<td>Delta Temp vs time Max signals: D1: -2.68ºC (No. 185, i.e. 11.6 s), D2: -3.54ºC (No. 141, i.e. 8.8 s), D3: -3.4ºC (No. 249, i.e. 15.6 s)<br>Note: To avoid division by zero, images No. 2,3,4,5, and 6 were deleted from the sequence.</td>
<td>Contrast vs time Max signals: D1: 0.445 (No. 438, i.e. 27.4 s), D2: -0.546 (No. 156, i.e. 9.8 s), D3: -0.641 (No. 396, i.e.24.8 s)</td>
</tr>
<tr>
<td> 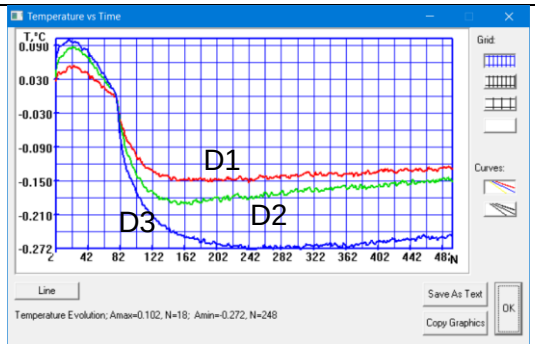
</td>
<td> 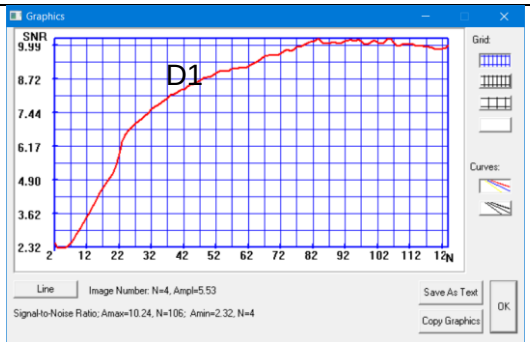
</td>
</tr>
<tr>
<td>Delta Temperature after sequence normalized by the end of heating, i.e. image No. 77, or 4.8 s</td>
<td>SNR for a raw sequence after averaging the sequence by 4 images<br>Source SNR=10.24 (No. 106, i.e. 6.6 s)</td>
</tr>
</table>

Figure 4.4: Temperature evolutions on front of cells filled with water at 25 %( D1), 50% (D2) and 100% (D3) and the Signal-to-Noise ratio.

## 4.3 Image Processing Protocol

The image sequence was recorded using an Optris pi 450i IR Camera (image format 382 × 288, temperature resolution 40 mK, spectral range $7.5 - 13\ \mu m$, frame rate 80Hz). The ThermoFit Pro software from TPU was used to process them.

At first, the image sequence is converted from the “FS” file to disc image format which can be used to create a scenario in the ThermoFit software. Normally, the first image of the scenario is assumed to be that of ambient temperature and therefore, the background option on the preview window is used to subtract the first image from the sequence to deal with excess temperatures only. The sequence with a specified mask is spatial filtered before appropriate processing algorithms are selected.

The differential temperature signals ($\Delta T_m$) and running temperature contrast ( $C_m$ ) can directly be determined on the preview window.

### 4.3.1 Signal-to-noise ratio (SNR)

SNR is a measure that compares the level of the desired signal to the level of background noise. In this analysis, the signal is typically the response of heat flow in a sample specimen, while noise refers to random fluctuations or errors in the measurement. In this analysis, high SNR indicates that the signal is much stronger than the noise, suggesting high-quality data with clear thermal events or transitions. Meanwhile, low SNR indicates that the noise level is comparable to or exceeds the signal level, which indicates poor detection and visibility of water in the cells. ThermoFit has built-in tools for SNR evaluation as indicated in Figure 4.5. As indicated in previous research by Vavilov et al. (2020), an SNR greater than 10 is good quality data suitable for analyses of subsurface defects.

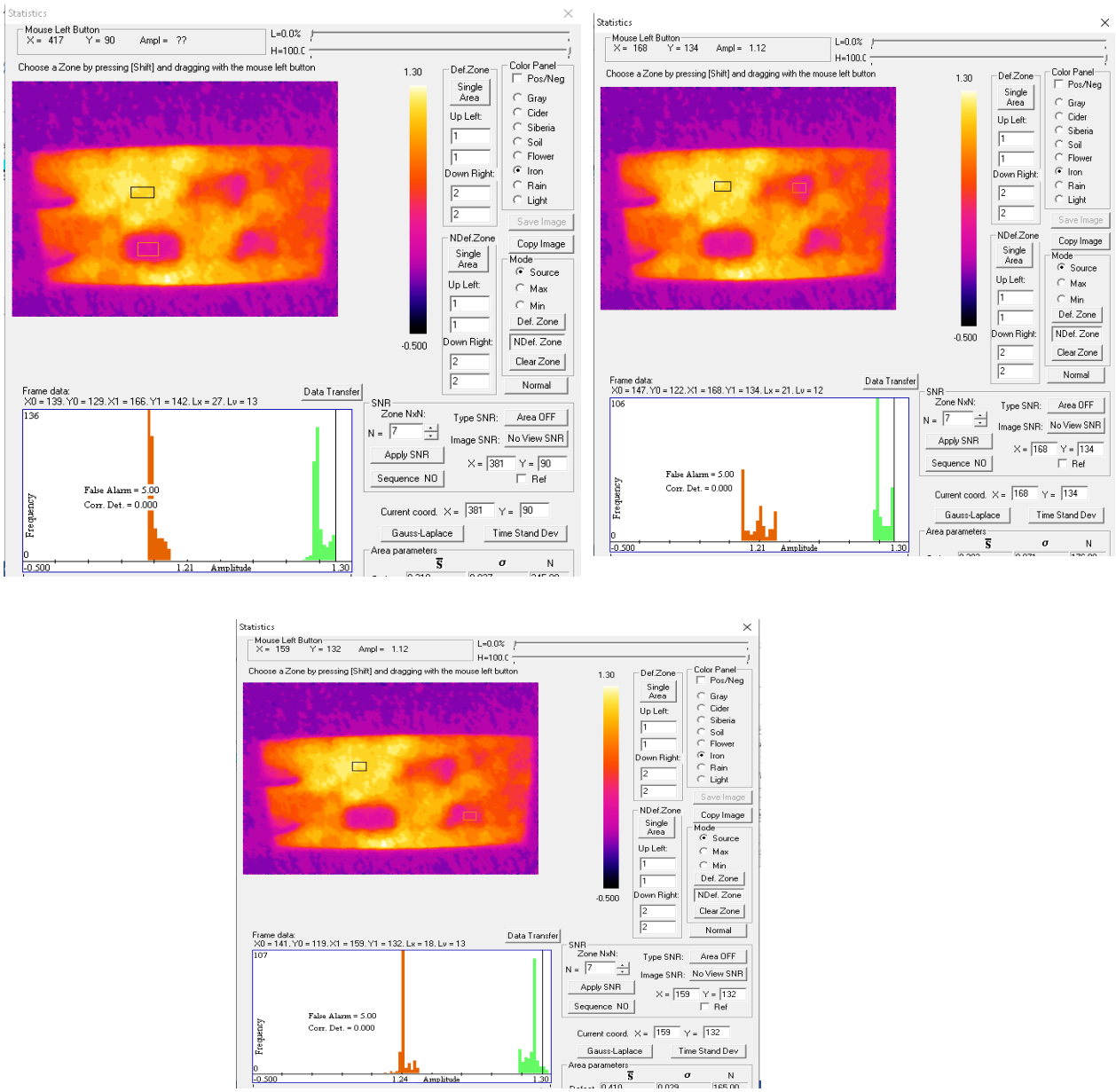


Figure 4.5. SNR of samples with water in cells at 25%, 50%, and 100%

In addition to section 4.6.5, image #74 from the horizontal samples specimen was selected for processing, and the SNR of different algorithms were compared. It demonstrates the effectiveness of different types of image-processing algorithms. The algorithm with relatively high SNR was preferred. In this case, the Fourier phase ($4^{th}$ harmonic) produces higher SNR across all cells (25%,50% and 100%). The same procedure was done for the rest of the images.

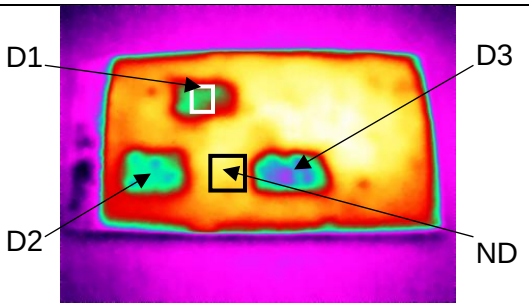


D1 Source SNR=9.8 (No. 74, i.e. 4.6 s)
Chosen defect and non-defect areas are shown

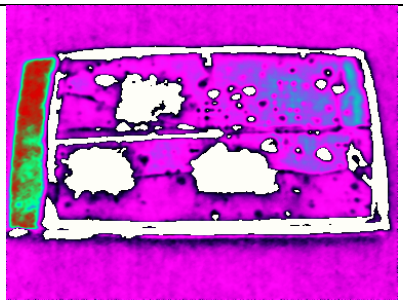

D1 Fourier Phase SNR=13.0 (No.4)

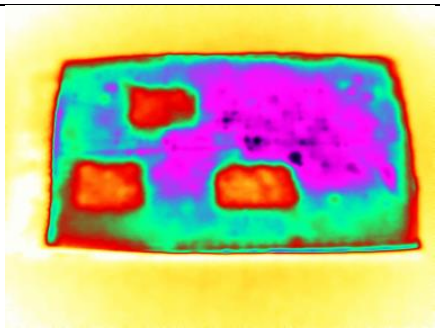

D1 PCA (1) SNR=9.7

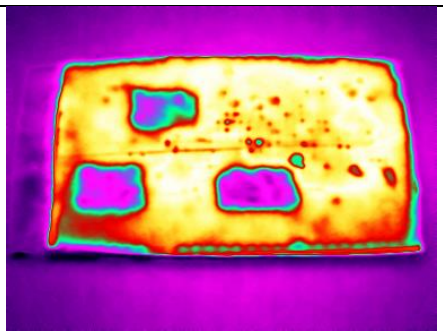

Correlogram SNR=24.19

Figure 4.6. Processed images for horizontal

| Image | SNR | | |
|---|---|---|---|
| | D1 | D2 | D3 |
| Source | 9.8 (No. 74, or 4.6 s) | 10.1 (no. 79, or 4.9 s) | 10.4 (no. 84, or 5.3 s) |
| Fourier phase | 69.9 (4$^{th}$ harmonic) | 88.1 (4$^{th}$ harmonic) | 77.1 (4$^{th}$ harmonic) |
| PCA | 9.7 (1$^{st}$ component) | 9.2 (1$^{st}$ component) | 9.7 (1$^{st}$ component) |
| Correlogram | 24.9 | 16.2 | 18.7 |

## 4.4 Experimental Protocol for an Inclined Specimen

Similarly, the same specimen was set in inclined positions $(30°, 45°, \text{and } 60°)$. To avoid non-uniform heating, the heating source was set perpendicular to the test sample. This section forms a key part of the objectives of this work, which is to investigate the effect of the panel's inclination to the detectability and visibility of water ingress in honeycomb cells.

Practically, the fuselage has honeycomb panels at different orientations and cells partially filled with entrapped water dictate the position of water in them. Therefore, detecting ingress in a full spectrum of the fuselage plate orientations is necessary.

The specimen is set as indicated in Figure 4.6, and a similar data acquisition technique and procedure, as indicated in section 4.6.3, was used.

### 4.4.1 The sample specimen positioned at 30 degrees inclination.

In this scenario, the same sample was rotated and set at 30° inclination, and parameters like those for the horizontal (180°) sample were recorded and analysed. Like a horizontal position, the presence of an air gap provides heat resistance through cells. It can be observed that based on the heating power, the temperature at the end of heating in a non-defect area (224,185 – a spot between D2 and D3) is 10.0$^{o}$C.

The absorbed power at this position is about 3 times less than in the horizontal position (compare excess temperatures at the end of heating) and the processed images are presented in figures 4.8

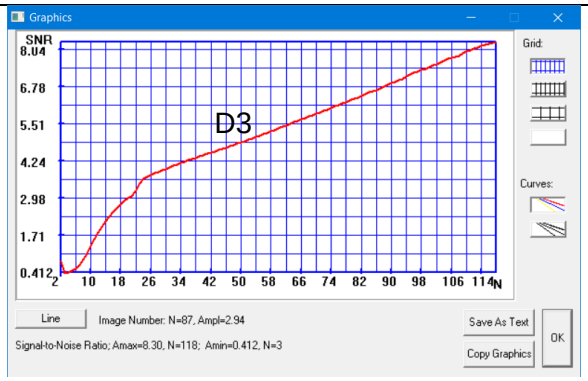


SNR for D3. Note that there is no maximum to compare to the horizontal position

Figure 4.7. SNR for the 30-degree inclined sample

| Image | SNR | | |
|---|---|---|---|
| | D1 | D2 | D3 |
| Source | 5.0 (No. 118, last in the reduced sequence, i.e. 29.5 s) | 6.5 (no. 117, or 29.3 s) | 8.3 (No. 118, last in the reduced sequence, or 29.5 s) |
| Fourier phase | 9.0 (3$^{rd}$ harmonic) | 13.3 (3$^{rd}$ harmonic) | 48.5 (3$^{rd}$ harmonic) |
| PCA | 4.5 (1$^{st}$ component) | 5.2 (1$^{st}$ component) | 5.9 (1$^{st}$ component) |
| Correlogram | 4.8 | 5.6 | 6.3 |

* Note that if a sample is under 30° the water in D1 and D2 changed configuration to compare to the horizontal position. Therefore, the defect areas D1 and D2 are not uniform in this case, which contributes to the changed SNR.

From the data above, the Fourier phase algorithm provides a better SNR of 48.5 (3rd harmonic) for cells D3(filled with 100% water). Also, it can be observed that the SNR is water content (m) dependent because 25% water has a lower SNR than 100% water-filled cells. It indicates that cells with 100% water content (contact with skin) can easily be visualised as opposed to those with air gaps. The sample of the processed images is presented in Figure 4.8

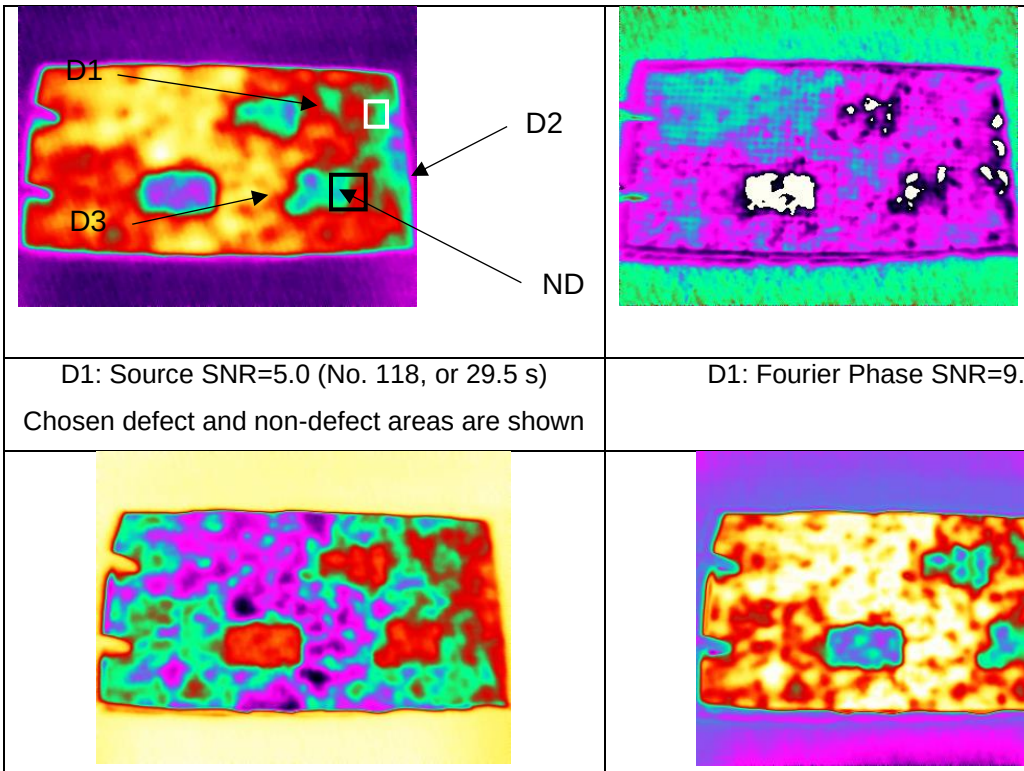


D1: Source SNR=5.0 (No. 118, or 29.5 s)
Chosen defect and non-defect areas are shown

D1: Fourier Phase SNR=9.0 (3rd)

D1: PCA (1st) SNR=4.5

D1: Correlogram SNR=4.8

Figure 4.8: results of image processing (30$^{o}$)

### 4.4.2 Sample specimen positioned at 60 degrees inclination.

It can be observed that based on the heating power, the temperature at the end of heating in a non-defect area (224,185 – a spot between D2 and D3) is 9.7°C.

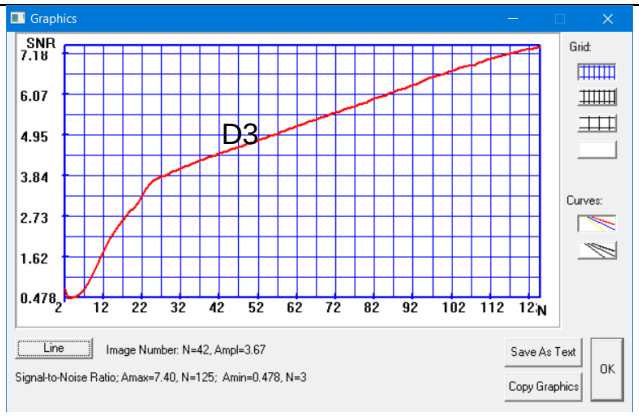


SNR for D3. Note that there is no maximum to compare to the horizontal position

Figure 4.9. SNR for the 60-degree inclined sample

| Image | SNR | | |
|---|---|---|---|
| | D1 | D2 | D3 |
| Source | 7.4 (No. 125, last in the reduced sequence, or 31.3 s) | 6.5 (no. 125, or 31.3 s) | 7.4 (No. 125, last in the reduced sequence, or 31.3 s) |
| Fourier phase | 16.8 (5$^{th}$ harmonic) | 21.9 (5$^{th}$ harmonic) | 26.2 (5$^{th}$ harmonic) |
| PCA | 5.5 (1$^{st}$ component) | 5.4 (1$^{st}$ component) | 5.8 (1$^{st}$ component) |
| Correlogram | 5.0 | 5.0 | 5.4 |

* Note that if a sample is under 60°, the water in D1 and D2 changed configuration compared to the horizontal position. Therefore, the defect areas D1 and D2 are not uniform in this case, contributing to a slightly higher end of heating temperature compared to the horizontal sample.

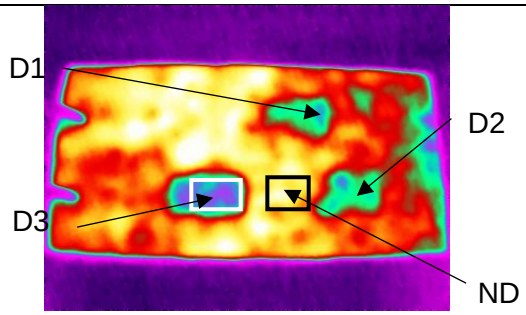


D3: Source SNR=7.4 (No. 125, or 31.3 s)
Chosen defect and non-defect areas are shown

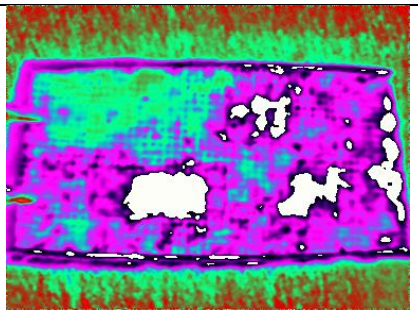

D3: Fourier Phase SNR=26.2 (5th)

| | |
|---|---|
| 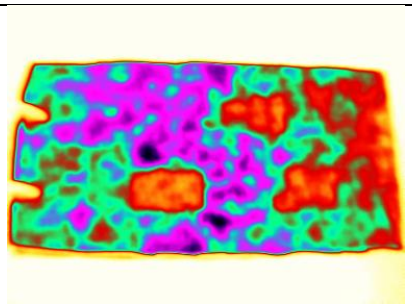 | 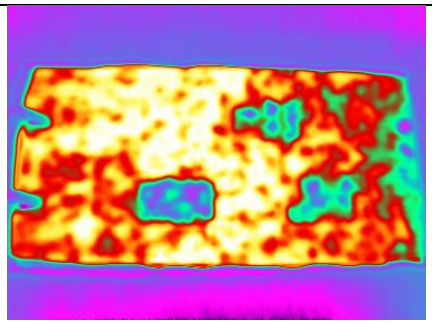 |
| D3: PCA (1st) SNR=5.8 | D3: Correlogram SNR=5.4 |

Figure 4.10. Results of image processing

### 4.4.3 Experimental protocol for the vertical inclination

In a vertical panel, water is in contact with the skin surface on both sides, and heat conduction only occurs through 25% and 50% of the water in the cells. These cells reveal a similar trend as that of 100% filled water. In fact, the significant deviation of the surface temperature variation is due to the presence of air in cases of 25% and 50%. It can be observed that based on the heating power, the temperature at the end of heating in a non-defect area (224,185 – a spot between D2 and D3) is 11.0$^{o}$C.

| | |
|---|---|
| 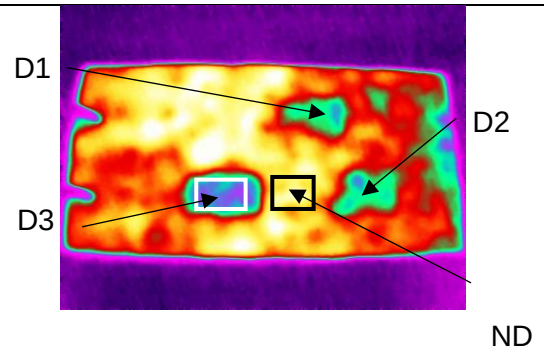 | 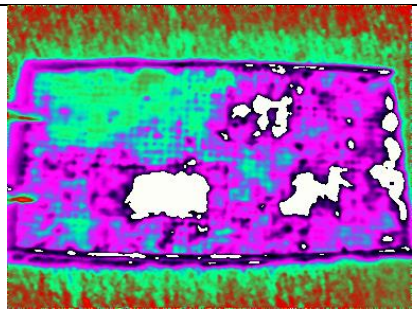 |
| D3: Source SNR=7.4 (No. 125, or 31.3 s) Chosen defects and non-defect areas are shown | D3: Fourier Phase SNR=50.3 (5th) |
| 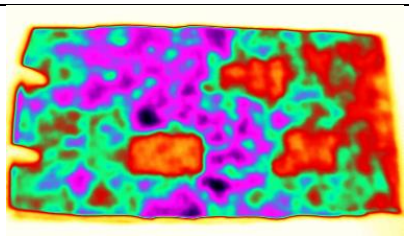 | 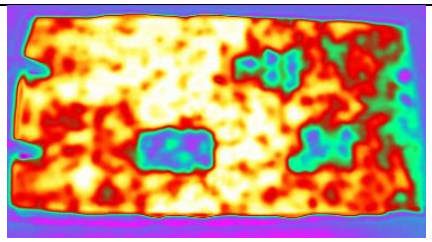 |
| D3: PCA (1st) SNR=5.3 | D3: Correlogram SNR=5.0 |

Figure 4.11 Results of image processing (90°)

| Image | SNR | | |
|---|---|---|---|
| | D1 | D2 | D3 |
| Source | 5.2 (No. 125, last in the reduced sequence, or 31.3 s) | 6.3 (no. 125, or 31.3 s) | 7.4 (No. 125, last in the reduced sequence, or 31.3 s) |
| Fourier phase | 17.5 ($5^{th}$ harmonic) | 20.2 ($5^{th}$ harmonic) | 50.3 ($5^{th}$ harmonic) |
| PCA | 4.2 ($1^{st}$ component) | 4.9 ($1^{st}$ component) | 5.3 ($1^{st}$ component) |
| Correlogram | 3.9 | 4.5 | 5.0 |

* Note that if a sample is in a vertical position, the water in D1 and D2 changed configuration compared to the horizontal position. Therefore, the defect areas D1 and D1 are not uniform in this case, which contributed to a slightly higher end of heating temperature compared to 30° and 60° inclined samples.

### 4.5 Comparison of Results

The comparison between the SNR values for different specimen orientations is presented in Table 4.3. Generally, the horizontal plate reveals higher SNRs for all applied logarithms, which translates into better visibility of water-filled cells. On the contrary, the 30° and 60° sample orientations are characterized by relatively low SNRs, and this could be explained by water leakage through the adhesive seal tap during rotation. Furthermore, the vertical orientation shows low SNR values, translating into image quality.

It was also observed that there is no particular algorithm which is the best for all scenarios when performing image processing.

Table 4.3. Efficiency of experimental data processing

| | **SNR (cells filled with 50% water)** | | | |
|---|---|---|---|---|
| **Sample orientation** | Source | Fourier phase | PCA | Correlogram |
| **Horizontal** | 10.1 | 88.1 | 9.2 | 16.2 |
| **$30^0$** | 6.5 | 13.3 | 5.2 | 5.6 |
| **$60^0$** | 6.5 | 21.9 | 5.4 | 5.0 |
| **Vertical** | 6.3 | 20.2 | 4.9 | 4.5 |

It is observed in Figure 4.10a, b that if a sample is positioned under 60º, the water in the defects D1 and D2 changed configuration compared to the horizontal position. As indicated previously, it could be because of leaks through the adhesive seal tap on the surface. Therefore, the defect areas D1 and D2 are not uniform in this case thus contributing to lower

SNR values, see results presented in sections 4.6.5.1, 4.6.5.2, and 4.6.5.3.

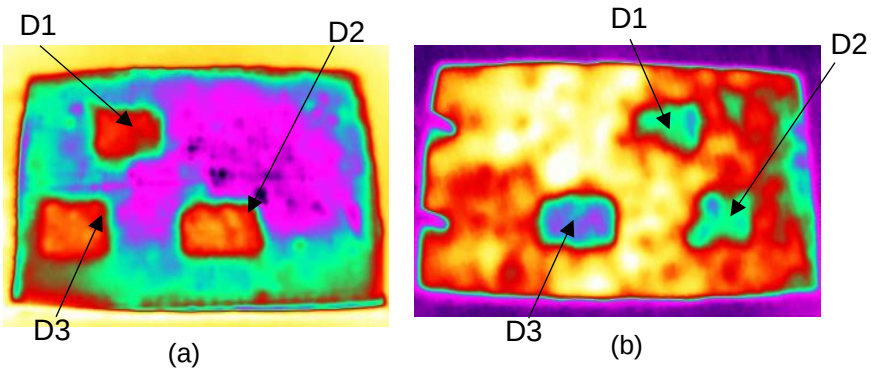


Figure 4.12: IR thermograms of the sample in different positions: a) horizontal (180°), b) Inclined at 60°

Table 4.4 Optimum water detection parameters (Fibreglass honeycomb, experimental results)

| | Scenario | Delta ($\Delta T_m$)℃ | Maximum time$t_m(\Delta T_m)s$ | Contrast $(C_m)$ | Maximum time$t_m(C_m)ms$ |
|---|---|---|---|---|---|
| **Front surface water (Separated by air gap)** | Cell filled with water (100%) in a Horizontal panel ($t_h = 5s$) | -6.5 | 0.72 | -0.7 | 5 |
| | Cell filled with water (50%) in a Horizontal panel $180^0$ ($t_h = 5s$) | -3.96 | 0.94 | -0.59 | 1.94 |
| | Cell filled with water (50 %) in a Vertical panel $90^0$ ($t_h = 5s$) | -4.8 | 0.75 | -0.55 | 2.5 |
| | Cell filled with water (50 %) in an inclined panel $30^0$ ($t_h = 5s$) | -3.71 | 0.83 | -0.58 | 1.76 |
| | Cell filled with water (50 %) in an inclined panel $60^0$ ($t_h = 5s$) | -4.5 | 0.72 | -0.51 | 3 |
| **Rear surface water (water is in contact with skin)** | Cell filled with water (50%) in a Horizontal panel $180^0$ ($t_h = 5s$) | -4.8 | 0.81 | -0.69 | 2.75 |
| | Cell filled with water (50 %) in a Vertical panel $90^0$ ($t_h = 5s$) | -4.8 | 0.75 | -0.55 | 2.5 |
| | Cell filled with water (50 %) in an inclined panel $30^0$ ($t_h = 5s$) | -6.2 | 0.87 | -0.72 | 1.32 |
| | Cell filled with water (50 %) in an inclined panel $60^0$ ($t_h = 5s$) | -4.8 | 0.58 | -0.67 | 1.56 |

## 4.6 Phase Change Evaluation

As indicated previously that when aircraft is under exploitation in high altitude, water ingress freezes (volumetric expansion) and upon landing, due to temperature difference, frozen water starts melting at 0°C. This process is critical in the detection of water ingress because water in a solid phase absorbs more heat energy than in a liquid phase. The delta temperature and contrast were higher with a shorter observation time$(t_m)$. The investigation of this phenomenon can either be done through passive or active heating. This work presents the results of both modes of heating.

The experimental procedure started by placing a sample with cells filled with water at 100%, 50% and 25% in a freezer for about 2 days for a complete phase change (liquid to solid). After that, a sample was placed in a thermographic “black chamber” for passive heating, and the surface temperature was monitored by an Optris pi 450i IR Camera. Passive heating is a practical phenomenon when the aircraft has landed after exploitation. In this experiment, the additional heat from the surroundings, the operators and other heat sources were avoided to obtain meaningful results.

The second step was to use active heating with double halogen lamps, 1kW each, producing a square pulse phase of 1Hz. The sample was heated for about two minutes and 30 minutes of cooling. It can be observed from Table 4.5 (a) that a cell filled with 100% water has higher SNR across all processing algorithms for both heating techniques. It means that this cell is better detected, as shown in Figure 4.12 Similarly, the data in Table 10 (b) show that this cell (100% water) has the highest $\Delta T$ and$C_m$.

Table 4.5 (a). Optimum water ingress detection parameters (effect of phase change).

| **Heating Technique** | **Image processing algorithm** | **Signal-to-Noise Ratio (SNR)** | | |
|---|---|---|---|---|
| | | 25% | 50% | 100% |
| **Passive** | Correlation | 30.2 | 37.4 | 50.2 |
| | Derivative | 4.8 | 5.3 | 5.8 |
| | Fourier | 27 | 28.2 | 75.8 |
| | PCA (3 Component) | 108.8 | 114.4 | 143.1 |
| **Active** | Correlation | 1.46 | 1.74 | 9.5 |
| | Derivative | 3.54 | 5.83 | 10.9 |
| | Fitting 2 | 3.71 | 5.9 | 38.3 |
| | Fourier | 3.47 | 5.52 | 28.9 |
| | PCA (3 Component) | 5.39 | 7.94 | 44.82 |

Table 4.5 (b). Optimum temperature signals and temperature contrast (phase change)

| | $\Delta T$, ℃ | | | $C_m$ | | |
|---|---|---|---|---|---|---|
| | 25% | 50% | 100% | 25% | 50% | 100% |
| Active Heating | -17.53 | -21.43 | -26.52 | -0.37 | -0.48 | -0.53 |
| Passive Heating | -10.14 | -10.65 | -10.72 | -0.467 | -0.469 | -0.473 |

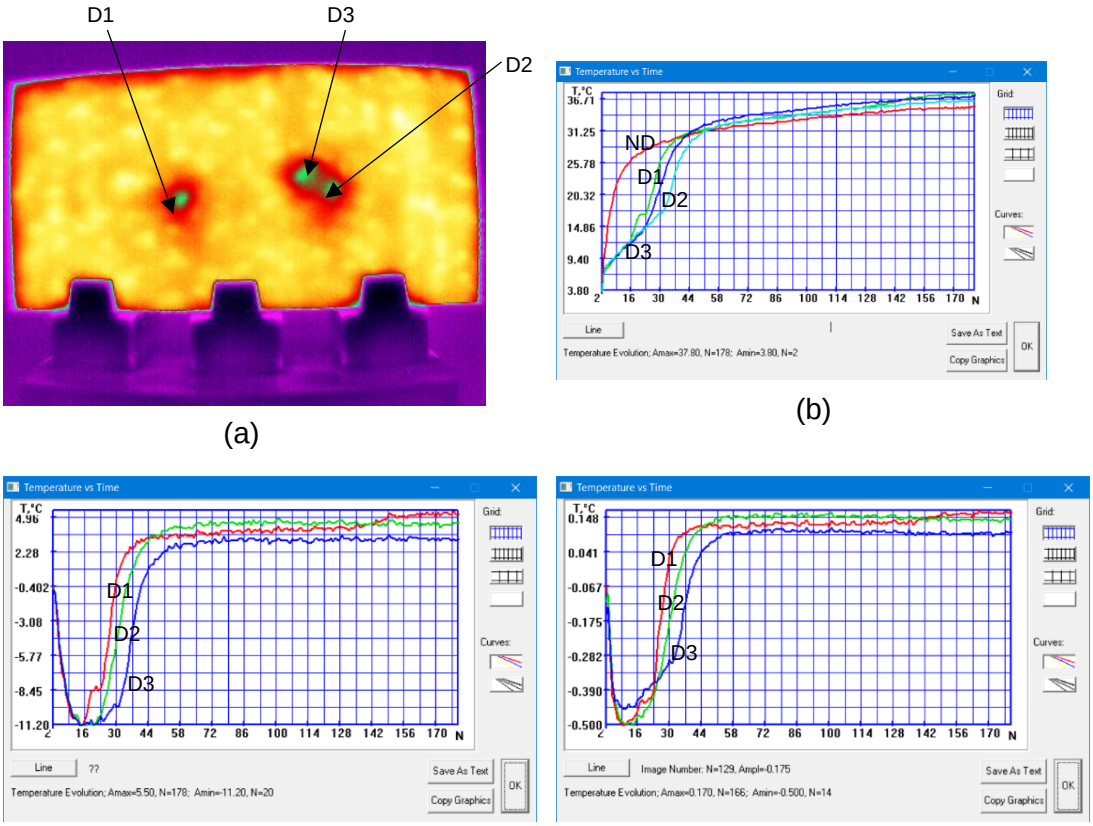


Figure 4.13: Phase change with passive heating a) raw image, b) Temperature variation c) Delta temperature variation d) Contrast

**Note**: D1 (25%); D2 (50%); D3 (100%); ND (Non-defect area)

### 4.6.1 Image processing

This section focuses on the Image processing of the image sequence of the samples with frozen water from passive and active heating. Initially, high-resolution thermal images are captured using infrared cameras, ensuring consistent environmental conditions to minimize noise and artifacts. Preprocessing steps such as noise reduction through Gaussian filtering and calibration for emissivity differences are critical in enhancing the image quality. Image processing algorithms such as Fourier phase, Principal component analysis (PCA), Time gram, Tomogram, Correlogram, and Tomography (negative time gram, upper threshold). The resulting images of these algorithms are compared and analysed.

The analysis of these cells with frozen water focuses on understanding their spatial distribution, which can inform structural integrity assessments and thermal performance evaluations. The processed images from the passive heating thermography (30s) of selected algorithms are presented in Figure 4.13.

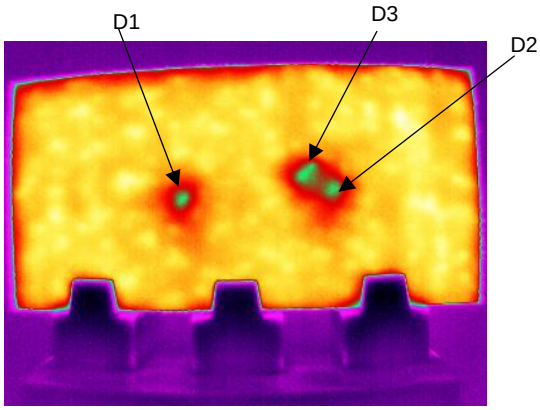


(a)

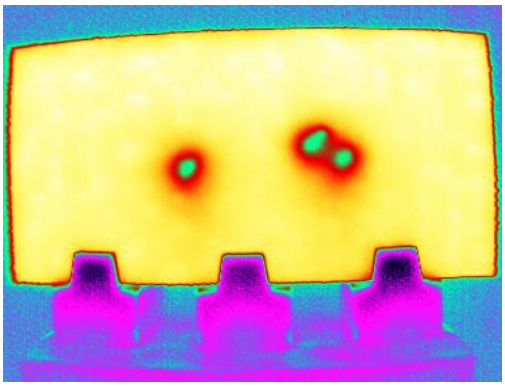

(b)

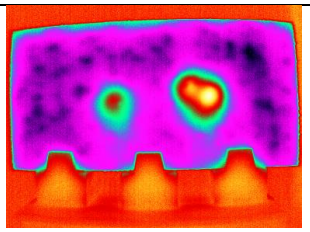

Fourier phase#4

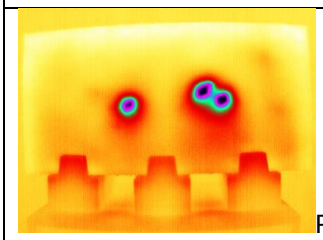

Principal component analysis (component 2)

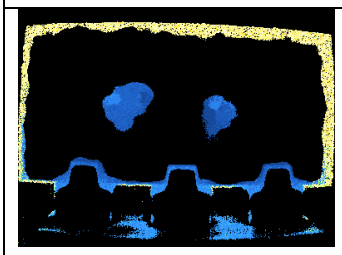

Time gram Upper threshold

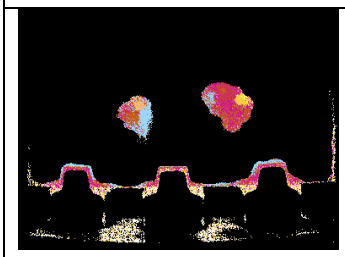

Tomogram

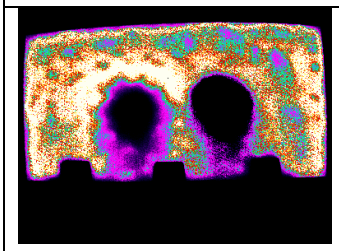

Correlogram

Figure 4.14: Image processing (passive heating) a) raw image, b) removed background

### 4.6.2 Active heating

Active heating was applied when the sample was taken from the freezer with a time step of 1 second. The surface temperature evolution was recorded. The original raw image was processed using similar algorithms as in passive heating. In this section, the raw image was

processed, and the background was subtracted. The results and image processing thermograms are presented in Figures 4.13 and 4.14.

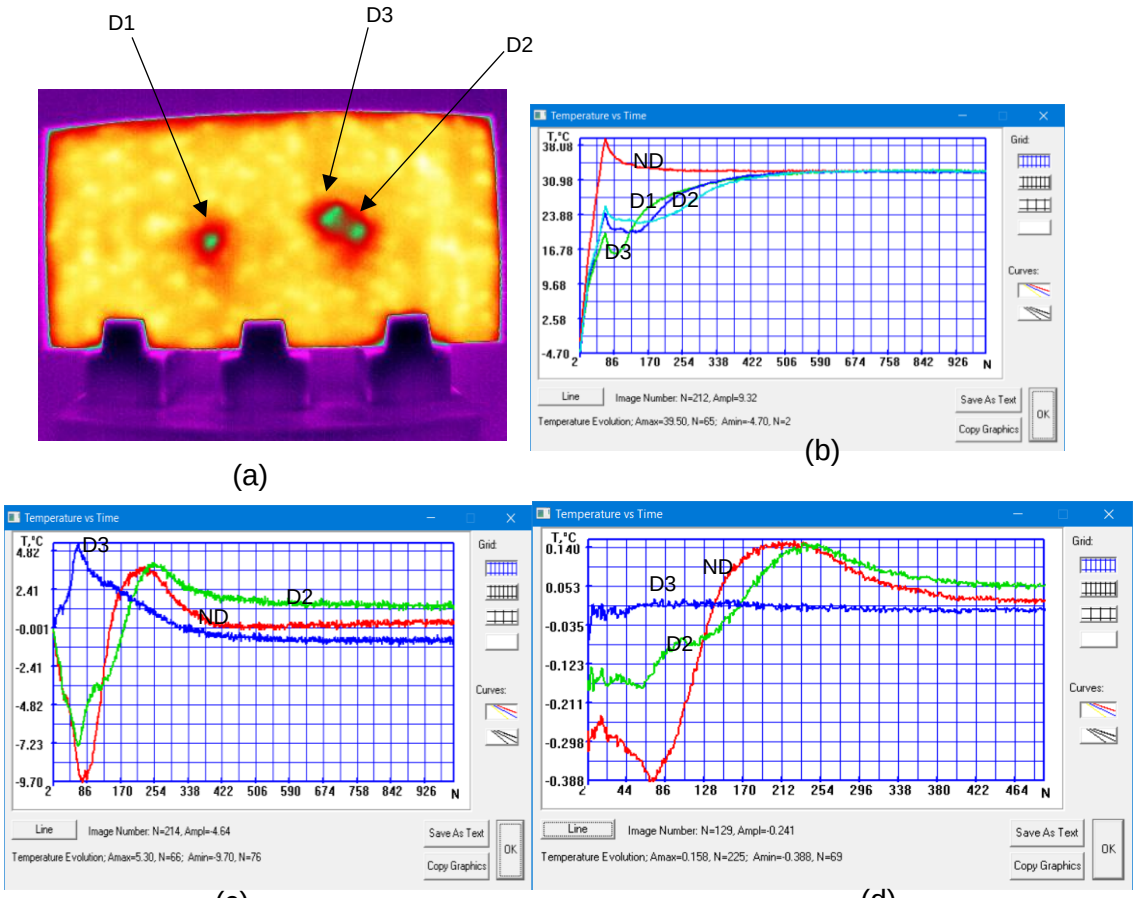


Figure 4.15: Phase change with active heating a) raw image, b) Temperature variation c) Delta temperature variation d) Contrast

**Note**: D1 (25%); D2 (50%); D3 (100%); ND (Non-defect area)

### 4.6.2.1 Image processing (active heating)

Due to high heating intensity in the active heating, the frozen water in cells melts quicker than when the passive heating is applied. It can be observed in the processed images below that with similar algorithms applied, the frozen water in cells is poorly detected and its visibility is also poor.

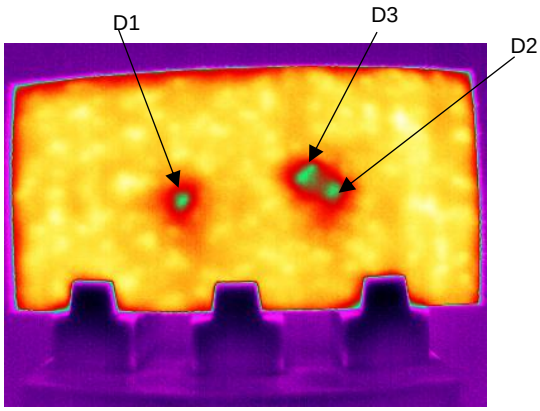


(a)

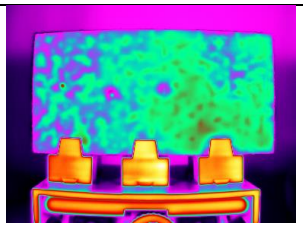

Fourier magnitude#3

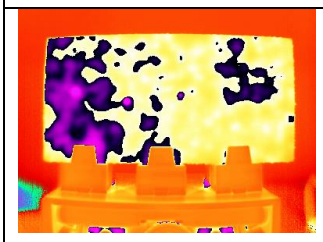

Fourier phase#3

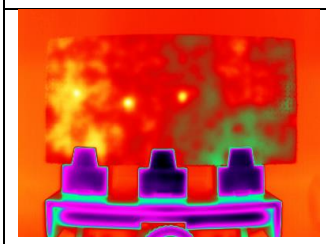

Principal component analysis (1)

Figure 4.16: Image processing with active heating a) raw image, b) removed background and noise

## 4.7 Water Mass (Content) Determination Technique

This section presents a calibration curve using the experimental data to estimate water content in the cells of honeycomb structures. The focus is on the depth and not in a lateral direction. According to Vavilov et al. (2016), the actual estimation of water content in the honeycomb cell is a challenging task. It requires water to be in contact with skin surface for estimation, which means if the inspection is from a rear side of a 50% water filled cell, the estimation will indicate that the cell is fully filled with water, which is not the case. If all cell walls (Nomex paper) are removed, the area occupied by water increases which has little or no effect to the temperature contrast and delta temperature.

However, in an aviation industry, the determination of the amount of water ingress in the fuselage typically involves several estimation methods and procedures. Such methods include visual Inspection whereby the aviation technicians and inspectors regularly visually inspect the exterior of the fuselage for signs of water accumulation and its severity. Cells filled with 100% water will have bigger water stains, streaks, or discoloration on the exterior surfaces opposed to partially water filled cells (25% and 50%). The Drainage and Collection technique is also used whereby Some aircraft are equipped with drainage systems designed to collect and expel water that enters the fuselage during flight or while on the ground. Water drained from various spots (cells) is quantified.

It has been proven that for cells with 100% water produce similar delta temperature regardless of the water quantity in x and y directions. The cells with 50% filled with water (z-direction) produce less delta temperature ($\Delta T_m$ ) to that of 100% water. Therefore, it suggests that water content (mass) has an effect to the delta temperature as well as the contrast ($C_m$). It was also found that the cells walls have an insignificant effect in $\Delta T_m$. The comparison between delta temperatures of the cell filled with100% water partitioned by walls, without walls, and the increased water occupation area is presented in Table 4.6.

Table 4.6 Water mass justification

| **Scenario** | $\Delta \boldsymbol{T_m}(℃)$ | $\mathbf{t_m}(\boldsymbol{s})$ |
|---|---|---|
| 100% water with walls | -56.17 | 6 |
| 100% water with no walls | -56.2 | 6 |
| 100% water with increased water occupation area | 57.57 | 6 |

Based on the data provided, this section will only emphasise on the method and procedure of quantifying water in cells (in z-direction) by introducing an approximate calibration curve of water mass in percentage vs delta temperature ($\Delta T_m$) is presented. This curve will be used as a guideline on how to quantify water if cells are100%, 50%,25% filled with water or in between depending on the recorded delta temperatures.

Considering the active thermography experimental data presented in table 4.5(b), the critical relationship between the water content in cells (in percentage of occupancy) and the optimum temperature signals ($\Delta T\ ^0c$). It can be observed that cells filled with 100% water reveal higher (-ve) surface temperature signals as opposed to 25% and 50%. The approximate calibration curve below could be of a great guiding tool for aviation engineers to estimate water content in honeycomb cells. Please note that the estimation is only in z- direction (depth). In fact, the water content in terms of mass and volume can be determined once the actual sizes of cells (depth and width) as well as water properties such as density are known.

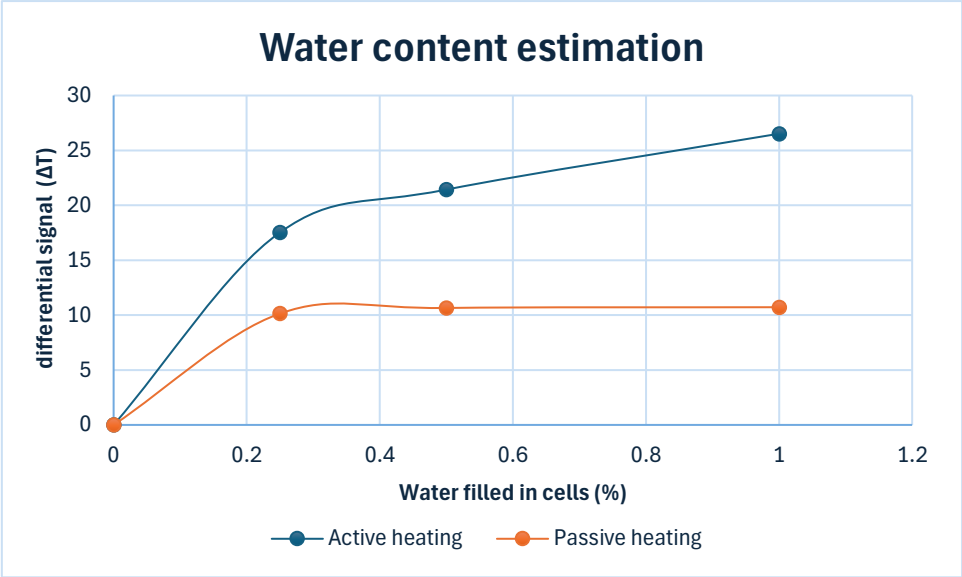


* The minus sign of $\Delta$T is omitted.

Figure 4.17: Approximate calibration curve

The calibration curve (Figure 4.17) provides essential data for estimating water content, illustrating the relationship between the intensity of the surface differential signal (ΔT, °C) and water content. Among the two heating methods tested (Active and Passive), the active heating technique shows a peak ΔT of 27°C, which corresponds to 100% water content, indicating that the cells are fully saturated with water (water in contact with the skin). At a ΔT of 20°C, the water content is approximately 32%, and at 25°C, it reaches around 80%. Water content can be expressed either by mass or by volume.

In contrast, with passive heating, the calibration curve rises with increasing water content until the ΔT reaches 12°C, corresponding to 34% water content. Beyond this point, the curve levels off, even as water content continues to increase. This could be due to rapid thermal equilibrium between the panel and its environment.

These results suggest that active heating yields a more dependable calibration curve, while passive heating is more effective for detecting water ingress.

## 4.9 Conclusion of the Results Obtained

The aircraft fuselage is primarily made up of honeycomb panels arranged in different orientations, and a one-sided thermographic inspection is typically performed after the aircraft lands. Experimental results show that panel orientation does not influence the signal-to-noise

ratio (SNR) values, indicating that the visibility of water trapped in the honeycomb cells remains unaffected by panel orientation.

At high altitudes, the low temperatures cause water in the cells to freeze. Upon landing, a sudden temperature change leads to melting, and during this process, experimental data indicates that the differential signals and contrast are greater than those observed in cells containing only water. Additionally, the observation times are shorter for cells with ice compared to those with liquid water. The significance of image processing in reducing noise and background irregularities has been highlighted to enhance water ingress detection.

Calibration curves for both active and passive heating suggest that cells with higher water content produce stronger differential signals in shorter observation times. These curves can serve as an effective method for estimating water content in the cells.

# CHAPTER 5:
# DISCUSSION OF EXPERIMENTAL AND NUMERICAL WORK

## 5.1 Introduction

In this chapter, the results of the numerical modelling (ThermoCalc-3D), Image processing (ThermoFit Pro) and the experiments using infrared thermography aimed at characterising water ingress in the honeycomb panels are discussed. The correlation between the variation of surface differential temperature signals over time, the running contrast, and their observation times are comprehensively discussed. The concept of SNR during water ingress detection and image processing is also discussed. Determining water content in honeycomb cells is a serious concern to aviation engineers. Therefore, the approximate calibration curve to estimate water content in cells is presented and discussed. For the numerical model (presented in Chapter 3), the results were obtained by the ThermoCalc-3D software and the ThermoDouble software for a 3D normalisation. The results from the experiments and the adopted protocol are presented and described in Chapter 4; the results (temperature), which were recorded by the infrared camera, are presented. The focus is on the presence of the water ingress as observed by the surface differential temperature signals on the specimens, running contrast, observation times and the SNR.

### 5.1.1 Numerical work (ThermoCalc 3D)

#### 5.1.1.1 Presence of water ingress in honeycomb panels

To illustrate the effect of the presence of water in cells of honeycomb panel, the numerical solutions of the surface differential temperature signals, running contrast, the observation times, and the signal to noise ratio (SNR) profile on the surface area of the specimen over the cells filled with water as well as the cells filled with air, were predicted during heating until the maximum heating period was reached. It was observed that a model with cells full of water (100%) can easily be detected, as shown in Figure 3.5 in Chapter 3.

#### 5.1.1.2 Differential temperature signals (ΔT) and the running thermal contrast ($C_{run}$)

The differential temperature signals on the surface of the model with water ingress at various depths and orientations were plotted in the ThermoCalc-3D software. Similarly, the running thermal contrast of the model with similar conditions as above were plotted as shown in figure 3.5 (b, c,d,e, and f) in Chapter 3. The difference in variation for differential temperature and running thermal contrast was observed at various water content in cells (25%, 50% and 100%) as indicated in the predicted results (sample figure 3.5 in chapter 3). The temperatures have

shown a very good distinction between water and air-filled cells. The deviation is significant because of the difference in thermal properties between water and air. The model was uniformly heated and with no induced noise. However, during image/sequence processing, there is an embedded noise, which can be observed through the signal-to-noise ratio factor.

As seen in Figure 3.14 in Chapter 3, the cell fully filled with water (with water in contact with the skin on both sides) generates higher peak ΔTm signals and shorter observation times (tm). A similar pattern is observed in the vertical panel, where both surfaces remain in contact with water desPIRTe having a smaller mass compared to the fully water-filled cells. These results align with previous studies, which found that observation time decreases with lower water content, and the presence of air gaps between the water and the skin makes both Cm and tm values more dependent on water content. When water is in contact with the skin, the temperature signals show only a weak dependence on the thickness of the water layer.

## 5.2 Signal-To-Noise Ratio for Numerical Image Sequences

SNR is a critical parameter in image processing. The image sequence obtained from the ThermCalc-3D numerical software was processed by several image processing algorithms in ThermoFit, using the SNR as a figure of merit. The SNR for each scenario (orientation and water content) was calculated. The horizontal plate generally produces higher SNRs across all applied logarithms, resulting in better visibility of the water-filled cells. In contrast, the $30^0$ and $60^0$ sample orientations exhibit relatively low SNRs, likely due to water leakage through the adhesive seal during rotation. Additionally, the vertical orientation shows lower SNR values, which affects the image quality. It was also noted that no single algorithm consistently performs best across all scenarios during image processing. It was also observed that if a sample is positioned under $60^o$, the water in the cells partially filled with water (25% and 50%) changed configuration compared to the horizontal position. it could be because of leaks through the adhesive seal tap on the surface. Therefore, the defect areas of these cells are not uniform in this case, thus contributing to lower SNR values.

## 5.3 3D Normalisation

3D normalisation is a scientific procedure where the numerical image is used as a mask image to enhance water ingress detection in the experimental images or sequence. ThermoDouble numerical software was used to generate 3D normalised images. Typical results are shown in Chapter 3, Figures 3.24 and 3.25. It was observed that there was an improvement in terms of water ingress detection and visibility. Figure 5.1 depicts the experimental image before and after the 3D normalisation.

| Experimental imagines(3s) | Calculated images with image #7 | 3D normalisation images (ThermoDouble) |
|---|---|---|

Figure 5.1: 3D normalization of the experimental

## 5.4 Experimental Work

### 5.4.1 Detection of water ingress in cells

The image sequence was recorded using an Optris pi 450i IR Camera (image format 382 × 288, Noise Equivalent Temperature Difference (NETD) 40 mK, spectral range $7.5 - 13\ \mu m$, frame rate 80Hz). The ThermoFit Pro software from TPU was used to process them.

At first, the image sequence is converted from the “FS” file to disc image format, which can be used to create a scenario in the ThermoFit software. Normally, the first image of the scenario is assumed to be that of ambient temperature and therefore, the background option on the preview window is used to subtract the first image from the sequence to deal with excess temperatures only. The sequence with a specified mask is spatial filtered before appropriate processing algorithms are selected.

The differential temperature signals ($\Delta T_m$) and running temperature contrast ( $C_m$ ) can directly be determined on the preview window.

### 5.4.2 Differential temperature signals (ΔT) and the running contrast ($C_{run}$)

The experimental results for these two parameters, shown in Table 5.1 extracted from Chapter 4, closely align with the theoretical data derived from the model with the same panel orientation ($180^0$ with air gap). Notably, the cells fully filled with water exhibit the highest values for both differential temperature signals (ΔT = -3.54°C) with the shortest observation time (8.8 seconds), and thermal contrast (C = 64.1%) with a somewhat longer observation time of 24.8 seconds. It is important to note that, as anticipated, the maximum temperature signals for the fully water-filled cells occur earlier than those for cells with air gaps. However, the thermal contrast behaves in a more complex manner, reaching its peak at a later time.

Table 5.1. Optimum water detection parameters
(horizontal panel with air gap, experimental results).

| Defect | $\Delta T_m$ (℃) | $t_m(\Delta T_m), s$ | $C_m$ | $t_m(C_m), s$ |
|---|---|---|---|---|
| 25% (D1) | 2.7 | 11.6 | 0.45 | 27.4 |
| 50% (D2) | 3.4 | 15.6 | 0.55 | 9.8 |
| 100% (D3) | 3.5 | 8.8 | 0.64 | 24.8 |

### 5.4.3 Signal–to-noise ratio for experimental image sequences

During the data processing of the numerical image sequence, SNR was used as a key parameter for detecting and visualizing water trapped in the cells of the honeycomb model. It was found that the SNR was higher in cells completely filled with water (100%) compared to both the sound areas and cells with 25% and 50% water content. Additionally, the SNR values for the vertical, horizontal, and inclined models were similar, indicating that the orientation of the structure had minimal impact on the detectability of water trapped in the cells.

Furthermore, it was observed that SNR values varied depending on the processing algorithm used, suggesting that no single algorithm is optimal for all scenarios.

The SNR data presented in Chapter 3 (Table 3.2) compares different orientations of a sample with cells filled to 50% with water. This also highlights the issue of uniform versus non-uniform heating, which is crucial in real-world scenarios such as water ingress assessment in aircraft fuselages. These results are compared with those from a sample with cells fully filled with water (100%).

## 5.5 Implication of the Study

The study of water ingress detection in honeycomb structures has significant implications for the aviation industry, particularly in ensuring aircraft safety, durability, and performance. Honeycomb structures are commonly used in aerospace due to their lightweight and high-strength properties, essential for reducing fuel consumption and enhancing the overall efficiency of aircraft. However, when water enters these structures, it can lead to a range of issues that can compromise the integrity and safety of the aircraft.

Water ingress in these structures has broad and far-reaching implications for the structural integrity and safety of the aircraft. Water ingress can weaken the structural strength of

honeycomb panels, potentially leading to delamination, corrosion, and other forms of material degradation. Over time, this can compromise the overall safety of the aircraft, especially in critical components like fuselages, wings, and tail sections.

This study focused on the numerical and experimental characterisation of water ingress in the cells of honeycomb structures, in particular, the structures at various orientations as well as specific water content in the cells. The findings from this study are scientifically contributing to improving maintenance practices in the aviation industry by enhancing predictive maintenance capabilities. Detecting and quantifying water ingress before it causes significant damage could reduce the need for extensive inspections and allow for more proactive maintenance scheduling, lowering costs and improving operational efficiency.

Therefore, by advancing methods to detect and manage water ingress as demonstrated in this work, the industry can improve the reliability and longevity of critical aircraft components, ensuring a safer and more cost-effective aviation environment.

## 5.6 Conclusions

Detecting water in honeycomb sandwich airframes is a crucial inspection task in the aviation industry. Among the available techniques, 3D modelling is the most effective method for obtaining quantitative data on water detection within honeycomb cells. This study used a quantitative comparison of key parameters, such as SNR, differential temperature signals, contrasts, and their corresponding observation times, across various test scenarios (horizontal, inclined, and vertical panels). Based on the results, the following conclusions were drawn:

- Panel orientation has minimal impact on the SNR values observed during experimental testing. In other words, the orientation of the panels does not significantly affect the visibility of water trapped within the honeycomb cells.
- Based on the comparison of SNR of various image processing algorithms across all computational and experimental test scenarios ( orientations), it was observed that no single post-processing algorithm was found to provide optimal inspection results
- The findings align with previous studies, confirming that water or ice in direct contact with the skin surface is most effectively detected.
- The use of an appropriate heating technique is critical to achieving the best inspection parameters.
- The experimental data can be used to estimate water content in the cells by introducing a parameter calibration curve.

- The issue of frozen water volume expansion, which could potentially damage cell walls, warrants further investigation.

# CHAPTER 6:
# THESIS CONCLUSIONS

## 6.1 Introduction

This study conducted qualitative and quantitative analysis using computational methods and IRT to detect water within honeycomb structures. It used key parameters, such as SNR, running contrast, differential signal temperature, and observation times. The chapter begins with a summary of the previous work and a report on the key findings from the numerical and experimental analyses. General conclusions are drawn from these two approaches, highlighting the insights gained. The chapter also addresses the critical challenges encountered throughout the study. Given the significance of this research for the aviation industry, the final section outlines additional areas that warrant further investigation.

## 6.2 Work Reported in This Thesis

This work was motivated by the real need for an effective technique or combination of techniques to detect and quantify water ingress in the honeycomb structures in the aircraft fuselage. This process requires a user-friendly method with high accuracy and low cost and can be used in complex structures at various orientations. In this context, the numerical modelling using ThermoCalc-3D software as a predictive technique and infrared thermography (Active and Passive) appeared to be a perfect match for characterising water ingress in a honeycomb structure. ThermoCalc-3D uses finite difference algorithms, which results in high accuracy in the differential temperature signals. Infrared thermography is a preferred thermal non-destructive testing method that allows for the control of a full spectrum of material during testing.

### 6.2.1 Numerical modelling and Image processing

A 3D heat conduction problem was analysed using ThermoCalc-3D. The model had cells filled with water at various depths (25%,50%, and 100%). The heat flux was applied on the top, front surface of this model when set at various inclinations (30°,45°, 60°, 90°, and 180°). In some instances, non-uniform heating was applied to the model, which aimed at introducing practical or real conditions on the aircraft fuselage. The comparison of the critical parameters (differential temperature signals, running contrast, observation times, and the SNR between cells with no water, partially filled and fully filled with water was presented. The image sequences obtained from ThermoCalc-3D were processed using ThermoFit Pro software. The results of this model, presented in Chapter 3, achieved the following:

- It was noted that the orientation of the panel has minimal effect on the SNR values during modelling, meaning the visibility of water trapped in the honeycomb cells is largely independent of panel orientation.
- It was found that 3D normalisation improves the detection of water ingress.
- No single post-processing algorithm produces the best inspection results for all model scenarios.
- The findings are consistent with previous research, confirming that the most accurate detection occurs when water or ice is in direct contact with the surface.

### 6.2.3 Infrared thermography testing and image processing

The primary focus was on active infrared thermography testing of honeycomb panels with water ingress at varying depths and orientations. Additionally, passive infrared thermography testing was performed on structures with frozen water. This approach is crucial for detecting water ingress, as water in its solid state absorbs more heat energy than in its liquid form. The temperature difference (delta T) and contrast are more pronounced with shorter observation times ($t_m$). As outlined in Chapter 4, key parameters were recorded and analysed, with the results presented in Table 4.4.

The surface temperature profiles observed on the thermograms (image sequence) were obtained during the heating and cooling process. Data from a heating pulse of 2s,3s, and 5s were recorded. The comparison between the output parameters of various orientations was presented and a general observation was that cells with water filled at 100% revealed high (-ve) differential temperature signals (ΔT) and running contrast ($C_m$) with shorter observation times for both ΔT and $C_m$.In the case of frozen water in cells, both the ΔT and $C_m$ were recorded as maximum and shortest observation times.

The image sequences obtained from both experimental procedures were processed using algorithms in the ThermoFit Pro software in terms of SNR. The algorithm with the highest SNR is the preferred for image processing for that scenario. The SNR of various image processing algorithms were compared, and the highest SNR was identified. In thermography, a higher SNR results in clearer images with less random noise interference, enhancing the ability to detect small variations, such as temperature differences between a defected and a non-defected area.

In general, after validation, the differential temperature signals and the running contrast are greatly influenced by the cell's structure, the quantity of water in cells, the phase of water (liquid or solid), and the experimental set-up standards.

A calibration curve was developed to quantify water ingress in honeycomb panels using both active and passive infrared thermography data. This curve establishes a relationship between the panel's thermal response (temperature differential signals) and the amount of water trapped within the cells. In active infrared thermography (heating), it was observed that the temperature differential signal increases with higher water content. As discussed in Chapter 4, cells completely filled with water (100%) exhibited the highest temperature differential signal of 27°C, while those with 50% water content showed a lower signal of 25°C. These variations indicate that the temperature changes are influenced by both the presence and the quantity of water in the cells. Similarly, in passive infrared thermography (without external heating), temperature variations due to environmental conditions were recorded, with the presence of water affecting heat transfer and cooling rates. The calibration curve reached a maximum temperature differential signal of 11°C at 37% water content, beyond which the signal remained constant.

Based on these observations, the active (heating) infrared thermography curve proved to be more reliable than the passive (heating) infrared thermography. By correlating the thermal data with known water content from experimental results, the calibration curve was established, enabling the quantification of water ingress in the panel. This allows for accurate detection and assessment of water content within the honeycomb structure's cells.

## 6.3 Research Work Challenges

As discussed in previous chapters, this research primarily focuses on both numerical and experimental aspects. The numerical simulations were conducted using software developed at Tomsk Polytechnic University (TPU) in Russia, including ThermoCalc-3D, ThermoFit Pro, and ThermoDouble. The experimental component involved active and passive thermography. During this study, several challenges were encountered:

- **Water injection in the cells:** The honeycomb specimens were injected with water through the rear surface, with adhesive tape applied to prevent leakage. However, in some cases, water leakage occurred, which impacted the results.
- **Experimental setup:** Active thermography requires uniform heating, meaning the centre of the heat source must be aligned perpendicularly with the centre of the specimen. This proved challenging for a first-time operator.

- **Positioning of test samples:** Setting the test samples at specific inclined angles (e.g., 30°, 45°, 60°) was also difficult due to the challenge of achieving accurate angles.

## 6.4 Future Work

This research primarily focused on thermal non-destructive testing (NDT) to both qualitatively and quantitatively characterise water ingress in honeycomb cells. However, an important aspect that requires further investigation is the phenomenon of frozen water volume expansion, which may potentially cause damage to the cell walls. Additionally, the long-term effects of water ingress on the overall lifespan of the panel, as well as the potential for physical damage due to water absorption and freezing, also warrant further study. Understanding how these factors influence the durability and structural integrity of honeycomb panels is crucial for developing more effective maintenance and design strategies in applications where water exposure is a concern.

## REFERENCES


Airbus. (2017). Infra-red water detector. [online] Available at: http://www.airbus.com.

Alexey Moskovchenko, Vavilov, V.P. and Chulkov, A.O. (2020). Comparing the efficiency of defect depth characterization algorithms in the inspection of CFRP by using one-sided pulsed thermal NDT. *Infrared Physics & Technology*, 107, pp.103289–103289. doi: https://doi.org/10.1016/j.infrared.2020.103289.

Avdelidis, N.P. and Moropoulou, A. (2003). Emissivity considerations in building thermography. *Energy and Buildings*, 35(7), pp.663–667. doi:https://doi.org/10.1016/s0378-7788(02)00210-4.

Brown, A. and Lee, M. (2022). Finite Element Analysis of Composite Materials. Springer

Chulkov A.O., Shagdirov B.I., Vavilov V.P., Kladov D.Yu., Stasevskii V.I. (2023), Detecting and evaluating water ingress in horizontally oriented aviation honeycomb panels by using automated thermal non-destructive testing. Rus. J. NDT, Vol. 59, No. 12, pp. 1272-1279. DOI: 10.1134/S1061830923600946.

Dua, G., Mulaveesala, R., Mishra, P. and kaur, J. (2021). InfraRed Image Correlation for Non-destructive Testing and Evaluation of Delaminations in Glass Fibre Reinforced Polymer Materials. Infrared Physics & Technology, p.103803. doi:https://doi.org/10.1016/j.infrared.2021.103803.

Fang, Q. and Maldague, X. (2020). A Method of Defect Depth Estimation for Simulated Infrared Thermography Data with Deep Learning. 10(19), pp.6819–6819.https://doi.org/10.3390/app10196819.

Grys, S. (2018). Determining the dimension of subsurface defects by active infrared thermography – experimental research. Journal of Sensors and Sensor Systems, 7(1), pp.153–160. https://doi.org/10.5194/jsss-7-153-2018.

Ibarra-Castanedo, C., Tarpani, J.R. and Maldague, X.P.V. (2013). Nondestructive testing with thermography. *European Journal of Physics*, 34(6), pp.S91–S109. doi:https://doi.org/10.1088/0143-0807/34/6/s91.

Ibarra-Castanedo, C., Genest, M., Servais, P., Maldague, X.P.V. and Bendada, A. (2007). Qualitative and quantitative assessment of aerospace structures by pulsed thermography. Nondestructive Testing and Evaluation, 22(2-3), pp.199–215. doi:https://doi.org/10.1080/10589750701448548.

Johnson, T., Williams, R., & Patel, S. (2018). Infrared Thermography in Non-Destructive Testing. Wiley.

Kaplan H. Practical Applications of Infrared Thermal Sensing and Imaging Equipment.-Tutorial Texts in Optical Engineering, SPIE Press V. TT34, 1999, USA, 164 p.

Katunin A., Dragan, K., Dziendzikowski M. (2015). Damage identification in aircraft composite structures: A case study using various non-destructive testing techniques. Composite Structures, Vol. 127, pp.1–9.
DOI:10.1016/j.compstruct.2015.02.080.

Kumar, R., & Patel, D. (2019). Thermal Response of Composite Materials. Elsevier.

LaPlante G., Marble A.E., MacMillan B., Lee-Sullivan P., Colpirtts B.G., Balcom B.J. (2005). Detection of water ingress in composite sandwich structures: a magnetic resonance approach. NDT & E International, 2005, Vol. 38, Issue 6, pp.501–507.
DOI: 10.1016/j.ndteint.2005.01.006.

Lee, J., Kim, H., & Chen, X. (2021). Challenges in Thermal Imaging for Composite Panels. Journal of Composite Science, 15(3), 215-230.

Liu, X. (2021). Aircraft maintenance and water detection in aerospace components. International Journal of Aerospace Engineering, 34(3), 89-97.

Manohar, A. and Lanza, F. (2014). Modeling 3D heat flow interaction with defects in composite materials for infrared thermography.66, pp.1–7. https://doi.org/10.1016/j.ndteint.2014.04.003.

Moskovchenko, A., Švantner, M., Vavilov, V. and Chulkov, A. (2021). Characterizing Depth of Defects with Low Size/Depth Aspect Ratio and Low Thermal Reflection by Using Pulsed IR Thermography. Materials, 14(8), p.1886. https://doi.org/10.3390/ma14081886

Nesteruk D.A.(2005). Thermal imaging control of water in aviation cellular panels during aircraft operation, Cand. Sci. (Eng.) Dissertation, Russia, Tomsk: Tomsk Polytech. Univ., 2005.

Nguyen, T., Zhang, Y., & Brown, C. (2020). Validation Techniques for Computational Models in Materials Engineering. Computational Mechanics, 40(5), 678-689.

Non-destructive Testing Handbook: Infrared and Thermal Testing (3rd ed.), 2001, ASNT, USA, 718 p.

Omar, M. and Zhou, Y. (2008). A quantitative review of three flash thermography processing routines. 51(4), pp.300–306. doi:https://doi.org/10.1016/j.infrared.2007.09.006.

Pawar, S.S. and Vavilov, V.P. (2016). Applying the heat conduction-based 3D normalization and thermal tomography to pulsed infrared thermography for defect characterization in composite materials. International Journal of Heat and Mass Transfer, 94, pp.56–65. doi: https://doi.org/10.1016/j.ijheatmasstransfer.2015.11.018

Pfeiffer, H., Heer, P., Ioannis PIRTropakis, Pyka, G., Greet Kerckhofs, Patitsa, M. and Wevers, M. (2012). Liquid detection in confined aircraft structures based on lyotropic percolation thresholds. Sensors and actuators. B, Chemical, 161(1), pp.791–798. doi:https://doi.org/10.1016/j.snb.2011.11.034.

Rani, A. and Mulaveesala, R. (2022). Novel pulse compression favourable excitation schemes for infrared non-destructive testing and evaluation of glass fibre reinforced polymer materials. Composite Structures, 286, p.115338. doi:https://doi.org/10.1016/j.compstruct.2022.115338.

Sharath, D. Menaka, M and Venkatraman, B. (2012). Defect Characterization Using Pulsed Thermography. 32(2), pp.134–141.https://doi.org/10.1007/s10921-012-0166-4.

Smith, D., & Evans, R. (2019). Techniques for moisture detection and management in aircraft systems. Aerospace Technology Journal, 41(2), 56-64.

Smith, J., & Jones, L. (2020). Aerospace Composite Materials: Performance and Testing. Aerospace Journal, 75(2), 120-135.

Smith, K., & Williams, P. (2024). Combined Methods for Water Ingress Assessment in Aerospace Panels. Journal of Advanced Composite Structures, 29(4), 345-359.

Taylor, A., Richards, J., & Green, D. (2023). Integrated Approaches in Structural Health Monitoring. Structural Health Monitoring, 22(1), pp50-65.

Tewary, S, at el (2009). Detection of Subsurface Defects using Active Infrared Thermography. In Academic of Science and Innovation Research. New Dehli, 4/8. Chandigarh, India: CSIR-Central Scientific Instruments Organization. 1-6.

Umar, M.Z., Vladimir Vavilov, Abdullah, H. and Ariffin, A.K. (2019). Low energy impact damages detection in carbon fibre reinforced carbon using ultrasonic – Stimulated infrared thermography. AIP conference proceedings.

doi: https://doi.org/10.1063/1.5089310.

Vavilov, V.P. and Burleigh, D.D. (2015). Review of pulsed thermal NDT: Physical principles, theory and data processing. *NDT & E International*, 73, pp.28–52. doi: https://doi.org/10.1016/j.ndteint.2015.03.003.

Vavilov, V. and Burleigh, D.D. (2020). Infrared thermography and thermal non-destructive testing. Cham: Springer.

Vavilov, V.P., Pan, Y., Moskovchenko, A.I. and Čapka, A. (2017). Modelling, detecting, and evaluating water ingress in aviation honeycomb panels. Quantitative InfraRed Thermography Journal, 14(2), pp.206–217.
doi: https://doi.org/10.1080/17686733.2017.1317443.

Vavilov, V.P (2022). 3D modeling of pulsed thermal NDT: Back to basic features and subtle phenomena. *NDT & E International*, 130, pp.102659–102659.
doi: https://doi.org/10.1016/j.ndteint.2022.102659.

Vavilov, V.P., Pan, Y. and Nesteruk, D.A. (2016). Infrared thermographic inspection of water ingress in composite honeycomb panels. Applied optics, 55(34), pp.120–135. doi: https://doi.org/10.1364/ao.55.00d120

Vavilov V., Marinetti S., Pan Y., Chulkov A .(2016) Detecting water ingress in aviation honeycomb panels: Qualitative and quantitative aspects. Polymer Testing, 2016, Vol. 54, pp. 270–280.
DOI: 10.1016/j.polymertesting.2016.07.023.

Wang P., Pei Y., Zhou L. Near-field microwave identification and quantitative evaluation of liquid ingress in honeycomb sandwich structures. NDT & E international, 2016, Vol. 83, pp.32–37. DOI: 10.1016/j.ndteint.2016.06.002.

Wei, Y., Xiao, Y., Li, S., Gu, X., Zhang, D., Li, H. and Chen, Y. (2024). Depth prediction of GFRP composite using long pulse thermography. Measurement, 237, pp.115259–115259. doi:https://doi.org/10.1016/j.measurement.2024.115259.

Wei, Y., Zhang, S., Luo, Y., Ding, L. and Zhang, D. (2021). Accurate depth determination of defects in composite materials using pulsed thermography. 267, pp.113846–113846. https://doi.org/10.1016/j.compstruct.2021.113846.

Whelan.D.A. (1995). Infrared Thermography: A Review of Techniques and Applications for Non-Destructive Testing. Journal of Non-destructive Evaluation, 14(1), pp. 3-15.

Xavier P.V. Maldague (1993). Nondestructive Evaluation of Materials by Infrared Thermography. Springer.

Zeng, N., Wu, P., Wang, Z., Li, H., Liu, W. and Liu, X. (2022). A Small-Sized Object Detection Oriented Multi-Scale Feature Fusion Approach with Application to Defect Detection. 71, pp.1–14. https://doi.org/10.1109/tim.2022.3153997.